Water mass transformations in the Barents Sea and linkages to the Polar Front

Vidar Surén Lien

Dissertation for the degree Philosophiae Doctor

July 2010

Geophysical Institute
University of Bergen
Norway

Water mass transformations in the Barents Sea and linkages to the Polar Front

Vidar Surén Lien

PhD Thesis in physical oceanography

July 2010

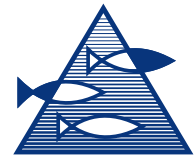

Geophysical Institute
University of Bergen
Norway

Institute of Marine Research
Bergen
Norway

Acknowledgements

This work would not have been possible without the help from my supervisors, Tor Gammelsrød, Bjørn Ådlandsvik and Øystein Skagseth, all of whom I owe a big thank you for your support and help along the way. We have had some good discussions which have helped a lot in the progress of the work.

In addition, I would like to thank all other who have contributed with discussion, help, and support during the last three years:
I owe Tor-Villy Kangas a thank you for deploying the moorings in the northeastern Barents Sea and "threading the path", although I never got to use the data. I would also like to honour the memory of Tor Ivar Halland - you made the stay at "Professor Boyko" a much better one. Ole Gjervik deserves a thank you for constructing our superb moorings, of which none failed - as usual! I thank Randi Ingvaldsen for constructive discussions. Harald Loeng and Tor Gammelsrød are acknowledged for having the courage and drive to go ahead and put moorings in Russian waters - it was at least worth a shot. I owe Ken Drinkwater a big thank you for fruitful discussions and careful reading of my manuscripts, and I also owe Frode Vikebø a thank you for help with ROMS and keeping up the momentum in our modeling efforts.

I also want to thank the rest of the oceanography group at IMR, for your openness, inclusiveness and for making IMR a great place to work!

I want to thank my family for your support, and for always encouraging me to pursue knowledge.

And last but not least, great hug to you, Bente, for your endless support and patience, and to you, Sigve, although you do not yet understand what daddy is doing at work.

Vidar S. Lien
Bergen, June 2010

Outline

This thesis consists of an introduction and 4 scientific papers. Paper I investigates the exchanges between the Barents Sea and the Arctic Ocean, while paper II focuses on the water masses and how they are transformed. Paper III investigates the Barents Sea Polar Front, by the use of a high-resolution numerical ocean model. Paper IV uses a regional numerical ocean model to improve the regional climate scenario produced by a global climate model.
List of papers:

- **Paper I:**
  Mass and heat transports in the NE Barents Sea: Observations and models
  T. Gammelsrød, Ø. Leikvin, V. Lien, W.P. Budgell, H. Loeng and W. Maslowski
  Journal of Marine Systems, 75, 56-69, 2009

- **Paper II:**
  Intermediate and deep water mass characteristics and transformations in the St. Anna Trough
  V.S. Lien and A.G. Trofimov
  Submitted to Deep-Sea Research I

- **Paper III:**
  The Barents Sea Polar Front - a model study
  V.S. Lien and B. Ådlandsvik
  Manuscript

- **Paper IV:**
  Using the Regional Ocean Modeling System (ROMS) to improve the oceanic circualtion from a GCM 20^{th} century simulation
  A. Melsom, V.S. Lien and W.P. Budgell
  Ocean Dynamics, 59, 969-981, 2009

Contents

Acknowledgements **v**

Outline **vii**

1 Introduction **1**

2 Scientific background **1**

2.1 General circulation and processes in the Barents Sea 1

2.1.1 Deep water formation 4

2.1.2 Barents Sea Polar Front 5

2.2 Numerical modeling 6

2.2.1 Numerical modeling efforts in the Barents Sea 6

2.2.2 Regional Ocean Modeling System (ROMS) 7

2.2.3 Model set-up used in this study 8

2.2.4 Validation and evaluation of numerical models 11

3 This study **11**

3.1 Objectives 11

3.2 Summary of papers 12

3.3 Main conclusions 14

3.4 Future perspectives 15

Bibliography **16**

Paper I **27**

Paper II **43**

Paper III **101**

Paper IV **151**

1 Introduction

The Barents Sea is an important area due to its vast marine resources. It hosts large commercial fish stocks, such as the Arcto-Norwegian cod *(Gadus morhua)* and capelin *(Mallotus villosus)* (Sakshaug et al. 2009), and in recent years large quantities of oil and gas has been discovered below the seabed. It is also an important area for both the regional and the global climate. Based on observations by Knipowitsch (1905), Roald Amundsen's expedition with *Gjøa* and observations from his own *Fram* expedition, Nansen (1906) pointed out that the Barents Sea is a production area for high-salinity shelf water due to ice-freezing and subsequent brine release, and hypothesized that the Barents Sea thereby contributes to the world oceans deep water. Large variability has been observed in both the climate (Ingvaldsen et al. 2003); (Levitus et al. 2009) and the marine resources (Sakshaug et al. 1994) of the Barents Sea. This calls for a better understanding of the processes determining the variability and its impacts.

Observations during recent decades have shown large changes in the Atlantic Water (AW) supply to the Arctic Ocean (Quadfasel et al. 1991); (Polyakov et al. 2005). Increasing temperatures have been observed upstream along the Norwegian continental slope (Orvik & Skagseth 2005), in the Barents Sea Opening (Skagseth et al. 2008), in the Fram Strait at the entrance to the Arctic Ocean (Schauer et al. 2004), and in the interior Arctic Ocean (Polyakov et al. 2005); (Dmitrenko et al. 2008a). Observations have shown that the global climate is warming, with an amplification in polar regions. This is supported by model projections of 21st century climate (IPCC-WG-I/8 2007) . In order to establish an ecosystem approach to sustainable harvest of marine resources, it is important to assess the impacts of possible climate change in advance. To do this, we have to rely on model projections. However, the global climate models are unsuitable for a regional assessment of climate change, especially at high northern latitudes (Fig. 1). Thus, there is a need for downscaling by applying regional models with higher spatial resolution in order to resolve processes that are important for the regional climate.

Another motivation for increasing our knowledge and understanding of the regional climate system, is the feedback from the regional processes to the global climate. It is therefore of great importance to apply our knowledge of regional climate change impacts to our knowledge of the global climate system.

2 Scientific background

2.1 General circulation and processes in the Barents Sea

The Barents Sea is one of the largest ($1.4*10^6$ km^2) and the deepest (average depth of 230 m) shelf sea adjacent to the Arctic Ocean (Fig. 2). It is bounded by the Norwegian

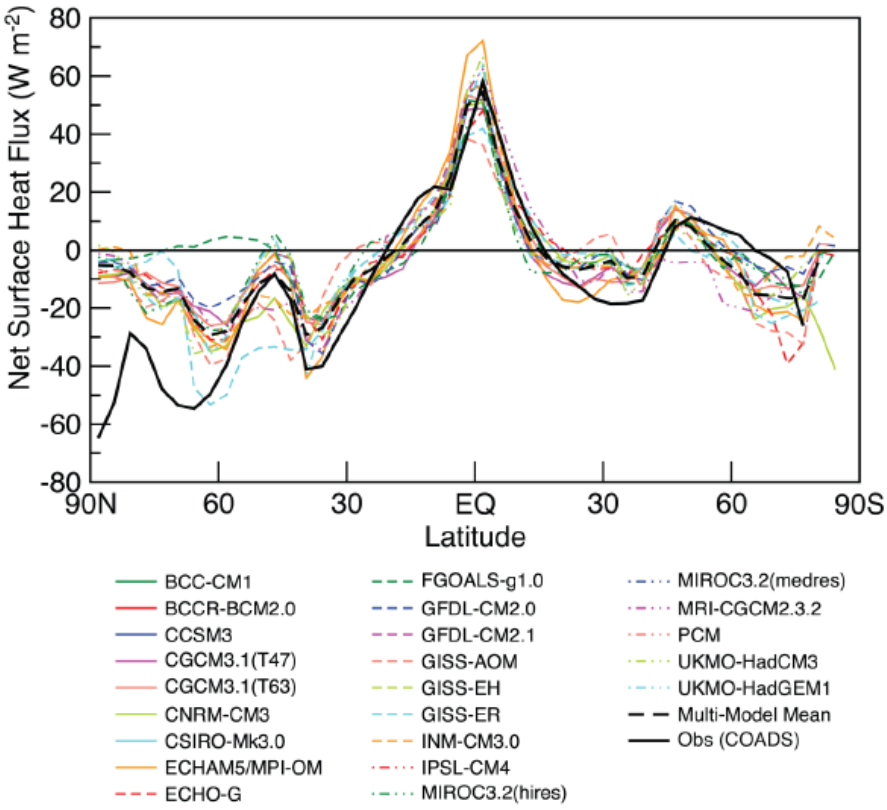

Figure 1: *Zonal mean net heat fluxes at the surface in the global climate models (colors) and from observations (thick, black line). The model ensamble mean is shown as broken thick, black line. (North towards left; from IPCC 4AR Ch. 8.3.1, Fig. 8.4)*

and Russian coast to the south, while Novaya Zemlya forms the eastern border. To the north, Svalbard and Franz Josef Land defines the corners of the Barents Sea's extension. The interior Barents Sea is dominated by several banks and basins, forming a complex topography, which puts a strong constraint on the current pattern. The main inflow occurs through Bjørnøyrenna (Bear Island Trough) between the coast of Norway and Bjørnøya (Bear Island), see e.g. Blindheim (1989), while the inflow between Bjørnøya and Svalbard is very low due to the presence of Svalbardbanken (the Svaldbard Bank) and Hopenbanken (the Hopen Bank). Main outflow occurs to the east, between Novaya Zemlya and Franz Josef Land, see e.g Loeng et al. (1993). There is also some exchange between the Barents Sea and the Arctic Ocean to the north, through the troughs

between Svalbard and Franz Josef Land (Mosby 1938); (Novitsky 1961); (Matishov et al. 2009).

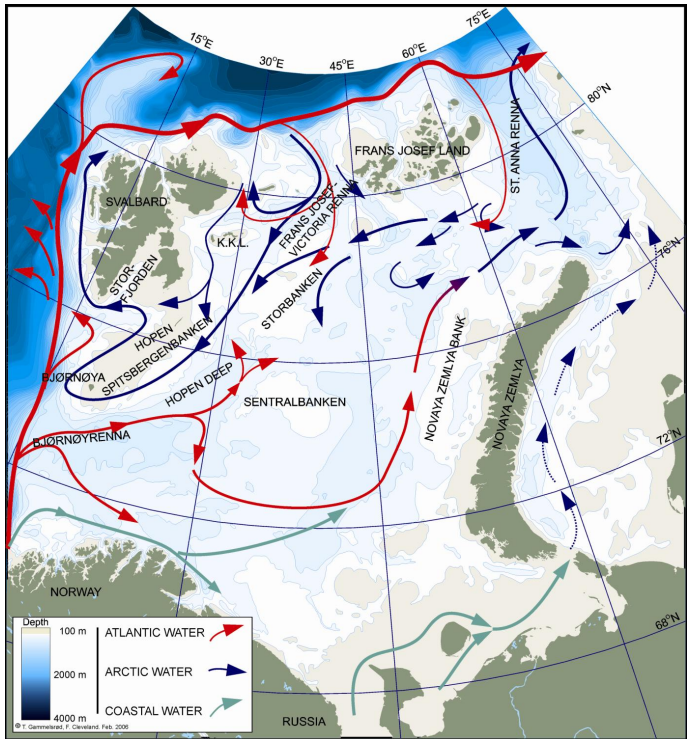

Figure 2: *Bathymetric map of the Barents Sea region. Arrows show general circulation patterns. (Courtesy by F. Cleveland and T. Gammelsrød)*

The inflow of warm and saline AW to the Nordic Seas follows the Norwegian continental slope as the Norwegian Atlantic Current (NwAC; Helland-Hansen & Nansen (1909)). Between Norway and the Svalbard Archipelago, the current bifurcates and one branch continues northward as the West Spitsbergen Current (WSC; Aagaard et al. (1987); Fig. 2). As the WSC enters the Nansen Basin through the Fram Strait, it submerges under the cold halocline in the Arctic Ocean and flows eastward as a slope current following the continental shelf break. This water mass is sometimes referred to as Fram Strait Branch Water (FSBW; see e.g. Schauer et al. (2002b)). North of the St. Anna Trough, the FSBW bifurcates and one branch enters the St. Anna Trough (Hanzlick & Aagaard 1980) and follows the topography into the northeastern Barents Sea between Novaya Zemlya and Franz Josef Land (Loeng et al. 1993), (Schauer et al. 2002a). This water mass is warmer than the water masses flowing eastward from

the Barents Sea, and it is therefore easily distinguishable (Loeng et al. 1993), (Schauer et al. 2002a).

The other branch of the NwAC, termed the North Cape Current (NCaC), carries between 1.5 and 2 Sv (1 Sv = 10^6 m^3s^{-1}) of AW into the Barents Sea (Blindheim 1989); (Ingvaldsen et al. 2002); (Skagseth et al. 2008). Here, AW is usually defined by $S > 35.0$, and the typical temperature range is 4.5 ^{o}C $< T <$ 6.5 ^{o}C (Midttun & Loeng 1987). In addition, the Norwegian Coastal Current (NCC) carries between 0.5 Sv and 1 Sv (Ingvaldsen et al. 2004b) of water with similar temperature as AW but with $S < 34.7$ (Sætre & Ljøen 1971), adding freshwater to the Barents Sea. In the Barents Sea, these water masses undergo considerable modifications through several different processes (Loeng 1991); (Pfirman et al. 1994), before they exit to the northeast between Novaya Zemlya and Franz Josef Land and flow into the Arctic Ocean (Loeng et al. 1993); (Schauer et al. 2002a). These processes include cooling through heat loss to the atmosphere (Aagaard et al. 1981), freshwater gain from the NCC, ice melt, runoff and net precipitation (Steele et al. 1995), input of salt through ice freezing and brine rejection (Midttun 1985); (Loeng 1991), and wind and tidal mixing (Sundfjord et al. 2007). This gives the Barents Sea water a wide range of densities before exiting into the Arctic Ocean (Rudels et al. 1994); (Schauer et al. 2002b). According to Rudels et al. (1994), the Barents Sea water entering the Arctic Ocean consists of 3 components. The most dense being AW that has been cooled through heat loss to the atmosphere and freshened through net precipitation. Above this layer is less dense AW that has recieved freshwater trough ice melting and has then been homogenized through ice freezing leading to brine release and haline convection the following winter. At the top is a layer stemming from the NCC with additional freshwater input from rivers, mainly through the Kara Sea. Thus, as the water from the Barents Sea leaves the St. Anna Trough, it occupies a 1000 m deep water column (Rudels et al. 1994). This water column deflects the FSBW from the upper slope to the lower slope in the Arctic Ocean, and partly descends below the less dense FSBW (Rudels et al. 1994); (Schauer et al. 2002b); (Dmitrenko et al. 2009a). Thereby, the Barents Sea is important for the ventilation and renewal of the water masses in the Arctic Ocean. Formation of water masses dense enough to sink to great depths may also contribute to the renewal of the deep water in the Arctic Ocean (Nansen 1906); (Midttun 1985); (Loeng et al. 1993); (Rudels et al. 1994); (Jones et al. 1995); (Schauer et al. 2002a).

2.1.1 Deep water formation

Through the processes mentioned above, the Barents Sea contributes with deep water to the Arctic Ocean (Jones et al. 1995). Through the Fram Strait, the Arctic Ocean contributes to the deep water in the Greenland and Norwegian Seas (Aagaard et al. 1985). Eventually, this deep water spills over the Greenland Scotland Ridge through

the Denmark Strait (Macrander et al. 2005) and the Faroe Shetland Channel (Hansen & Østerhus 2007), and thereby contributes to the renewal and ventilation of the world oceans deep water. Formation of high-salinity shelf water through ice-freezing in the Barents Sea was proposed by Nansen (1906) and evidence of such production was observed by Midttun (1985). Observations in the western Barents Sea supports the idea that such a process may produce water with density large enough to sink to great depths in the Arctic Ocean (Quadfasel et al. 1992); (Schauer & Fahrbach 1999); (Skogseth et al. 2008); (Geyer et al. 2009).

The water masses entering the Arctic Ocean from the Barents Sea are less saline, but colder and also more dense than water masses at similar depths in the Eurasian Basin (Hanzlick & Aagaard 1980), (Schauer et al. 1997), and part of it submerges under the FSBW at the Arctic Ocean continental slope (Rudels et al. 2000a). Water flowing along the bottom of St. Anna Trough enters the Nansen Basin at 1000 m depth, below the FSBW. Therefore, no warmer water will be entrained on the way down the slope. This will lead to a cooling of the deep ocean water masses if the initial temperature of the outflow is lower than the temperature in the deep water (Rudels et al. 2000a). However, increasing temperature and salinity towards the bottom of the Eurasian Basin, indicates another source of deep water than the Barents Sea water (Jones et al. 1995). They suggest the area around Severnaya Zemlya as a potential formation area of Arctic Ocean bottom water, as these islands favor ice-freezing in lee polynas, leading to formation of high-salinity shelf water. However, this high-salinity water with temperature at the freezing point enters the Nansen Basin at only 100 m depth, and therefore have to pass through a layer of Atlantic derived water in the Circumpolar Boundary Current before reaching the deeper layers. This will increase the temperature of the descending water masses (Jones et al. 1995).

2.1.2 Barents Sea Polar Front

The Barents Sea Polar Front (BSPF) forms the transition zone between the relatively warm and saline AW in the south and the colder and less saline Polar Water (PW) in the north (Loeng 1991). One of the first exstensive investigations of the frontal structure was made by Johannessen & Foster (1978), and they concluded that the front is topographically steered and follows approximately the 100 m isobath. Later studies have confirmed that the front is topographically steered (Gawarkiewicz & Plueddemann 1995); (Parsons et al. 1996) and that it is dependent on the width of the NCaC carrying AW into the Barents Sea (Ingvaldsen 2005). The BSPF also defines the maximum extension of the sea-ice cover in the western Barents Sea (Vinje & Kvambekk 1991).

The seasonal ice cover provides for a high biological productivity due to a strongly stratified water column during late spring and summer (Loeng 1991); (Sakshaug et al. 1994); (Falk Petersen et al. 2000); (Reigstad et al. 2002), due to input of freshwater

through sea-ice melt and heating through insolation. In winter, wind mixing and thermal and haline convection supplies the surface layer with nutrients from below through mixing (Wassmann et al. 1999); (Sakshaug et al. 2009). Thus, processes connected to the seasonal ice cover is important for the onset of the algal bloom to the north of the BSPF.

2.2 Numerical modeling

Several factors contribute to make the Barents Sea a challenging area to model. The seasonal ice cover interacts with the ocean through adding freshwater during the melt season and creating a two-layer system with a strong pycnocline in summer, while wind mixing, and thermal and haline convection causes the mixed layer depth to reach the bottom in winter. On banks, ice freezing and subsequent brine rejection may create dense, high-salinity bottom water. Such bottom water has been observed cascading down the continental shelf (Blindheim 1989) in highly baroclinic currents. Strong tidal currents enhance the ocean mixing and create tidal fronts on the shallowest banks. In a numerical test experiment, Harms et al. (2005) found that including tides had a significant impact on the heat fluxes in the marginal ice zone (MIZ), over shallow banks, and in the BSPF-area. Being located at high latitudes strongly influences the internal Rossby-radius, and thus the length scale of the mesoscale activity in the Barents Sea. In a two-layer system, the internal Rossby radius R_i is given by

$$R_i = \frac{\sqrt{g'H}}{f}$$

where g' is the reduced gravity and f is the Coriolis parameter. H is the thickness of the upper layer.

Setting the reduced gravity to 0.005 (corresponding to e.g. ρ_1=1027.5 kg m^{-3} and ρ_2=1028 kg m^{-3}), assuming a surface layer of 30 m thickness, and setting the latitude to 75^{o}N, gives an internal Rossby-radius of 2.75 km.

From the above it is clear that high resolution, both horizontally and vertically, is needed in the model in order to adequately resolve the processes transforming the water masses in the Barents Sea. To further complicate the picture, any numerical ocean model is dependent on atmospheric forcing, which is expected to be of inadequate quality in the Barents Sea region due to very few observation stations.

2.2.1 Numerical modeling efforts in the Barents Sea

Pioneering work in using density driven, three dimensional numerical models in the Barents Sea include the works of Slagstad et al. (1989); Støle-Hansen & Slagstad (1991), focusing on ice-ocean interaction and vertical mixing. Ådlandsvik & Loeng (1991) used a purely wind-driven, barotropic model to study the influence of wind on the inflow to

the Barents Sea. In later years, a wide range of model studies have been conducted in the Barents Sea. Kärcher et al. (2003b) used a regional model to look at interannual climate variability in the northeastern Barents Sea, while Maslowski et al. (2004) used a model covering the Arctic Ocean and adjacent areas to estimate budgets of volume, heat, and salt in the Barents Sea. Budgell (2005) performed a dynamical downscaling from a coarse model covering the North Atlantic and Arctic Oceans to a regional model covering the Barents and Kara Seas. In a sensitivity study, Harms et al. (2005) found that the atmosphere-ocean heat exchange in the Barents Sea is sensitive both to changes in the inflowing water and the overlying atmosphere, and also to internal processes such as tidal mixing.

All of the above mentioned numerical experiments can be categorized as regional model studies, covering the whole Barents Sea and to some degree adjacent areas. The advantage of this approach is that the open boundaries are relatively far away from the area of interest, which reduces the direct influence of the boundary conditions. The drawback of regional applications is the horizontal resolution. The large computational demand puts a constraint on the resolution, and regional applications typically have a horizontal resolution on the order of 10 km. The above calculation showed that the typical length scale of mesoscale activity in the Barents Sea is as low as $\sim$3 km. Thus, the regional models are unable to resolve the mesoscale dynamics, although they may be categorized as "eddy-permitting" models, i.e. eddies are not resolved but are "permitted" to exist.

Process-oriented model studies require high resolution, and therefore usually apply models covering smaller areas, i.e. a fjord or an estuary. Examples include modeling of Storfjorden at Svalbard (Skogseth et al. 2007); (Fer & Ådlandsvik 2008), and the MIZ in the northern Barents Sea (Sundfjord et al. 2008). However, new advances in supercomputer modeling has made it feasible to move towards the eddy-resolving regime even for regional applications.

2.2.2 Regional Ocean Modeling System (ROMS)

In this thesis, we have used the numerical ocean model ROMS (Regional Ocean Modeling System), which is a three-dimensional baroclinic ocean general circulation model (OGCM). It is an open source community model, developed at Rutgers University (see http://www.myroms.org/). It is described in several papers, see Shchepetkin & McWilliams (2005) and Haidvogel et al. (2008) for details. ROMS uses topography-following generalized sigma coordinates in the vertical. This ensures high vertical resolution even in shallow and well-mixed areas, as opposed to models using z-coordinates or isopycnic coordinates in the vertical. In addition, stretching (packing) of the vertical layers towards the surface and bottom enhances the resolution further in the surface and bottom boundary layers.

The sigma-coordinate system puts a constraint on the slope of the bathymetry in the model grid. A factor r, representing the normalized slope of the bottom in the model grid, is defined (Beckmann & Haidvogel 1993)

$$r = \frac{\Delta h}{2h}$$

According to Haidvogel & Beckmann (1999), empirical studies have shown that reliable results are obtained if r does not significantly exceed 0.2. To ensure that the r-value does not get too high, the bathymetry needs to be smoothed. This is often done by applying a Shapiro-filter (Shapiro 1970), which reduces the bottom slope and thus also the r-value. Another desirable effect of the shapiro filter is that it effectively removes 2Δx-noise in the grid. However, depending on the horizontal resolution of the model grid, the smoothing removes topographic features that may potentially play important roles in the local dynamics. The need to smooth the bathymetry is therefore a disadvantage of the sigma-coordinate models.

In the horizontal, the model uses orthogonal curvilinear coordinates. Advantages include laterally variable resolution, which enables the ability to focus on specific areas of interest or areas that need enhanced resolution for proper treatment, such as frontal areas. On the downside, errors with for instance eddies propagating from areas where they are resolved to areas where they are not resolved may arise. A short discussion on this matter is provided in section 3.1.4 in Haidvogel & Beckmann (1999).

For the model to be appliccable at high latitudes, an ice module is coupled to the model system (Budgell 2005). Two ice layers and one snow layer are included, in addition to a molecular sub-layer (Mellor & Kantha 1989) between the bottom of the ice and the upper ocean. The inclusion of a molecular sub-layer improved the freezing and melting rates substantially (Budgell 2005). The ice dynamics are based on the elastic-viscous-plastic (EVP) rheology by Hunke & Dukowicz (1997) and Hunke (2001), while the thermodynamics is based on Mellor & Kantha (1989) and Häkkinen & Mellor (1992).

2.2.3 Model set-up used in this study

One problem in sigma-coordinate models is the problem with internal pressure gradients generated in areas with steep topography. Computing the internal pressure gradient along sigma-surfaces rather than along geopotential isolines, creates internal pressure gradient forces that set up artificial currents. This problem has been widely discussed during the last decades, see Mesinger (1982); Haney (1991); Beckmann & Haidvogel (1993); Mellor et al. (1994); Shchepetkin & McWilliams (2003). In this thesis, spline density Jacobian are used to compute the pressure gradients, as described in Shchepetkin & McWilliams (2003). The artificial currents set up by the internal

pressure gradient error was found to be relatively small in a regional application, and higher resolution should decrease this problem further.

Another topic which has been a focus of interest concerning sigma-coordinate models, is the issue of spurious diapycnal mixing (see e.g.Barnier et al. (1998)). Mixing in the ocean is dominated by isopycnic mixing, i.e. the mixing occur along isopycnals, while in sigma-coordinate models mixing is computed along sigma surfaces. In coastal areas where density is depressed towards the coast, e.g. through downwelling, the isopycnals can be oriented unaligned with the bathymetry and therefore also the sigma surfaces (see Fig. 3). This leads to spurious diapycnal mixing (as opposed to the dominating isopycnal mixing). In two of the model experiments in this thesis (paper III and IV), the mixing is rotated along geopotential surfaces to reduce the diapycnal mixing. This has been found to substantially reduce the diapycnal mixing (Marchesiello et al. 2009). However, some diapycnal mixing occurs naturally through wind and tidal mixing in shelf areas such as the Barents Sea.

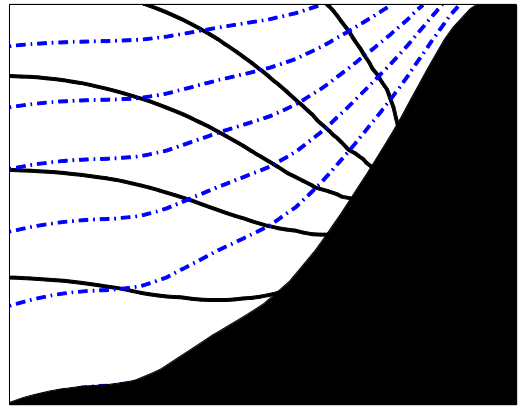

Figure 3: *Schematic of nearshore downwelling, making the isopycnals (black lines) unaligned with the sigma-layers (blue, broken lines).*

As a default, ROMS uses a third order biased upwind scheme for advection of tracers. This scheme has some numerical diffusion, and therefore no explicit diffusion is applied to the advection of tracers. One of the benefits of using this scheme, is that we avoid issues with over- and undershooting. In the high-resolution model study of the BSPF (paper III), however, we have applied a fourth order centered scheme for the advection of tracers. The motivation behind this was to reduce the spurious numerical diffusion in order to better retain strong gradients in the frontal areas. In addition, a

new version of the vertical coordinate was applied (Shchepetkin & McWilliams 2005), in which the vertical layers above a prescribed depth (here set to 30 m, which should be close to the pycnocline depth in summer) are close to level. This reduces the spurious diapycnal mixing in the upper ocean, which has the potential to cause problems in ice-covered areas, as it may artificially transfer heat from a warmer subsurface layer to an ice-covered surface.

In the model runs presented in papers I, III, and IV, the atmospheric forcing applied have a low horizontal resolution compared to the model grids. As the horizontal resolution in model studies improve, this will increasingly become a limitation, as the atmospheric forcing will be smooth and without strong horizontal gradients compared to the modeled ocean. Also, in areas with sparsely distributed observation points, the error of the atmospheric reanalysis will increase. This is especially the case in high latitudes, where observations are very limited.

All numerical ocean models, except global simulations, need input on the lateral open boundaries. This requires a proper treatment of the information crossing the open boundaries. A nudging and radiation scheme proposed by Marchesiello et al. (2001) were used for the three-dimensional velocity components and tracers in papers III and IV. The nudging was applied as a cosine function covering the 10 outer cells. In paper I, a Flow Relaxation Scheme (FRS; Engedahl (1995)) was applied at the open boundaries. In all model studies in this thesis (paper I, III and IV) Flather (1976) open boundary conditions were used for barotropic normal velocity components, while Chapman (1985) open boundary conditions were used for free surface.

Generic-length-scale mixing scheme (Warner et al. 2005a) was chosen as vertical turbulent mixing closure of both momentum and tracers in the model studies in papers I and III. The scheme is a modified form of the Mellor-Yamada 2.5 closure (Mellor & Yamada 1982). The GLS-scheme has been found to produce good results in shallow areas where tidal mixing is important (Warner & Geyer 2005b), and is therefore regarded as a suitable option in the Barents Sea. In the basin scale model applied in the climate downscaling experiment presented in paper IV, the LMD (Large-McWilliams-Doney) mixing scheme was applied. This scheme has been shown to produce a good agreement with observed mixed layer behaviour and the effects of langmuir circulation are well represented through empirical parameterizations (Large & Gent 1999).

Tidal velocities and free surface height from 8 tidal constituents from the Arctic Ocean Tidal Inverse Model (AOTIM; Padman & Erofeeva (2004)) were included, and the tidal elevation and velocities were added to the free surface and barotropic velocity open boundary conditions, respectively.

2.2.4 Validation and evaluation of numerical models

An OGCM is a complicated, highly non-linear set of partial differential equations. Therefore, estimating the model uncertainties through conventional statistical methods is not feasible, since the model includes a wide range of variables with non-linear inter-dependencies. Further, the chaotic nature of some physical processes means that a model realisation becomes just one out of many possible outcomes. Therefore, a thorough and robust validation of the model is needed in order to assess the quality of the model results. By *thorough* is meant an extensive evaluation of the model's performance, and *robust* is to be understood as parameters with a high signal-to-noise ratio and tests that represent challenges for the model. The relationship between observations and models may be viewed as an analogue to the need for calibration when taking measurements with various instruments. Thus, numerical models are still dependent on observations to keep control of the model's deviation from reality. Yet, any OGCM is dependent on vertical and/or lateral boundary conditions, as well as atmospheric forcing, which themselves contain sources of error and uncertainties. Thus, even with a "perfect" model, it would still be impossible to produce "perfect" results.

3 This study

3.1 Objectives

The main objectives of this study are summarized as follows. There has, however, been some changes to these objectives during the course of the study.

- **Quantify the exchanges between the Barents Sea and the Arctic Ocean**

The main goal of this thesis has been to improve our knowledge of the exchanges between the Barents Sea and the Arctic Ocean, with respect to water masses and fluxes. To accomplish this, an existing data set of CTD-measurements (Conductivity-Temperature-Depth) and a one-year record of current meter measurements (Loeng et al. 1993); (Schauer et al. 2002a) was combined with results from two numerical ocean models (paper I). In addition, an extensive array of CTD-measurements was carried out, along with an array of five oceanographic moorings, carrying a total of 13 instruments measuring current, temperature, salinity, and pressure. Unfortunately, at the time of writing, the data from the moored instruments have not yet, 21 months after successful recovery, been made available by Russian authorities due to security inspections. But an analysis of the water masses based on the CTD-measurements have been carried out (paper II).

- **Investigate the variability of the Barents Sea Polar Front by utilizing a high-resolution numerical ocean model**

As part of the International Polar Year, an extensive measuring program was carried out in the Polar Front region in summer 2007 and spring 2008. The objective of paper III was to use observations to evaluate the numerical ocean model, and combine the different datasets in a study of the structure and variability of the BSPF.

- **Assess the improvement by using a regional ocean model to downscale the results from a global climate model**

The objective of paper IV was put forward to get papers I, II, and III into a larger context. The regional climate plays an important role for the local processes in the Barents Sea, which in turn provide feedback to the regional and subsequently the global climate. Improving the quality of climate scenarios are therefore of great importance in order to understand how the Barents Sea may be affected by climate change.

3.2 Summary of papers

Numerical models are powerful tools capable of providing new insights in a wide range of spatial and temporal scales, from local processes to climate variability. A huge advantage of models over observations is that models provide data in 4-D, while observations below the sea surface often consist of measurements that are one-dimensional in space and taken at a single time (e.g. CTD), or measurements at a single point over a period of time (e.g. current meter). In paper I, we have utilized both observations and models to investigate the exchanges of volume, heat, and salt between the Barents Sea and the Arctic Ocean through the strait between Novaya Zemlya and Franz Josef Land. A good agreement between observations and the models was found, and both showed that the heat flux from the Barents Sea to the Arctic Ocean is small, and it cannot be ruled out that the Barents Sea acts as a heat sink rather than a heat source for the Arctic Ocean. Thus, the major part of the $\sim$50 TW of heat carried by the NwAC into the Barents Sea in the west (Skagseth et al. 2008), is given up to the atmosphere before the remains of the AW exits the Barents Sea in the northeast. Although there was a good agreement between the observations and the models in paper I, the models indicated that the current meter moorings were not placed at optimal locations. We therefore propose that models could be used for optimizing the geographical locations of oceanographic mooring arrays.

After estimating the fluxes of volume, heat, and salt between the Barents Sea and the Arctic Ocean, we turned our focus (paper II) to investigate the water masses and how they are transformed into the water masses that are observed downstream at the Arctic Ocean continental slope (Schauer et al. 2002b); (Dmitrenko et al. 2009a). Based

on a total of 142 CTD-measurements from the very sparsely sampled St. Anna Trough, we found evidence of two water masses of Atlantic origin within the St. Anna Trough. A cold ($\Theta < 1$) and saline ($S > 34.9$) mode of AW was found in the southern parts of the trough, while a warmer ($\Theta \sim 1$) and less saline ($S \sim 34.8$) mode of AW was found in the western and northern parts. The warmer AW is a branch of the FSBW that enters the St. Anna Trough from the north, and is documented in the literature (Hanzlick & Aagaard 1980); (Loeng et al. 1993); (Schauer et al. 2002a,b); (paper I). The colder AW has earlier been reported as Cold Bottom Water (CBW), defined by $\Theta < 0$ (paper I), but in 2008 it was observed to exhibit temperatures well above 0 °C. We attributed this to interannual variability, and pointed at differences in heat loss patterns between the years 1991 and 2008 (paper II), along with interannual variability in the water mass characteristics in the inflowing water masses in the western Barents Sea (Skagseth et al. 2008). The presence of water masses with a density sufficient to penetrate to at least 2000 m depth in the Arctic Ocean (paper II), shows that the Barents Sea contributes to the ventilation of the deep water masses in the Arctic Ocean even though the Barents Sea is currently in a warm climatic phase (Levitus et al. 2009).

In paper III, we shifted our focus to the BSPF in the western Barents Sea. A high-resolution numerical ocean model was set up to study the seasonal variability of the front, and its linkages to the seasonal sea-ice cover. The model results showed that the position of the front is determined by a topographically steered warm core jet, that carries AW along the Svalbardbanken slope with the shallow water on its right side (retrograde). Although the jet is variable in strength, its spatial variability is small, and the front is more or less locked to the barhymetry through the year, with some variations along the flank of Svalbardbanken.

The seasonal stratification of the water column plays a critical role in the spring-bloom system in the Barents Sea (Sakshaug et al. 2009). Two mechanisms contribute to this stratification in the MIZ by reducing the density of the surface mixed layer: *i)* Freshwater input from sea-ice melt reduces the salinity, and *ii)* solar insolation increases the temperature in the surface mixed layer (Loeng 1991). However, the model results in paper III points to a third, more local process, where the water column is stratified due to advection of dense bottom water along the slope of Svalbardbanken. At the shallow parts of the slope, the bottom layer of cold, brine-enriched water may be sufficient to provide a stratification shallow enough to support the onset of an algal bloom. At one model station, advection of dense bottom water made the conditions favorable for primary production one month earlier than the preceeding year, when no dense bottom water was advected past the station.

According to the International Panel on Climate Change (IPCC), it is very likely that the earth will experience warming within the next hundred years, due to a human induced increase in the atmospheric levels of CO_2. It is also projected that higher latitudes will experience amplified warming compared to the rest of the globe (IPCC-

WG-I/10 2007). This calls for a regional assessment of the climate change impacts in the Barents Sea, because a large change in the physical environment will affect the marine ecosystems (Drinkwater et al. 2010), and provide feedback to the global climate system. In papers I and II we addressed the contribution from the Barents Sea to the ventilation of deep water in the Arctic Ocean, and thereby also the global thermohaline circulation. In paper II, we also addressed some of the important processes which transform warm and saline AW into cold and dense deep water. Local processes important for the biological productivity in the vicinity of the Barents Sea Polar Front were studied in paper III. To assess the impacts from climate change on all of these processes, global climate projections need to be downscaled to an adequate resolution.

To assess the value of performing a downscaling, we used a regional model forced by the output from a global climate model to run a 20 year hindcast (paper IV). The output from the regional model were compared with the results from the global model as well as available observations. The intercomparison revealed a substantial improvement of the model results. Most importantly, the too weak heatflux into the Barents Sea in the global model (16 TW) was increased to realistic values in the regional model (46 TW), compared to observations (48 TW; Skagseth et al. (2008)). The increase in heat transport was due to an increase in both the volume flux and the temperature. The unrealistically low inflow of AW to the Barents Sea caused an excessive ice extent in the global model. This is reported to be a common problem of global climate models (Arzel et al. 2006); (Overland & Wang 2007). From this, another problem that needs attention arises. With the excessive ice cover present in the global model, the overlying atmosphere will also be too cold. When this atmosphere is used to force the regional model, the heat loss from the open ocean to the atmosphere will be far too high, which results in excessive cooling in the regional model. Nevertheless, the improvement of the performed downscaling is encouraging, and shows that the effort is worthwile and should be pursued in the assessment of future climate change in the Barents Sea region.

3.3 Main conclusions

- The heat flux from the Barents Sea to the Arctic Ocean is small, and it cannot be ruled out that the Barents Sea may act as a heat sink rather than a heat source for the Arctic Ocean

- Water masses dense enough to ventilate the deeper layers of the Arctic Ocean are formed in the northeastern Barents Sea, although the Barents Sea is currently in a warm climatic phase

- Advection of dense, brine-enriched bottom water along the Svalbardbanken slope may cause the onset of the spring-bloom to locally be shifted up to one month in time

- Downscaling global climate model results by applying a regional model significantly improves the model output. This gives hope that global climate projections can be used for regional assessment of climate change impacts

3.4 Future perspectives

The northeastern Barents Sea and the St. Anna Trough are sadly undersampled, and although the data presented in papers I and II have improved our knowledge about the water masses and water mass transformations in this area, an increase in sampling frequency is badly needed. A regular monitoring by the use of conventional techniques such as CTD-measurements and moored current meter arrays, will provide a giant leap towards closing the budgets of volume, salt, and heat for the Barents Sea. Also, regularly updated time series will improve our knowledge of the variability of key parameters on shorter (seasonal to annual) and longer (interannual to decadal) time scales. High-resolution models, together with strategically placed moorings containing high-resolution ADCP (Acoustic Doppler Current Profiler) and temperature and conductivity sensors should be utilized to investigate the outflow of dense bottom water into the St. Anna Trough. This will require increased efforts of bi-lateral cooperation between Norway and Russia, which is a prerequisite for an integrated monitoring of the Barents Sea-Arctic Ocean exchanges.

References

Aagaard, K., Coachman, L. K. & Carmack, E. C. (1981), 'On the halocline of the Arctic Ocean', *Deep-Sea Res. Part A* **28**, 529–545.

Aagaard, K., Foldvik, A. & Hillman, S. R. (1987), 'The west spitsbergen current: Disposition and water mass transformation', *J. Geophys. Res.* **92**, 3778–3784.

Aagaard, K., Swift, J. H. & Carmack, E. C. (1985), 'Thermohaline circulation in the Arctic Mediterranean Seas', *J. Geophys. Res.* **90**, 4833–4846.

Ådlandsvik, B. & Loeng, H. (1991), 'A study of the climatic system in the Barents Sea', *Polar Res.* **10(1)**, 45–49.

Arzel, O., Fichefet, T. & Goosse, H. (2006), 'Sea ice evolution over the 20th and 21st centuries as simulated by current AOGCMs', *Ocean Model.* **12**, 401–415.

Barnier, B., Marchesiello, P., de Miranda, A., Molines, J. & Coulibaly, M. (1998), 'A sigma-coordinate primitive equation model for studying the circulation in the South Atlantic. Part I: model configuration with error estimates', *Deep-Sea Res. I* **45**, 543–572.

Beckmann, A. & Haidvogel, D. B. (1993), 'Numerical simulation of flow around a tall isolated seamount. Part I: Problem formualtion and model accuracy', *J. Phys. Oceanogr.* **23**, 1736–1753.

Blindheim, J. (1989), 'Cascading of Barents Sea bottom water into the Norwegian Sea', *ICES/CIEM* **188**, 49–58.

Budgell, W. P. (2005), 'Numerical simulation of ice-ocean variability in the Barents Sea region; Towards dynamical downscaling', *Ocean Dynamics* **55**, 370–387.

Chapman, D. C. (1985), 'Numerical treatment of cross-shelf open boundaries in a barotropic coastal ocean model', *J. Phys. Oceanogr.* **15**, 1060–1075.

Dmitrenko, I. A., Bauch, D., Kirillov, S. A., Koldunov, N., Minnett, P. J., Ivanov, V. V., Höleman, J. A. & Timokhov, L. A. (2009a), 'Barents Sea upstream events impact the properties of Atlantic water inflow into the Arctic Ocean: Evidence from 2005 to 2006 downstream observations', *Deep Sea Res. I* **56**, 513–527.

Dmitrenko, I. A., Polyakov, I. V., Kirillov, S. A., Timokhov, L. A., Frolov, I. E., Sokolov, V. T., Simmons, H. L., Ivanov, V. V. & Walsh, D. (2008a), 'Toward a warmer Arctic Ocean: Spreading of the early 21st century Atlantic Water warm anomaly along the Eurasian Basin margins', *J. Geophys. Res.* **113**, C05023.

Drinkwater, K., Beugrand, G., Kaeriyama, M., Kim, S., Ottersen, G., Perry, I., Pörtner, H.-O., Polovina, J. & Takasuka, A. (2010), 'On the processes linking climate to ecosystem changes', *J. Mar. Sys.* **79**, 374–388.

Engedahl, H. (1995), 'Use of the flow relaxation scheme in a three-dimensional baroclinic ocean model with realistic topography', *Tellus* **47A**, 365–382.

Falk Petersen, S., Hop, H., Budgell, W. P., Hegseth, E. N., Korsnes, R., Løyning, T. B., Ørbæk, J. B., Kawamura, T. & Shirasawa, K. (2000), 'Physical and ecological processes in the marginal ice-zone of the northern Barents Sea during the summer melt period', *J. Mar. Sys.* **27**, 131–159.

Fer, I. & Ådlandsvik, B. (2008), 'Descent and mixing of the overflow plume from Storfjord in Svalbard: an idealized numerical model study', *Ocean Sci.* **4**, 115–132.

Flather, R. A. (1976), 'A tidal model of the northwest European continental shelf', *Mem. Soc. Roy. Sci. Liege* **6(10)**, 141–164.

Gawarkiewicz, G. & Plueddemann, A. (1995), 'Topographic control of thermohaline frontal structure in the Barents Sea Polar Front on the south flank of Spitsbergen Bank', *J. Geophys. Res.* **100**, 4509–4524.

Geyer, F., Fer, I. & Eldevik, T. (2009), 'Dense overflow from an Arctic fjord: Mean seasonal cycle, variability and wind influence', *Cont. Shelf Res.* **29**, 2110–2121.

Haidvogel, D. B., Arango, H., Budgell, W. P., Cornuelle, B. D., Curchitser, E., Di Lorenzo, E., Fennel, K., Geyer, W. R., Hermann, A. J., Lanerolle, L., Levin, J., McWilliams, J. C., Miller, A. J., Moore, A. M., Powell, T. M., Shchepetkin, A. F., Sherwood, C. R., Signell, R. P., Warner, J. C. & Wilkin, J. (2008), 'Ocean forecasting in terrain-following coordinates: Formulation and skill assessment of the Regional Ocean Modeling System', *J. Comput. Phys.* **227(7)**, 3595–3624.

Haidvogel, D. B. & Beckmann, A. (1999), *Numerical ocean circulation modeling*, Imperial College Press. ISBN 1-86094-114-1.

Häkkinen, S. & Mellor, G. L. (1992), 'Modelling the seasonal variability of a coupled arctic ice-ocean system', *J. Geophys. Res.* **97**, 20285–20304.

Haney, R. L. (1991), 'On the Pressure Gradient Force over Steep Topography in Sigma Coordinate Ocean Models', *J. Phys. Oceanogr.* **21**, 610–619.

Hansen, B. & Østerhus, S. (2007), 'Faroe Bank Channel overflow 1995-2005', *Prog. Oceanogr.* **75**, 817–856.

Hanzlick, D. & Aagaard, K. (1980), 'Freshwater and Atlantic Water in the Kara Sea', *J. Geophys. Res.* **85(C9)**, 4937–4942.

Harms, I. H., Schrum, C. & Hatten, K. (2005), 'Numerical sensitivity studies on the variability of climate-relevant processes in the barents sea', *J. Geophys. Res.* **110**, C06002.

Helland-Hansen, B. & Nansen, F. (1909), 'The Norwegian Sea: Its Physical Oceanography based upon the Norwegian Research 1900-1904, Part 1, No. 2', *Fiskeridir. Skr. Ser. Havunders.* **3**, 390pp.

Hunke, E. (2001), 'Viscous-plastic sea ice dynamics with the evp model: linearization issues', *J. Comput. Phys.* **170**, 18–38.

Hunke, E. & Dukowicz, J. (1997), 'An elastic-viscous-plastic model for sea ice dynamics', *J. Phys. Oceanogr.* **27**, 1849–1867.

Ingvaldsen, R. (2005), 'Width of the North Cape Current and location of the Polar Front in the western Barents Sea', *Geophys. Res. Lett.* **32**, L16603.

Ingvaldsen, R., Asplin, L. & Loeng, H. (2004b), 'The seasonal cycle in the Atlantic transport to the Barents Sea during the years 1997-2001', *Cont. Shelf Res.* **24**, 1015–1032.

Ingvaldsen, R. B., Loeng, H. & Asplin, L. (2002), 'Variability in the Atlantic inflow to the Barents Sea based on a one-year time series from moored current meters', *Cont. Shelf Res.* **22**, 505–519.

Ingvaldsen, R., Loeng, H., Ottersen, G. & Ådlandsvik, B. (2003), 'Climate variability in the Barents Sea during the 20th century with a focus on the 1990s', *ICES Mar. Sci. Sym.* **219**, 160–168.

IPCC-WG-I/10, Meehl, G., Stocker, T., Collins, W., Friedlingstein, P., Gaye, A., Gregory, J., Kitoh, A., Knutti, R., Murphy, J., Noda, A., Raper, S., Watterson, I., Weaver, A. & Zhao, Z.-C. (2007), 'Global Climate Projections', *In: Solomon, S., Qin, D., Manning, M., Chen, Z., Marquis, M., Averyt, G.B., Tignor, M. and Miller, H.L. (eds) Climate change 2007: the physical science basis. Contribution of working group I to the fourth assessment report of the intergovernmental panel on climate change. Cambridge University Press, Cambridge* .

IPCC-WG-I/8, Randall, D., Wood, R., Bony, S., Colman, R., Fichefet, T., Fyfe, J., Kattsov, V., Pitman, A., Shukla, J., Srinivasan, J., Stouffer, R., Sumi, A. & Taylor, K. (2007), 'Climate models and their evaluation', *In: Solomon, S., Qin, D., Manning, M., Chen, Z., Marquis, M., Averyt, G.B., Tignor, M. and Miller, H.L.*

(eds) Climate change 2007: the physical science basis. Contribution of working group I to the fourth assessment report of the intergovernmental panel on climate change. Cambridge University Press, Cambridge .

Johannessen, O. M. & Foster, L. A. (1978), 'A Note on the Topographically Controlled Oceanic Polar Front in the Barents Sea', *J. Geophys. Res.* **83**, 4567–4571.

Jones, E. P., Rudels, B. & Anderson, L. G. (1995), 'Deep waters of the Arctic Ocean: origins and circulation', *Deep-Sea Res. I* **42(5)**, 737–760.

Kärcher, M., Kulakov, M., Pivovarov, U., Schauer, U., Kauker, F. & Schlitzer, R. (2003b), 'Atlantic water flow to the kara sea: Comparing model results with observations', *Proceedings in Marine Science; In: Siberian River Run-off in the Kara Sea: Characterisation, Quantification, Variability and Environmental Significance [Stein, R., K. Fahl, D.K. Fütterer and E. Galimov (Eds.)]* pp. 47–69.

Knipowitsch, N. (1905), 'Hydrologische Untersuchungen im Europäischen Eismeer', *Ann. Hydro. Mar. Met.* **33**, 241–260.

Large, W. & Gent, P. (1999), 'Validation of vertical mixing in an equatorial ocean model using large eddy simulations with observations', *J. Phys. Oceanogr.* **29**, 449–464.

Levitus, S., Matishov, G., Seidov, D. & Smolyar, I. (2009), 'Barents Sea multidecadal variability', *Geophys. Res. Lett.* **36**, L19604.

Loeng, H. (1991), 'Features of the physical oceanographic conditions of the Barents Sea', *Polar Res.* **10(1)**, 5–18.

Loeng, H., Ozhigin, V., Ådlandsvik, B. & Sagen, H. (1993), 'Current measurements in the northeastern Barents Sea', *ICES CM* **40**, 22pp.

Macrander, A., Send, U., Valdimarsson, H., Jnsson, S. & Kase, R. H. (2005), 'Interannual changes in the overflow from the Nordic Seas into the Atlantic Ocean through Denmark Strait', *Geophys. Res. Lett.* **32**.

Marchesiello, P., Debreu, L. & Couvelard, X. (2009), 'Spurious diapycnal mixing in terrain-following coordinate models: The problem and a solution', *Ocean Modell.* **26**, 156–169.

Marchesiello, P., McWilliams, J. C. & Shchepetkin, A. F. (2001), 'Open boundary conditions for long-term integration of regional ocean models', *Ocean Modell.* **3**, 1–20.

Maslowski, W., Marble, D., Walczowski, W., Schauer, U., Clement, J. L. & Semtner, A. J. (2004), 'On climatological mass, heat and salt transports through the Barents Sea and Fram Strait from a pan-Arctic couples sea-ice model simulation', *J. Geophys. Res.* **109(C03032)**.

Matishov, G. G., Matishov, D. G. & Moiseev, D. V. (2009), 'Inflow of atlantic-origin waters to the barents sea along glacial troughs', *Oceanologia* **51**, 321–340.

Mellor, G. L., Ezer, T. & Oey, L.-Y. (1994), 'The pressure gradient conundrum of sigma coordinate ocean models', *J. Atmos. Oceanic Technol.* **11**, 1126–1134.

Mellor, G. L. & Kantha, L. (1989), 'An ice-ocean coupled model', *J. Geophys. Res.* **94**, 10937–10954.

Mellor, G. L. & Yamada, T. (1982), 'Developement of a turbulence closure-model for geophysical fluid problems', *Rev. Geophys.* **10(4)**, 851–875.

Mesinger, F. (1982), 'On the convergence and error problems of the calculation of the pressure gradient force in sigma coordinate models', *Geophys. Astrophys. Fluid Dyn.* **19**, 105–117.

Midttun, L. (1985), 'Formation of dense bottom water in the barents sea', *Deep-Sea Res. A* **32**, 1233–1241.

Midttun, L. & Loeng, H. (1987), 'Climatic variations in the Barents Sea. In: H. Loeng (ed) The effect of oceanographic conditions on the distribution and population dynamics of commercial fish stocks in the Barents Sea, Third Soviet-Norwegian symposium. Murmansk', pp. 13–28.

Mosby, H. (1938), 'Svalbard Waters', *Geofysiske publikasjoner* **12(4)**, 1–85.

Nansen, F. (1906), 'Northern waters: Captain roald amundsens oceanographic observations in the arctic seas in 1901', *Vitenskabs-Selskapets Skrifter* **1**, 145pp.

Novitsky, V. P. (1961), 'Permanent currents of the northern barents sea', *Trudy Gosudarstvennogo Okeanograficheskogo Instituda, Translated by U.S.N.O. 1967, Leningrad* **64**, 1–32.

Orvik, K. A. & Skagseth, Ø. (2005), 'Heat flux variations in the eastern Norwegian Atlantic Current toward the Arctic from moored instruments, 1995-2005', *Geophys. Res. Lett.* **32**.

Overland, J. & Wang, M. (2007), 'Future regional Arctic sea ice declines', *Geophys. Res. Lett.* **34**, L17705.

Padman, L. & Erofeeva, S. (2004), 'A barotropic inverse tidal model for the Arctic Ocean', *Geophys. Res. Lett.* **31**.

Parsons, A., Bourke, R., Muench, R., Chiu, C.-S., Lynch, J., Miller, J., Plueddemann, A. & Pawlowicz, R. (1996), 'The Barents Sea Polar Front in summer', *J. Geophys. Res.* **101**, 14201–14221.

Pfirman, S. L., Bauch, D. & Gammelsrød, T. (1994), 'The Northern Barents Sea: water mass dirstribution and modification. In: Johannessen, O.M., Muench, R.D., Overland, J.E. (Eds.), The Polar Oceans and Their Role in Shaping the Global Environment: The Nansen Centennial Volume', *Geophysical Monograph* **85**, 77–94.

Polyakov, I., Beszczynska, A., Carmack, E., Dmitrenko, I., Fahrbach, E., Frolov, I., Gerdes, R., Hansen, E., Holfort, J., Ivanov, V., Johnson, M., Kärcher, M., Kauker, F., Morison, J., Orvik, K., Schauer, U., Simmons, H., Skagseth, Ø., Sokolov, V., Steele, M., Timokhov, L., Walsh, D. & Walsh, J. (2005), 'One more step toward a warmer Arctic', *Geophys. Res. Lett.* **32(17)**, L17605.

Quadfasel, D., Rudels, B. & Selchow, S. (1992), 'The Central Bank vortex in the Barents Sea: Water mass transformation and circulation', *ICES Mar. Sci. Symp.* **195**, 40–51.

Quadfasel, D., Sy, A., Wells, D. & Tunik, A. (1991), 'Warming in the Arctic', *Nature* **350**.

Reigstad, M., Wassmann, P., Wexels Riser, C., S., Ø. & Rey, F. (2002), 'Variations in hydrography, nutrients and chlorophyll *a* in the marginal ice-zone and the central Barents Sea', *J. Mar. Sys.* **38**, 9–29.

Rudels, B., Jones, E. P., Anderson, L. G. & Kattner, G. (1994), 'On the intermediate depth waters of the Arctic Ocean. In: Johannessen, O.M., Muench, R.D., Overland, J.E. (Eds.), The Polar Oceans and Their Role in Shaping the Global Environment: The Nansen Centennial Volume', *Geophysical Monograph* **85**, 33–46.

Rudels, B., Muench, R. D., Gunn, J., Schauer, U. & Friedrich, H. J. (2000a), 'Evolution of the Arctic Ocean boundary current north of the Siberian shelves', *J. Mar. Sys.* **25**, 77–99.

Sætre, R. & Ljøen, R. (1971), 'The Norwegian Coastal Current. In: ANON (ed) Proceeding of the first international Conference on Port and Ocean Engeneering under Arctic Conditions, Vol II. Norwegian Institute of Technology, Trondheim', pp. 514–535.

Sakshaug, E., Bjørge, A., Gulliksen, B., Loeng, H. & Mehlum, F. (1994), 'Structure, biomass distribution and energetics of the pelagic ecosystem in the Barents Sea - A synopsis', *Polar Biology* **14(6)**, 405–411.

Sakshaug, E., Johnsen, G. & Kovacs, K. (2009), *Ecosystem Barents Sea*, Tapir Academic Press. ISBN 978-82-519-2461-0.

Schauer, U. & Fahrbach, E. (1999), 'A dense bottom water plume in the western Barents Sea: Downstream modification and interannual variability', *Deep-Sea Res.* **46**, 2095–2108.

Schauer, U., Fahrbach, E., Østerhus, S. & Rohardt, G. (2004), 'Arctic warming through the Fram Strait: Oceanic heat transport from 3 years of measurements', *J. Geophys. Res.* **109**, 14.

Schauer, U., Loeng, H., Rudels, B., Ozhigin, V. K. & Dieck, W. (2002a), 'Atlantic Water flow through the Barents and Kara Seas', *Deep-Sea Res. I* **49**, 2281–2298.

Schauer, U., Muench, R. D., Rudels, B. & Timokhov, L. (1997), 'Impact of eastern arctic shelf water on the nansen basin intermediate layers', *J. Geophys. Res.* **102**, 3371–3382.

Schauer, U., Rudels, B., Jones, E. P., Anderson, L. G., Muench, R. D., Bjørk, G., Swift, J. H., Ivanov, V. & Larsson, A.-M. (2002b), 'Confluence and redistribution of Atlantic water in the Nansen, Amundsen and Makarov basins', *Ann. Geophys.* **20**, 257–273.

Shapiro, R. (1970), 'Smoothing, filtering and boundary effects', *Rev. Geophys. Space Res.* **8**, 359–387.

Shchepetkin, A. F. & McWilliams, J. C. (2003), 'A method for computing horizontal pressure-gradient force in an oceanic model with a nonaligned vertical coordinate', *J. Geophys. Res.* **108**.

Shchepetkin, A. F. & McWilliams, J. C. (2005), 'The Regional Ocean Modeling System (ROMS): A split-explicit, free-surface, topography-following coordinates ocean model', *Ocean Modell.* **9**, 347–404.

Skagseth, Ø., Furevik, T., Ingvaldsen, R., Loeng, H., Mork, K. A., Orvik, K. A. & Ozhigin, V. (2008), 'Volume and heat transports to the Arctic via the Norwegian and Barents Seas', *In: 'Arctic-Subarctic' Ocean fluxes. In: Dickson, R., Meincke, J., Rhines, P. (Eds), Defining the role of the Northern Seas in Climate. Sringer, Netherlands* .

Skogseth, R., Sandvik, A. & Asplin, L. (2007), 'Wind and tidal forcing on the ineso-scale circulation in Storfjorden, Svalbard', *Cont. Shelf Res.* **27**, 208–227.

Skogseth, R., Smedsrud, L., Nilsen, F. & Fer, I. (2008), 'Observations of hydrography and downflow of brine-enriched shelf water in the Storfjorden polynya, Svalbard', *J. Geophys. Res.* **113**, C08049.

Slagstad, D., Støle-Hansen, K. & Loeng, H. (1989), 'Density-driven currents in the Barents Sea calculated by a numerical model', *ICES Paper CM* **1989/C:20**, 14 pp.

Steele, M., Morison, J. H. & Curtin, T. B. (1995), 'Halocline water formation in the barents sea', *J. Geophys. Res.* **100**, 881–894.

Støle-Hansen, K. & Slagstad, D. (1991), 'Simulation of currents, ice melting, and vertical mixing in the Barents Sea using a 3-D baroclinic model', *Polar Res.* **10(1)**, 33–44.

Sundfjord, A., Ellingsen, I., Slagstad, D. & Svendsen, H. (2008), 'Vertical mixing in the marginal ice zone of the northern Barents Sea - Results from numerical model experiments', *Seep-Sea Res. II* **55**, 2154–2168.

Sundfjord, A., Fer, I., Kasajima, Y. & Svendsen, H. (2007), 'Observations of turbulent mixing and hydrography in the marginal ice zone of the Barents Sea', *J. Geophys. Res.* **112**.

Vinje, T. & Kvambekk, Å. (1991), 'Barents sea drift ice characteristics', *Polar Res.* **10(1)**, 59–68.

Warner, J. C. & Geyer, W. R. (2005b), 'Numerical modelling of an estuary: a comprehensive skill assessment', *J. Geophys. Res.* **110**.

Warner, J., Sherwood, C. R., Arango, H. G. & Signell, R. P. (2005a), 'Performance of four turbulence closure methods implemented using generic length scale method', *Ocean Model* **8**, 81–113.

Wassmann, P., Ratkova, T., Andreassen, I., Vernet, M., Pedersen, F. & Rey, F. (1999), 'Spring bloom development in the marginal ice zone and the central Barents Sea', *Mar. Ecol. PZNI* **20**, 321–346.

I

Paper I

T. Gammelsrød, Ø. Leikvin, V. Lien, W.P. Budgell, H. Loeng and W. Maslowski
Mass and heat transports in the NE Barents Sea: Observations and models
Journal of Marine Systems, 75, 56-69, 2009

Journal of Marine Systems 75 (2009) 56–69

Contents lists available at ScienceDirect

Journal of Marine Systems

journal homepage: www.elsevier.com/locate/jmarsys

Mass and heat transports in the NE Barents Sea: Observations and models

Tor Gammelsrød [a,b,*], Øyvind Leikvin [a,b,e], Vidar Lien [c], W. Paul Budgell [c], Harald Loeng [c], Wieslaw Maslowski [d]

[a] Geofysisk Institutt, University of Bergen, 5007 Norway
[b] The University Centre in Svalbard, P.O. Box 156, 9171 Longyearbyen, Norway
[c] Institute of Marine Research, P.O. Box 1870, Nordnes, 5817 Bergen, Norway
[d] Oceanography Department, Naval Postgraduate School, Monterey, California, USA
[e] Akvaplan-niva, Polar Environmental Centre, 9296 Tromsø, Norway

ARTICLE INFO

Article history:
Received 17 March 2008
Received in revised form 17 July 2008
Accepted 21 July 2008
Available online 26 July 2008

Keywords:
Barents Sea
Current measurements
Numerical models
Ocean circulation
Thermohaline circulation
Water masses

ABSTRACT

The strait between Novaya Zemlya and Frans Josef Land, here called the Barents Sea Exit (BSX) is investigated using data obtained from a current-meter array deployed in 1991–1992, and two numerical models (ROMS and NAME). Combining the observations and models the net volume flux towards the Arctic Ocean was estimated to 2.0±0.6 Sv (1 Sv = 10^6 m^3s^{-1}). The observations indicate that about half of this transport consists of dense, Cold Bottom Water, which may penetrate to great depths and contribute to the thermohaline circulation. Both models give quite similar net transport, seasonal variations and spatial current structures, and the discrepancies from the observations were related to the coarse representation of the bottom topography in the models. Also the models indicate that actual deployment did not capture the main in- and outflows through the BSX. A snapshot of the hydrographic structure (CTD section) indicates that both models are good at reproducing the salinity. Nevertheless, they react differently to atmospheric cooling, although the same meteorological forcing was applied. This may be due to the different parameterisation of sea ice and that tides were included in only one of the models (ROMS). Proxies for the heat transport are found to be small at the BSX, and it can not be ruled out that the Barents Sea is a heat sink rather than a heat source for the Arctic Ocean.

1. Introduction

Processes within the Arctic Ocean and the Arctic Mediterranean produce dense water and therefore contribute to the global thermohaline circulation. Cooling and ice formation with subsequent brine release is most effective in polynyas on the vast shallow shelves in the Arctic. The Barents Sea is of particular interest since it is one of the largest shallow shelves adjacent to the Arctic Ocean, and also the deepest shelf with an average depth of about 230 m. Some of the dense water formed here (Midttun, 1985) is observed to contribute to the deep water formation in the Arctic, e.g. Rudels (1987), Quadfasel et al. (1988), Rudels et al. (1994), Schauer et al. (1997) and Schauer et al. (2002).

Observations (e.g. Schauer et al., 2002) and model experiments, (Karcher and Oberhuber, 2002; Maslowski et al., 2004; Budgell, 2005) indicate that most of the locally produced dense water will leave the Barents Sea via the strait between Novaya Zemlya and Frans Josef Land (Fig. 1), here designated as the Barents Sea Exit (BSX). This water continues via St. Anna Trough (Schauer et al., 2002) and enters the Eurasian Basin, where it may sink to more than 1000 m depth (Rudels et al., 1994).

The major influx to the Barents Sea takes place via the strait between Fugløya and Bjørnøya, often called the Barents Sea Opening (BSO). Based on a current-meter array, (Ingvaldsen et al., 2002, 2004), now extended to 10 years (1997–2006) Skagseth et al. (2008), found that the net flow into the Barents Sea was 1.8 Sv. The inflow consisted mainly of warm and saline Atlantic Water (AW). This compares well with the estimate by O'Dwyer et al. (2001) of 1.6 Sv based on hydrography and ADCP sections repeated 13 times in the period 1997–1999.

* Corresponding author. Geofysisk Institutt, University of Bergen, 5007 Norway.
E-mail address: torg@gfi.uib.no (T. Gammelsrød).

0924-7963/$ – see front matter © 2008 Elsevier B.V. All rights reserved.
doi:10.1016/j.jmarsys.2008.07.010

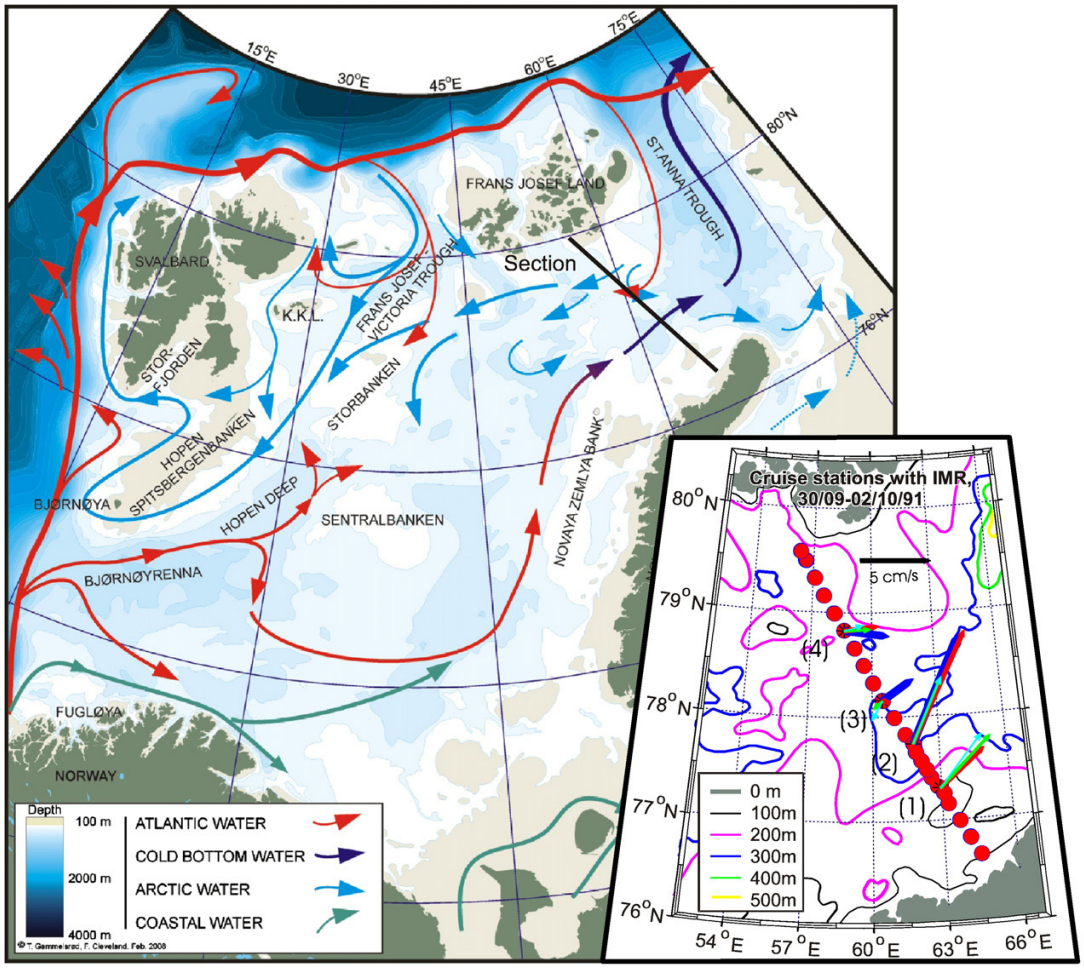

Fig. 1. Barents Sea bottom topography and schematic current system. Inset: Section between Frans Josef Land and Novaya Zemlya. The filled circles denote the 23 CTD-casts during deployment of the current-meter moorings, while the tails of the arrows and the numbers in parenthesis denote the mooring locations (1–4). The arrows represent the mean current vectors with the deepest instrument having the thickest arrow. Dark blue: deepest instrument, Red: 2nd from bottom, Green: 3rd from bottom, Light blue: closest to the surface. Note that at the southernmost station, there are only 3 instruments.

Changes in the oceanographic climate in the Arctic Ocean have been linked to anomalous heat transport in the AW from the Nordic Seas. Furevik (2001), using 16 years of data, discussed the variability of the AW inflow to the Barents Sea and related it to variability in the AW inflow to the Norwegian Sea, changes in the advection speed and interactions with the atmosphere. The variability of the AW flow may in turn be linked to the North Atlantic Oscillation; e.g. Furevik and Nilsen (2005). Two model experiments presented in Drange et al. (2005), and the experiments by Zhang et al. (1998) and Maslowski et al. (2004) indicate that the Norwegian Atlantic Current splits up into two major branches, one entering the Barents Sea via the BSO, while the other continues northwards as the West Spitsbergen Current (WSC). WSC dives below the surface and becomes insulated from direct atmospheric cooling, and is believed to be the larger heat source for the Arctic Ocean of the two branches. On the contrary, in the relatively shallow Barents Sea the AW is effectively modified by cooling and mixing due to wind and tidal currents and gradually looses its heat content on its way to the Arctic Ocean (Pfirman et. al., 1994). This denser, modified water is probably directly contributing to the deep water formation and therefore the thermohaline circulation; see for instance Meincke et al. (1997), Schauer et al. (1997) and Schauer et al. (2002).

The modification of the water masses in the Barents Sea critically depends on the ice cover and polynya activity (Pease, 1987; Martin and Cavalieri, 1989; Ivanov and Shapiro, 2005). In their model experiments Gerdes et al. (2003) demonstrate how an anomalous low heat inflow via the BSO in the 1960's did not produce a similar low signal in the heat flow through the BSX, because the Barents Sea was ice-covered and thus protected from atmospheric cooling. Conversely, a high heat inflow

through the BSO in the 1990's did not result in a strong signal in the BSX, when the ice extent was less. The sea-ice extent, in turn, seems to be connected to the cyclone activity in the East Siberia and south of the Barents Sea (Sorteberg and Kvingedal, 2006). High cyclonic activity in the East Siberia seems to be related to cold winds from the north, stimulating ice growth and transport of ice from the Arctic into the Barents Sea (Kwok et al., 2005). In addition, a high cyclonic activity south of the Barents Sea also supports a large sea-ice extent, because the winds then seem to slow down the inflowing warm AW.

The Barents Sea provides for an important fishing area. It has been shown that a vast year to year variation of the biomass of the different stocks is the rule rather than the exception (Sakshaug et al., 1994). This variability is closely linked to the climatic variability in the Barents Sea, which in particular influences the spring bloom regarding time and intensity (Olsen et al., 2003). Our investigation area is situated downstream of a vast off-shore oil and gas field on the Novaya Zemlya shelf, and the ecosystem in the region is, of course, extremely vulnerable to eventual hazards.

Since the water masses entering the Arctic Ocean via the BSX may contribute to both the global thermohaline circulation and to the melting of the arctic ice cap, it is of particular interest to investigate this area in detail. While the AW inflow through the BSO has been monitored since 1997 (Skagseth et al., 2008), the BSX is sadly under-sampled.

In order to assess the physical oceanography of the area, we seek assistance from both historical data and output from numerical models. The observational data set consists of an array of 4 current-meter moorings deployed for almost 1 year from 1991 to 1992 (Loeng et al., 1993), see Fig. 1 for positions. Also CTD-casts across the strait during deployment and recovery of the moorings were obtained. The same data set was used by Schauer et al. (2002) in a study of the fate of the AW in the Barents and Kara Seas. Here, the water mass characteristics, currents and fluxes through the BSX are discussed. Results from two numerical models: NPS Arctic Modelling Effort (NAME) by Maslowski et al. (2004) and a new experiment based on the Regional Ocean Model System (ROMS) are also presented. Both models were forced with the same atmospheric fields. In the next section we present the data sources and the numerical models. Thereafter, the hydrographical conditions, as well as the spatial and temporal structure of the observed currents in the BSX, are discussed. The volume transport calculations derived from the current-meter array are used for validation of the models, and the simulated current fields are analyzed and discussed to improve our transport estimates. The reasons for the apparent discrepancies between observations and models are commented upon. A proxy for heat transport calculations based on models and observations are compared. The different behaviours of the models are also discussed as well as the role of winds, tides and ice cover. Some conclusions from this study are given in the final summary.

2. Instruments and methods

2.1. Current measurements

An array of four moorings carrying 15 current meters in total, located between 77°19′N, 62°56′E and 78°50′N, 58°39′E (Fig. 1), was deployed on September 24th (mooring 4) and October 1st (mooring 1–3) 1991 and recovered in September 1992. A fifth mooring located further north was not recovered. The mooring array spanned approximately 200 km, with a distance between two adjacent moorings ranging from 60 km in the south to 80 km in the north. Aanderaa RCM-7 current meters were utilised, except at mooring 4 at 180 m depth, where a RCM-4 was used. These current meters use rotors to measure speed. Positions, observation depths and dates of recovery are given in Table 1. For convenience, the current meters are identified using a code where for instance 2c240 is the instrument at the second mooring, instrument no. 3 from the top and situated at 240 m depth. The sampling interval was 20 min for all the instruments, except for 4c180, which was set to one hour intervals.

The RCM registered speed, direction, temperature and conductivity accurate to ±1 cm/s, ±5°, ±0.05 °C and ±0.1 mmho/cm, respectively. The conductivity data showed a negative drift for some of the instruments, which did not match the CTD surveys at deployment and recovery. This obscures the interpretation of the salinity recordings on seasonal and longer time scales. The RCM data were checked,

Table 1
List of the current meters utilised in the analysis

Instrument ID	Depth [m]	Last measurement	*U* [cm/s]	*V* [cm/s]	*Sal*	*Temp* [°C]	Dir [deg]	Speed [cm/s]	St. dev. [cm/s]
1a60	60	09.07.	3.1	3.7	34.66	−1.09	40	4.9	4.5
1b100	100	13.07.	3.7	3.6	34.90	−0.29	46	5.2	4.6
1c144	144	08.09.	3.3	2.8	34.79	−0.20	49	4.3	4.9
2a65	65	25.07.	2.2	4.7	34.52	−1.15	25	5.2	4.6
2b105	105	08.09.	2.1	4.7	34.72	−0.01	24	5.1	5.1
2c240	240	08.09.	4.0	8.0	35.04	−0.36	26	8.9	5.4
2d333	333	06.09.	3.5	7.7	34.90	−0.39	24	8.5	6.1
3a65	65	07.09.	−0.7	−1.4	34.42	−1.50	208	1.5	2.5
3b170	170	07.09.	−0.6	−0.6	34.80	1.12	227	0.9	2.8
3c270	270	07.09.	0.6	−0.0	34.94	0.43	90	0.6	2.3
3d343	343	07.09.	2.2	1.6	34.86	−0.39	55	2.7	4.0
4a75	75	13.08.	1.3	0.4	34.44	−1.57	73	1.4	2.2
4b115	115	19.07.	1.9	0.1	34.52	−1.16	86	1.9	2.4
4c180	180	09.09.	2.4	0.4	–	−0.39	82	2.5	2.1
4d230	230	25.08.	3.2	−0.4	34.87	−0.33	96	3.2	2.8

The observation depths (the lowermost current meters at each mooring were located about 10 m above the seabed), date of last measurements (1992) and average values from the sensors are given. The current meters were deployed September 24th (mooring M4) and October 1st (moorings M1, M2, M3) 1991. For further details, see Schauer et al. (2002).

and obvious erratic points were replaced by interpolation from the same time series. Erratic data, found at the end of the data series due to failure in the rotors, were removed. For transport calculations (see Section 2.3), such missing data periods were reconstructed by extrapolation using instruments located nearby.

To eliminate tidal signals, the data series were filtered using a pl64tap-filter (Rosenfeld, 1983), with a cut-off-period of 33 h. The time series are folded over and cosine tapered at each end to return a filtered, phase preserving time series of the same length. For the purpose of error estimates, the degrees of freedom (M) were determined by the time taken for the autocorrelation function to fall to $1/e$, usually 3 to 5 days. The standard error was obtained by dividing the standard deviations by $\sqrt{M}$. This error was then combined with other sources of error such as choice of area representing each current meter to produce the final error estimates for the transports.

2.2. CTD measurements

A Neil Brown CTD system was used. The accuracy of the temperature sensors is better than 0.005 °C. The conductivity sensor was calibrated using water samples analyzed on a Guideline Portasal salinometer, and the accuracy of the salinity was found to be better than 0.01. The data were averaged over 5 dbar bins.

2.3. Mass transport calculations

To calculate mass transport, a simple objective method was applied; each current meter has been designated an area for mass transport calculation. The division lines were set half-way between the instruments both in the horizontal and vertical plane. The outer moorings were given a horizontal dimension equal to the distance to the neighbouring instrument. In the vertical the water column is naturally limited by the surface and the bottom. As can be observed from Table 1, some of the instruments failed before the recovery 7–9 September 1992. The missing records are reconstructed using the nearest instrument at the same mooring. The least square linear regression was used for calculating the actual values. This method worked for all moorings except mooring 1, where all rotors measuring speed had failed by August 8. Therefore the record 1c144 was prolonged first using the instruments 2b105 and 2c240. Then the procedure described above was used to construct 1b100 and 1a60. Since all current-meter moorings were recovered by September 9th, this month is under-sampled.

2.4. Model experiments

In addition to the current-meter data and CTD sections, we have analyzed data from two different ice-ocean numerical model experiments. Both models were forced with atmospheric fields from the European Centre for Medium Range Weather Forecasting (ECMWF).

2.4.1. The NAME model

This is a pan-Arctic simulation called NAME (Naval Postgraduate School Arctic Modelling Effort), described by Maslowski et al. (2004). The model domain was chosen to include all major out- and inflows to the Arctic Ocean far from the artificial boundaries in the Atlantic and Pacific Oceans. The model boundaries are closed, and an artificial channel through Canada is introduced to balance the net northward transport through the Bering Strait. The model grid size is typically 9 km, and in the vertical there are 45 z-coordinate levels. In the Arctic, the 2.5 km resolution digital bathymetry data set from Jakobsson et al. (2000) is utilised. The model applies a free surface. The ice model uses the plastic ice rheology (Zhang and Hibler, 1997) and the heat conduction through ice following Semtner (1976). The surface heat budget proposed by Parkinson and Washington (1979) is applied. The model was initialized using the temperature and salinity fields from the University of Washington Polar Science Center Hydrographic Climatology (Steele et al., 2001). A 27-year period of spin up was performed using 15-year mean, annual cycle of daily forcing fields (ERA15) from the ECMWF. To approach the initial conditions for the actual 1979–2001 experiment, the model was forced for 20 years using combinations of daily averages for 1979 as well as for the 1979–1981 period. The 23 years run was forced with ERA40. More model details and results of the simulations are given in Maslowski et al. (2004).

2.4.2. The ROMS model

The Regional Ocean Model System (ROMS), see e.g. Shchepetkin and McWilliams (2003), utilises topography following s-coordinates in the vertical that allows for enhanced resolution near the surface and bottom. The ROMS experiment presented here applies the same atmospheric forcing (the ERA40 data set from ECMWF) as in NAME to facilitate the comparisons between the two models. In Budgell (2005) the NCEP (Kalnay et al., 1996) wind stress was applied, otherwise the two model set ups are the same. Surface heat fluxes were calculated with cloud fractions modified using satellite derived data from the International Satellite Cloud Climatology Project (Schiffer and Rossow, 1985). The grid spacing in the Barents Sea corresponds to that of the NAME model, ~9 km resolution in the horizontal, and with 32 layers in the vertical. The model was forced at the boundaries using 5-day mean fields from a regional model covering the North Atlantic, and with tidal velocities and free surface heights from the 8 dominant constituents provided by Padman and Erofeeva (2004). The ice model component is based on the elastic-viscous-plastic rheology, see Hunke (2001). The ice thermodynamics is taken mainly from Häkkinen and Mellor (1992), and uses two ice layers and a snow layer (Mellor and Kantha, 1989). Initial conditions for the Barents Sea model were taken from 5-day averages of the regional model from January 1, 1990. The period 1990–2002 was simulated.

3. Results and discussion

3.1. Observations

3.1.1. Water masses

A T–S diagram obtained from the CTD-casts at the mooring positions during fall 1991 is shown in Fig. 2, where water mass definitions also are indicated. Since these measurements were performed from late September to early October, the Surface Water (SW) is still influenced by summer heating and melting.

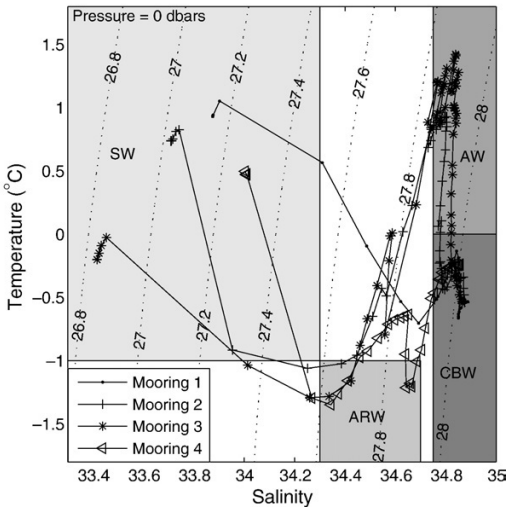

Fig. 2. *T–S* diagram covering the CTD stations (September–October 1991) corresponding to the four moorings deployed between Frans Josef Land and Novaya Zemlya, 1991–1992. The markers are placed at 5 m depth intervals. The major water mass definitions, Arctic Water (ARW), Atlantic Water (AW), Cold Bottom Water (CBW) and Surface Water (SW), are also marked.

Atlantic Water (AW) was observed at moorings 2 and 3, while the moorings in the extreme south and north were more influenced by the Arctic Water (ARW). Cold Bottom Water (CBW) was observed at all 4 locations.

The temperature and salinity time series at mooring 1 are shown in Fig. 3. Here we observe that from the middle of December, the temperature was close to the freezing point for a few months at the uppermost instrument (60 m). Simultaneously, the salinity was gradually increasing, an indication of freezing and brine rejection. However, this signal never penetrated down to the instruments at 100 or 144 m. Thus the process was not strong enough to provoke convection to the bottom. Similar patterns were observed at the other 3 moorings. This does not rule out that dense water may have formed in the polynya west of Novaya Zemlya, cascading through the BSX south of our mooring array (Midttun, 1985; Martin and Cavalieri, 1989; Ivanov and Shapiro, 2005). Weekly ice distribution maps, compiled by Kvingedal (personal communication, 2007) and presented in Fig. 4, illustrate the ice distribution and its variation during March 1992. It seems that a substantial polynya activity took place; early in this month there were large areas with open drift ice, only to disappear in the middle of the March and re-establish as drift ice together with young ice by the end of the month. This indicates that conditions were favourable for surface cooling, ice formation and brine rejection and thus formation of CBW.

3.1.2. Current measurements

The mean observed velocity vectors are plotted on the map in Fig. 1, see also Table 1. The currents show mainly a component towards North-East and East, with the strongest current in the southern and deepest part of the section. Also note that the currents tend to amplify towards the bottom. The maximum average current (9 cm/s) was observed at 240 m depth at mooring 2.

The nature of the time variability is given in Fig. 5, where the de-tided current vectors at 60 m for the southernmost mooring (M1) are shown. There are episodes with high speeds (>25 cm/s) in December, and the currents are rather uni-directional.

The monthly averaged cross-section velocity component (Fig. 6) shows a significant seasonal variability. Compared to the pattern in October, the December pattern seems to be a barotropic increase in the outward current speed of 4–5 cm/s at the two southernmost moorings. The December current structure is associated with the strongest horizontal and vertical shear of the whole year. During summer the currents were weaker. The return flow near mooring M3 was present throughout the year with a maximum in September. Even in December, when the outflow at mooring M2 was the strongest, the counter-current penetrated down to ~200 m depth. The monthly averages for each individual current meter are given in Schauer et al. (2002).

The marked seasonal variations of the current field (Figs. 5 and 6) are believed to be caused by changes in the wind field. The average winter (DJFM) and summer (JJAS) atmospheric circulations are shown in Fig. 7. During winter a low pressure in the central Barents Sea sets up strong winds towards the north in the study area. The corresponding Ekman transport will be towards the east, and water may pile up at the Novaya Zemlya coast giving a high water level there. The corresponding barotropic component of the current structure, see Fig. 6, may be due to the sea level sloping upwards towards Novaya Zemlya.

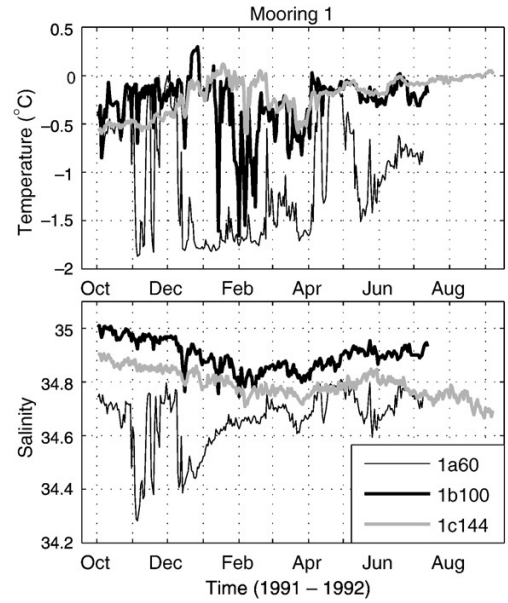

Fig. 3. Daily averaged values of a) temperature and b) salinity at mooring 1. The apparent trend in the salinity data at 144 m depth is obviously due to a drift in the conductivity cell.

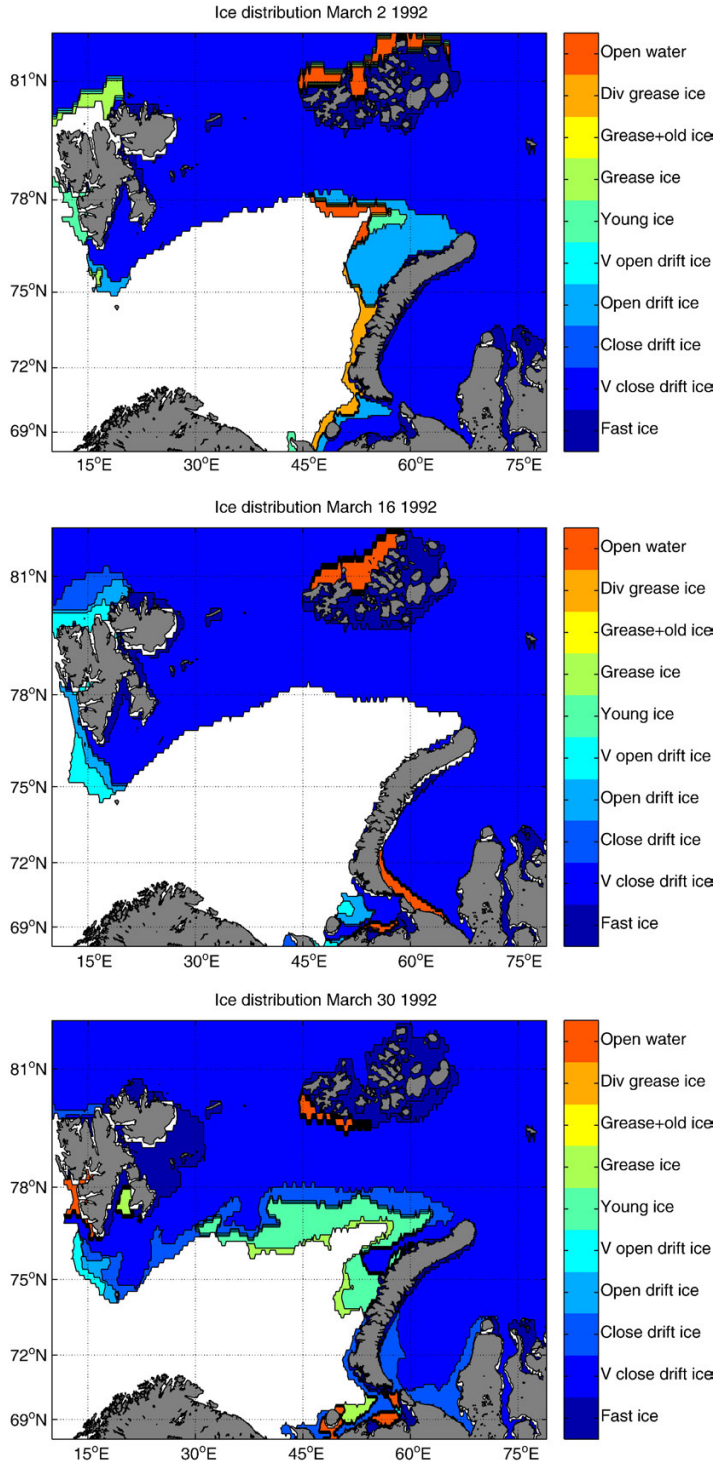

Fig. 4. Ice distribution variability in the Barents Sea, 1992, a) March 2nd, b) March 16th and c) March 30th (Kvingedal, pers. comm., 2007). See also Kvingedal (2005).

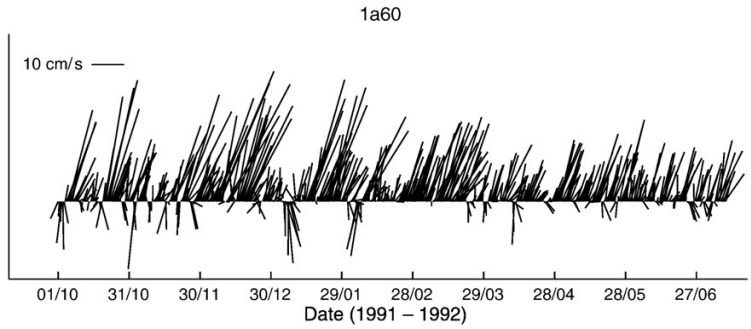

Fig. 5. De-tided time series from instrument 1a60 illustrating current vector stick-plot. One vector every 12th hour is shown.

3.1.3. Volume transports

The daily averages of the volume transports towards the Arctic Ocean (defined as positive), into the Barents Sea and the net transports are given in Fig. 8. As expected from the current structures discussed above, the net transport was mainly towards the Arctic. However, occasionally the flow reversed with amplitudes up to nearly 4 Sv for a few days. The average net transport through the BSX for the whole time series was found to be 1.6±0.5 Sv (Table 2), consistent with the calculations by Loeng et al. (1993) and Schauer et al. (2002).

The monthly averaged volume transports shown in Fig. 9 illustrate that the maximum transport (>3 Sv) occurred in December and the minimum in late summer (<1 Sv). The yearly averaged volume transport was found to be 2.2 Sv out of the Barents Sea with a return flow of 0.6 Sv, see Table 2. The atmospheric pressure difference between Frans Josef Land and Novaya Zemlya (P_{FJL}–P_{NZ}), also shown in Fig. 9, indicates that the maximum net transport coincides with the maximum pressure difference in December. During late summer and fall 1992 the pressure difference is increasing while the observed net transports are decreasing. However, in this period an increasing number of current meters failed, and September is under-sampled (see Table 1).

3.2. Comparison with models

3.2.1. Volume transports

The results from the model transport calculations for the RCM (reduced) section are also shown in Table 2 and Fig. 9. Table 2 shows that yearly averaged net transports are slightly higher for the two models than for the observations, as well as the out- and inflows. Fig. 9 shows that the seasonal signals of the models are smaller than the observed. The observations and the ROMS model showed a maximum transport in

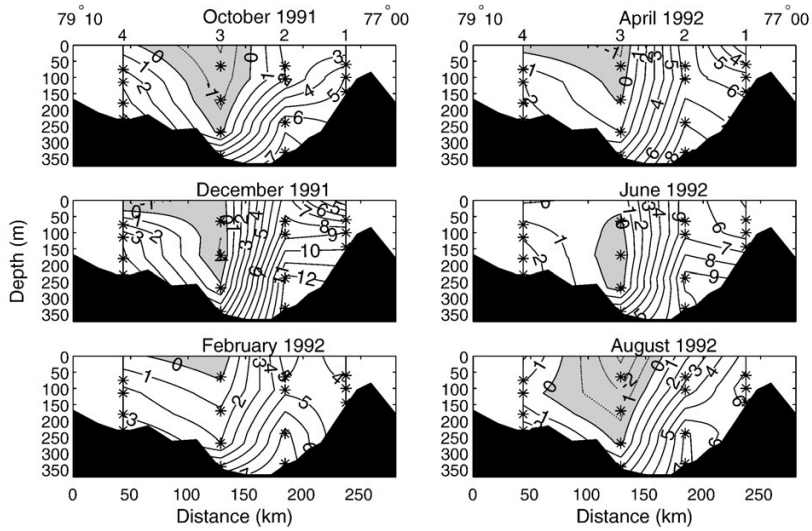

Fig. 6. Monthly averaged velocities (cm/s) perpendicular to the cross-section, interpolated from the current-meter array illustrated by the asterisks. The values for August are partially obtained by interpolation, see section 2.3. Positive values indicate flow towards the northeast, out of the Barents Sea. Negative values are shaded.

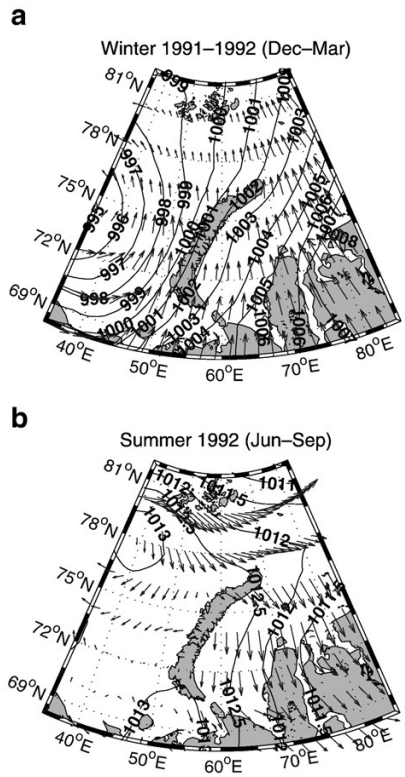

Fig. 7. The average wind during a)winter (December–March) and b)summer (June–September) 1991–1992 plotted together with the mean isobars at sea level in the area of study. The data are from the ERA40 re-analysis (European Center for Medium range Weather Forecast (ECMWF)).

December, while the peak transport in the NAME model occurred in January. Both models also seem to respond to an increase in the pressure difference towards the end of the

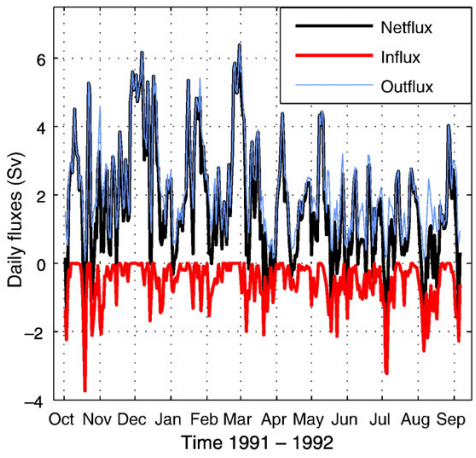

Fig. 8. Volume fluxes (Sv) through the strait between Frans Josef Land and Novaya Zemlya 1991–1992. The positive values are towards the Arctic Ocean.

Table 2
Volume transports (Sv) through the BSX 1991–1992 calculated from current-meter data (RCM) and the ROMS and NAME models for the corresponding 'reduced' section

Method	RCM			ROMS			NAME		
	Net	Out	In	Net	Out	In	Net	Out	In
RCM section	1.6	2.2	−0.6	1.9	3.3	−1.4	2.0	3.1	−1.1
AW	0.0	0.2	−0.2	0.1	0.2	−0.1	1.2	1.9	−0.7
CBW	1.0	1.0	0.0	1.7	2.7	1.0	0.0	0.1	−0.1
ARW	0.2	0.4	−0.2	0.0	0.1	−0.1	0.0	0.1	−0.1
SW	0.1	0.1	0.0	0.0	0.0	0.0	0.3	0.3	0.0
Whole section	–	–	–	2.6	3.9	−1.4	2.3	3.4	−1.1
AW	–	–	–	0.3	0.4	−0.1	1.3	2.0	−0.7
CBW	–	–	–	2.1	3.0	−0.9	0.1	0.2	−0.1
ARW	–	–	–	0.0	0.0	0.0	0.0	0.1	−0.1
SW	–	–	–	0.0	0.0	0.0	0.1	0.2	0.0

In the lower half of Table 2, model calculations for the whole section are shown. Positive values are out of the Barents Sea and into the Arctic Ocean. The transports divided into the major water masses are also given.

time series, while the observations indicate a decrease in volume transport, but again the month of September was under-sampled. Panteleev et al. (2004), using a CTD station set defining a closed area in the eastern Barents Sea obtained

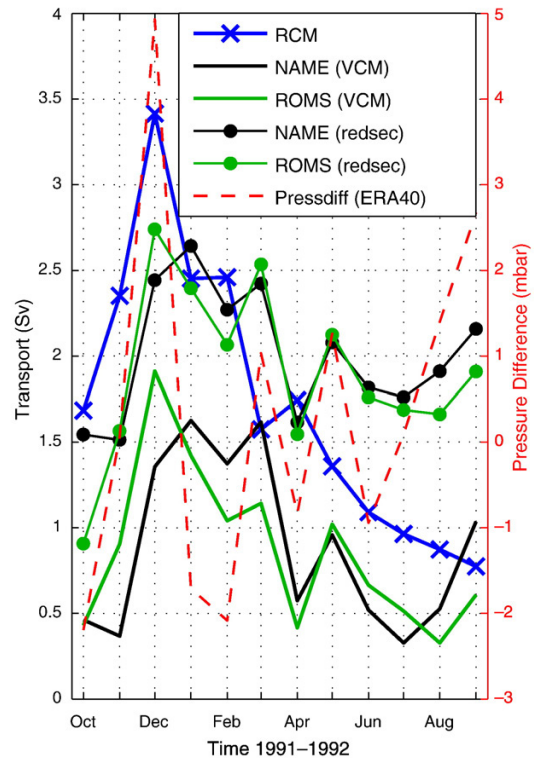

Fig. 9. Monthly average volume transports (net) based on observations, ROMS and NAME models for the section corresponding to the RCM array (redsec) and the data for the section constructed by Virtual Current Meters (VCM) only. The atmospheric pressure difference (ERA40) between Frans Josef Land and Novaya Zemlya is also given.

in September 1997, found that the transport through the BSX on that occasion was close to zero.

As the model velocities represent an area of roughly 9×9 km^2, a comparison with point measurements is not straightforward. From Figs. 1 and 6 it seems like the currents are steered by the topography. This is justified by the conservation of potential vorticity argument. The best way of comparing data with the models would probably be to select positions where the model bottom inclination compares with the inclination at the moorings. As there are different representations of the vertical in the two models (ROMS is terrain-following whereas NAME uses a fixed level z-coordinate), we have instead chosen to interpolate the model outputs to the exact positions of the current-meter moorings. Thereafter, the model values were interpolated in the vertical to the depths corresponding to the individual instruments. Theoretical volume transports were calculated based on these Virtual Current Meters (VCM) only. These results are also given in Fig. 9. The VCM model calculations for the net transport are 0.9 Sv too small, although the relative seasonal amplitude is comparable with the full model estimate. An inspection of the modelled current fields compared to the observations is needed to clarify this discrepancy.

3.2.2. Current structure

In Fig. 10 the yearly averages of the current fields normal to the section are given for the models and observations. The current fields of the models (Fig. 10, middle and Fig. 10, lower) indicate that the moorings M1, M2 and M4 are situated in areas with large horizontal velocity gradients. Taking into consideration that the currents are steered by the topography, and the fact that the model topographies do not match (compare the bottom profiles in Fig. 10), the discrepancy between the observations and the models may at least partly be explained by the coarse representation of the topography. It was sufficient to move the model virtual moorings one grid point (~9 km) to obtain a better fit with the observations; 0.2 Sv too low for NAME and 0.4 Sv too low for ROMS. However, the poor horizontal resolution of the 4 current-meter moorings is also an obvious explanation for the difference between the observational and simulated current fields at the BSX.

The model simulations indicate that the current-meter moorings were located such that they missed the current flow maxima (Fig. 10, middle and Fig. 10, lower). The major outflow seems to be situated between moorings 1 and 2, and the maximum inflow was modelled between moorings 3 and 4 in both models. This information may be used as guidelines for future field experiments.

The current measurements (Fig. 10, upper) indicate that the flow is mainly barotropic, except for a bottom intensified NE flow, particularly at mooring 2. This bottom intensification, which is likely to be related to a density driven behaviour of the current, is not reproduced by the models. One reason could be an absence or shortage of such dense water near the bottom; e.g. lack of CBW in the NAME model (Table 2). Another possibility could be the different representation of bottom topography in the models. Fig. 1 illustrates that the moorings were situated east of a saddle point with a downslope gradient towards the Arctic. The density section given

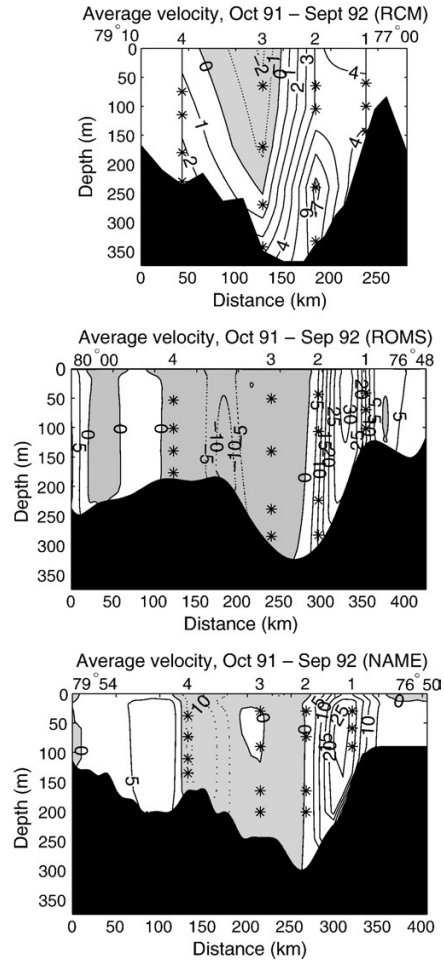

Fig. 10. Yearly averages (1991–1992) of velocity components normal to the section for observations (upper), the ROMS model (middle) and the NAME model (lower). Current-meter positions (real and virtual) are indicated with *. Negative values are shaded.

by Schauer et al. (2002), displays a pycnocline about 100 m above the bottom hugging the southern slope. This indicates a dense (σ_θ>28) bottom layer, which may be subject to a downslope acceleration. Too strong bottom friction in the models may also explain the lack of the bottom intensified current.

It is remarkable how well the two quite different modelling approaches discussed here compare. The models agree on the positions and strength of the jets in the central part of the section. In the northern part of the section both models indicate a jet (5–10 cm/s) towards the Arctic. Except for the topography-related differences from the observed current fields, it can not be concluded that the models fail to reproduce a realistic picture of the current fields. The model transport calculations for the whole section are given in Table 2 and show that the ROMS model gives a net transport of 2.6 Sv and the NAME model 2.3 Sv. Only future measurement campaigns will show if the model transports are closer

to reality than the calculations based on the widely spaced current meters. Results from another model experiment in the area, conducted by the Alfred Wegener Institute (AWI) (Gerdes et al., 2003), have been kindly provided by Michael Karcher. Based on monthly averages, we calculated a volume transport of 1.8 Sv through the BSX for the measuring period.

It is interesting to note that both models seem to respond to the secondary maximum in the pressure difference in March, and to a less extent to the third maximum in May, see Fig. 9. These features are not captured by the measurements. An inspection of the weekly ice maps (Fig. 4) illustrates that the BSX was completely covered by close drift ice as the ice edge was oriented E–W at the latitude of the northern tip of Novaya Zemlya in March 1992. This may have changed the wind stress on the ocean surface. Representing sea ice in numerical models is still a major challenge, and model experiments with ice forced into the model from satellite data might turn out useful in this respect. However, inspecting the individual current meters, Schauer et al. (2002) found that M1 showed the secondary transport maximum in March 1992, and some of the current meters revealed the May maximum at M1, M2 and M3. Hence, with a different weighting of contributions from each mooring, it is possible to remove this apparent discrepancy between the observations and the models.

3.3. Heat transport through the BSX

A proxy for the heat flux (Q_j) passing a current meter representing an area A_j is traditionally calculated as:

$$Q_j = c_w \rho_w A_j \sum_i v_i (T_i - T_{\mathrm{ref}}) \quad (1)$$

where v_i is the observed velocity and T_i is the temperature at the time step i, c_w is the specific heat of seawater assumed to be 4000 J kg^{-1} K^{-1}, ρ_w is the water density, and T_{ref} is a reference temperature. The recommended value for the reference temperature, when studying heat budgets for the Arctic Ocean, is $T_{\mathrm{ref}}=-0.1$ °C (Simonsen and Haugan, 1996). This is the estimated temperature of the overall outflow from the Arctic Ocean (Aagaard and Greisman, 1975). Although this value probably is not the most representative for the Barents Sea heat budget, we use $T_{\mathrm{ref}}=-0.1$ °C in order to make comparisons with previous estimates (e.g. Maslowski et al., 2004). The latent and sensible heat exchanges due to melting/freezing of sea ice and advection of sea ice are also neglected here.

The results are given in Table 3, where positive values indicate a heat flux from the Barents Sea towards the Arctic. The current meters indicate a small (−3.6 TW) net westward heat transport from the Arctic towards the Barents Sea. The ROMS model also shows a westward heat transport across the RCM section, while NAME indicates an eastward heat transport of 7.5 TW. When extended to the whole section, the heat transport of the two models only changed with a small amount. When splitting the net transports into water mass transports, we note from Table 2 that in the ROMS model only a small fraction of the transport through the BSX is AW. Most of the water is transformed to CBW, while in the NAME model most of the water is identified as AW, see also salt transports (Table 4). This also explains why the net heat transports in the two models have opposite signs (Table 3). To investigate this discrepancy, we look into the temperature and salinity structure at the BSX, comparing both models with a CTD section.

Table 3
Same as Table 2 for heat transports (TW)

Method	RCM			ROMS			NAME		
	Net	Out	In	Net	Out	In	Net	Out	In
RCM section	−3.6	2.6	−6.2	−6.0	5.9	−11.9	7.5	10.5	−3.0
AW	−0.3	0.8	−1.0	0.2	0.4	−0.2	5.5	7.2	−1.7
CBW	−1.1	0.1	−1.2	−6.5	3.9	−10.4	0.0	0.1	−0.1
ARW	−1.3	1.4	−2.7	−0.1	0.3	−0.4	0.1	0.3	−0.3
SW	−0.1	0.0	−0.2	0.1	0.1	0	0.2	0.5	−0.2
Whole section	–	–	–	−5.6	5.3	−10.9	7.4	11	−3.6
AW	–	–	–	0.8	1.0	−0.2	5.7	7.4	−1.7
CBW	–	–	–	−7.7	3.7	−11.4	−0.2	0.1	−0.3
ARW	–	–	–	−0.1	0.2	−0.3	−0.1	0.3	−0.5
SW	–	–	–	0.0	0.2	−0.2	0.2	0.4	−0.2

The CTD section obtained over 3 days in September–October 1991 (Fig. 11) shows that the upper ~50 m was dominated by Surface Water (SW), separated from the Arctic Water (ARW) below by a strong thermocline and halocline. The SW with temperature typically above −0.1 °C is probably formed from ARW by summer warming and melting of sea ice and river run-off. A core of Atlantic Water (AW) was found near the centre of the section with maximum temperature above 1.5 °C and salinity above 34.8. This AW is believed to enter the Arctic Ocean via the Fram Strait, following the continental slope and flow around Frans Josef Land to enter the Barents Sea from the east, see Schauer et al. (2002). The dense Cold Bottom Water (CBW) dominated the near bottom layers with temperatures down to −0.7 °C and maximum salinities at about 34.9, with $\sigma_\theta > 28$, see Fig. 2. However, the extremely dense CBW occasionally reported from the area with temperature near freezing point and salinities above 35 (Midttun, 1985), was not observed on this occasion.

In Fig. 11, daily model averages (October 1st) of temperature and salinity distributions are also shown. The model salinities compare very well with the observations, both in absolute values and in structure. The salinity is dominating the density structure in this area, and the temperature may be considered more like a tracer. Both models span the same temperature range as the observations (from −1.5 °C to +2.0 °C). Table 2 shows that in the ROMS model CBW is dominating the transport, while in the NAME model AW yields the major contribution to the BSX transport. The same impression is given by Fig. 11 as the deep saline layers in the ROMS model seem to be on the cold side and in the NAME model at the warm side compared to observations. Although the snapshots given in Fig. 11 could change substantially, as eddies of time scales of a few days may pass through the BSX, we will look into possible explanations for the different behaviour of the two models.

The present hindcast with the ROMS model seems to give too high heat content in the Barents Sea interior. This is manifested by a 0.6 °C bias (model too high) between observed and modelled temperature in the Kola Section at 33°30′E (not shown). This may cause too much ice melting, which in turn gives a higher rate of heat loss to the atmosphere in the eastern Barents Sea. If NAME tends to have too much ice, this will lead to an insulation of the water

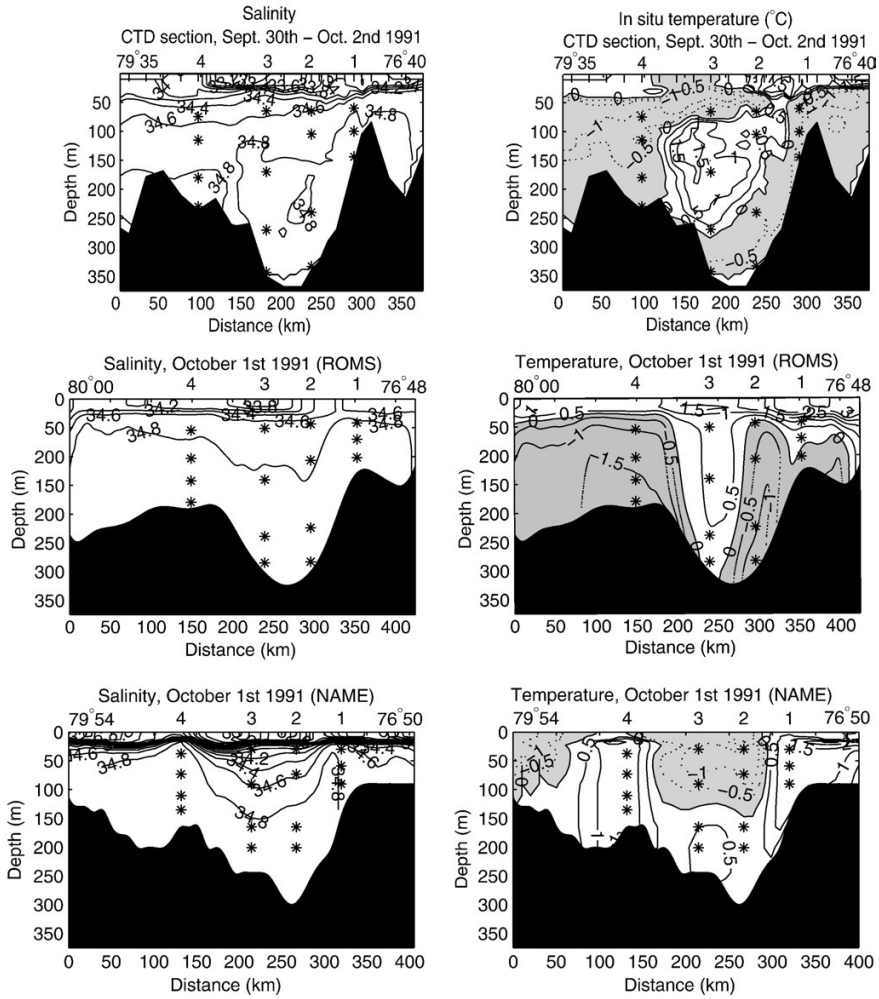

Fig. 11. Snapshot of salinity (left) and temperature (right) from CTD section (upper) compared with ROMS (middle) and NAME (lower) models. Temperatures below zero are shaded.

below, allowing AW to survive all the way to the BSX, as demonstrated by Gerdes et al. (2003). Furthermore, tides are included in ROMS, but not in NAME. Tides keep polynyas open, particularly near coasts and islands, and also produce divergences in the open ocean. Harms et al. (2005) found that tidal mixing contributes significantly to the air-sea heat budget in the Barents Sea; see also Martin and Cavalieri (1989). Another possible explanation of the cooling discrepancy is the different parameterisations of sea-ice processes in the two models.

It is worth noting that the differences from different atmospheric forcing data sets using a single model are larger than the differences between models using the same forcing data, i.e. compare the ROMS hindcast presented here with the NCEP forced experiment presented by Budgell (2005). The large sensitivity of atmospheric forcing parameterisation was

Table 4
Same as Table 2 for salt transports (kT/s)

Method	RCM			ROMS			NAME		
	Net	Out	In	Net	Out	In	Net	Out	In
RCM section	51	72	−21	65	114	−49	65	105	−40
AW	0	8	−8	4	8	−4	43	68	−25
CBW	33	34	−2	60	94	−34	−1	3	−4
ARW	7	15	−8	0.0	2	−2	0	2	−2
SW	0.0	0.0	0.0	0.0	1	−1	3	5	−1
Whole section	–	–	–	89	137	−48	82	122	−40
AW	–	–	–	11	14	−3	48	73	−25
CBW	–	–	–	74	104	−30	3	8	−5
ARW	–	–	–	0.0	2	−2	1	3	−2
SW	–	–	–	65	114	−49	65	105	−40

also demonstrated by Harms et al. (2005) applying the HAMSOM model in the Barents Sea.

3.4. Comparing fluxes through the BSO and the BSX

The nearly 10-year long (1997–2006) current measurement program in the BSO gave a net volume flux into the Barents Sea of 1.8 Sv, with a positive trend of about 0.1 Sv/year, (Skagseth et al., 2008). This current-meter array did not include the Norwegian Coastal Current (NCC). According to the model experiments discussed here, NCC contributes with about 1 Sv, adding up the total transport through the BSO to 2.8 Sv. Our estimate for the BSX is of the same order of magnitude, (2.0±0.6 Sv). Various model simulations indicate that the exchanges via the other openings are about one order of magnitude smaller, e.g. Gerdes et al. (2003) and Maslowski et al. (2004), in accordance with the few observations available from the area (Aagaard et al., 1983). Obviously, the BSX and the BSO are the main openings for the Barents Sea.

The heat flux into the Barents Sea via the current-meter array in the BSO was estimated to be 48 TW (Skagseth et al., 2008), and to 40 TW from the repeated combined ADCP and hydrography section by O'Dwyer et al. (2001). Including the contribution from NCC, the total heat flux is about 65 TW according to the 23-year model mean given by Maslowski et al. (2004) and 73 TW from the ROMS climatic mean. The model simulations reported by Drange et al. (2005), indicate 49 TW (NOASIM model) and 86 TW (MICOM model).

Observations show that the subsurface layers at the BSX are dominated by water of Atlantic origin (AW), with maximum temperature less than 1.5 °C, and Cold Bottom Water (CBW), see Table 2 and Fig. 11. The latter is presumably formed by direct cooling of AW and/or ice formation and brine release on the shallow shelves in the NE Barents Sea (Schauer et al., 2002), see Figs. 2 and 3. Thus, the water masses are subject to a strong modification when crossing the Barents Sea. The heat transport across the BSX based on the current-meter observations, was small but negative (−3.6 TW), indicating a heat flux from the Arctic Ocean into the Barents Sea.

The NAME (7.4 TW) and ROMS (−5.6 TW) models also gave small heat transports in the BSX in 1991–1992, and the 23-year model mean by Maslowski et al. (2004) indicate that the heat transport is not significantly different from zero (2.2± 3.5 TW). These results indicate a heat loss of about 70 TW from the water on its journey through the Barents Sea. Simonsen and Haugan (1996) investigated several parameterisations of the atmospheric surface heat fluxes and found that the average atmospheric cooling of the Barents Sea is about 140 TW. Thus the ocean heat transport by advection, as we have calculated here, do not balance the average atmospheric cooling estimated by Simonsen and Haugan (1996). We have tested the sensitivities of the reference temperature T_{ref} for the proxy heat calculation by varying it from freezing point to +1 °C, but the heat fluxes stayed low; between 24 TW (T_{ref}=−1.8 °C) for NAME and −22 TW (T_{ref}=+1 °C) for ROMS.

4. Summary and conclusions

Measurements from CTD-casts and a current-meter array deployed in the NE Barents Sea between Frans Josef Land and Novaya Zemlya (BSX) for almost a year in 1991–1992, are presented. The prevailing currents were towards NE, out of the Barents Sea, and evident bottom intensification was found in the central part of the strait. The range of day to day variability of volume transport was up to 10 Sv (Fig. 8), and the seasonal amplitude was found to be above 2 Sv (Fig. 9) with maximum in December–January. The seasonality seems mainly to be related to changes in the atmospheric pressure conditions and the belonging wind fields. The average net transport through the section, defined by the current meters, was found to be 1.6 Sv.

The current-meter array was compared with the NAME and ROMS models by extracting model values from the exact positions of the instruments. Both models gave the same (Fig. 9), but too low average transports (0.9 Sv) compared to the calculations based on the current meters. The models indicate (Fig. 10, middle and Fig. 10, lower) that three out of four moorings were situated in areas with strong horizontal velocity gradients. Therefore, it can not be concluded that the models fail to simulate realistic currents, but exact positioning is distorted because of the coarse representation of the bottom topography. Using all grid points in the 'reduced' section corresponding to the current meters, gave higher transports; 2.0 Sv for NAME and 1.9 Sv for ROMS (see Table 2). The model current structures (Fig. 10, middle and Fig. 10, lower) indicate that the deployed instruments missed the major outflow jet from the Barents Sea towards the Arctic Ocean.

The current-meter array covered only about half of the section (Fig. 10, upper vs. Fig. 10, middle and Fig. 10, lower). The total transport through the whole section was calculated from the models as 2.3 Sv for NAME and 2.6 Sv for ROMS. Combining the two model results with the observations, we estimate the net transport through the BSX to be 2.0±0.6 Sv.

The estimated influx of ~1.8 Sv to the Barents Sea in the west via the BSO between Fugløya and Bjørnøya (Skagseth et al., 2008) is larger than the BSX transport with error margins, when the contribution of the NCC (~1.0 Sv from the ROMS model set up) is added. However, the BSO transport is found to have a positive trend of 0.1 Sv/year, suggesting that a de-trended value of the BSO transport would resemble that of the estimated 1991–1992 BSX transport. The BSO water consists mainly of AW with an average temperature of about 6 °C (Blindheim, 1995). Observations show that the subsurface layers at the BSX are dominated by water of Atlantic origin (AW) with maximum temperature less than 1.5 °C and Cold Bottom Water (CBW) less than 0 °C, see Figs. 2, 11 and Table 2. Thus the water masses are subject to a strong modification crossing the Barents Sea, see also Schauer et al. (2002).

The cooling of the water masses was stronger in the ROMS- than in the NAME-simulations. This may be because the two models use different parameterisations of ice and/or the lack of tides in the NAME model. The tides seem to be important for the air-sea heat transfer in the Barents Sea (Harms et al., 2005). This resulted in different signs on the heat transports in the BSX for the NAME (7.4 TW) and ROMS (−5.6 TW) models. We have also seen here with ROMS, as also confirmed by HAMSOM (Harms et al., 2005), that the models are highly sensitive to the atmospheric forcing. This indicates that the choice of atmospheric forcing could be more important than the type of model.

Maslowski et al. (2004), using the whole 1979–2001 period simulation, found the average heat flux to be 2.2± 3.5 TW. Thus it remains open if the Barents Sea is a heat sink for the Arctic Ocean, rather than a heat source.

The CBW water passing the BSX is so dense, that it has the potential to reach below the depth of the sills (~800 m) of the Arctic Mediterranean between Greenland and Scotland and therefore contribute to the overflow and renewal of the world ocean deep water. Based on the current meters the CBW transport in the BSX is estimated to 1 Sv. Schauer et al. (2002) indicate that most of this water cascades via the St. Anna Trough as a bottom intensified flow towards the Arctic Ocean, where it penetrates down below the AW stemming from the Fram Strait. Observations (Foldvik et al., 2004) and models (Killworth, 1977) of Cold Bottom Water plumes indicate that the volume flux may increase by a factor of 2 to 4 by entrainment of surrounding water when cascading towards great depths. The Greenland–Scotland overflow is estimated to 6 Sv (Hansen and Østerhus, 2000), so the BSX contribution may be significant.

Acknowledgements

This study has received support from the IPY project Bipolar Atlantic Thermohaline Circulation (BIAC, IPY Cluster # 23) supported by The Norwegian Research Council.

References

Aagaard, K., Foldvik, A., Gammelsrød, T., Vinje, T., 1983. One year records of currents and bottom pressure in the Strait between Nordaustlandet and Kvitøya, Svalbard, 1980–1981. Polar Res. 1, 107–113.

Aagaard, K., Greisman, P., 1975. Toward new mass and heat budgets for the Arctic Ocean. J. Geophys. Res. 80 (27), 3821–3827.

Blindheim, J., 1995. Report on the working group on oceanic hydrography. Oban. ICES, pp. 26–28. April 1995.

Budgell, P., 2005. Numerical simulation of ice-ocean variability in the Barents Sea region: towards dynamical downscaling. Ocean Dyn. 55, 370–387. doi:10.1007/s10236-005-0008-3.

Drange, H., Gerdes, R., Gao, Y., Karcher, M., Kauker, F., Bentsen, M., 2005. Ocean general circulation modelling of the Nordic Seas. In: Drange, H., Dokken, T., Furevik, T., Gerdes, R., Berger, W. (Eds.), The Nordic Seas: An Integrated Perspective. Geophysical Monograph Series, vol. 158. AGU, Washington DC, pp. 199–219. doi:10.1029/158GM14.

Foldvik, A., Gammelsrød, T., Østerhus, S., Fahrbach, E., Nicholls, K.W., Padman, L., Woodgate, R.A., Rohardt, G., Schröder, M., 2004. Ice shelf water overflow and bottom water formation in the southern Weddell Sea. J. Geophys. Res. 109, C02015. doi:10.1029/2003JC001811.

Furevik, T., Nilsen, J.E.O., 2005. Large-scale atmospheric circulation variability and its impacts on the nordic seas ocean climate — a review. In: Drange, H., Dokken, T., Furevik, T., Gerdes, R., Berger, W. (Eds.), The Nordic Seas: An Integrated Perspective. Geophysical Monograph Series, vol. 158. AGU, Washington DC, pp. 105–137.

Furevik, T., 2001. Annual and interannual variability of the Atlantic Water temperatures in the Norwegian and the Barents Seas: 1980–1996. Deep Sea Res. I 48, 383–404.

Gerdes, R., Karcher, M.J., Kauker, F., Schauer, U., 2003. Causes and development of repeated Arctic Ocean warming events. Geophys. Res. Lett. 30 (19), 1980. doi:10.1029/2003GL018080.

Häkkinen, S., Mellor, G.L., 1992. Modelling the seasonal variability of a coupled arctic ice-ocean system. J. Geophys. Res. 97C (12), 20285–20304.

Hansen, B., Østerhus, S., 2000. North Atlantic–Nordic seas exchanges. Prog. Oceanogr. 45, 109–208.

Harms, I.H., Schrum, C., Hatten, K., 2005. Numerical sensitivity studies on the variability of climate-relevant processes in the Barents Sea. J. Geophys. Res. 110, C06002. doi:10.1029/2004JC002559.

Hunke, E.C., 2001. Viscous-plastic sea ice dynamics with the EVP model: linearization issues. J. Comput. Phys. 170 (1), 18–38.

Ingvaldsen, R., Asplin, L., Loeng, H., 2004. The seasonal cycle in the Atlantic transport to the Barents Sea. Cont. Shelf Res. 24 (9), 1015–1032. doi:10.1016/j.csr.2004.02.011.

Ingvaldsen, R., Loeng, H., Asplin, L., 2002. Variability in the Atlantic inflow to the Barents Sea based on a one-year time series from moored current meters. Cont. Shelf Res. 22 (3), 505–519. doi:10.1016/S0278-4343(01)00070-X.

Ivanov, V.V., Shapiro, G.I., 2005. Formation of a dense water cascade in the marginal ice zone in the Barents Sea. Deep Sea Res. I 52 (9), 1699–1717. doi:10.1016/j.dsr.2005.04.004.

Jakobsson, M., Cherkis, N., Woodward, J., Coakley, B., Macnab, R., 2000. A new grid of Arctic bathymetry: a significant resource for scientists and mapmakers. EOS Transactions. AGU. 81, 89, 93, 96.

Kalnay, E., Co-authors, 1996. The NCEP/NCAR 40 year re-analyses project. Bull. Am. Met. Soc. 77 (3), 437–471.

Karcher, M.J., Oberhuber, J.M., 2002. Pathways and modification of the upper and intermediate waters of the Arctic Ocean. J. Geophys. Res. I07 (C6), 3049. doi:10.1029/2000JC000530.

Killworth, P.D., 1977. Mixing on Weddel Sea continental slope. Deep Sea Res. 24 (5), 427–448.

Kvingedal, B., 2005. Sea ice extent and variability in the Nordic Seas, 1967–2002. In: Drange, H., Dokken, T., Furevik, T., Gerdes, R., Berger, W. (Eds.), The Nordic Seas: An Integrated Perspective. Geophysical Monograph Series, vol. 158. AGU, Washington DC, pp. 39–51.

Kwok, R., Maslowski, W., Laxon, S.W., 2005. On large outflows of Arctic sea ice into the Barents Sea. Geophys. Res. Lett. 32 (22), L22503. doi:10.1029/2005GL024485.

Loeng, H., Sagen, H., Ådlandsvik, B. and Ozighin, V., 1993. Current measurements between Novaya Zemlya and Frans Josef Land, September 1991–September 1992. Institute of Marine Research, Norway. Department of Marine Environment. Report 2/1993, pp 23 + 4 appendices.

Martin, S., Cavalieri, D.J., 1989. Contributions of the Siberian shelf polynyas to the Arctic Ocean intermediate and deep-water. J. Geophys. Res. 94 (C9), 12725–12738.

Maslowski, W., Marble, D., Walczowski, W., Schauer, U., Clement, J.L., Semtner, A.J., 2004. On climatological mass, heat, and salt transports through the Barents Sea and Fram Strait from a pan-Arctic coupled ice-ocean model simulation. J. Geophys. Res. 109, C03032. doi:10.1029/2001JC0010139.

Meincke, J., Rudels, B., Friedrich, H.J., 1997. The Arctic Ocean–Nordic Seas thermohaline system. ICES J. Mar. Sci. 54 (3), 283–299.

Mellor, G.L., Kantha, L., 1989. An ice-ocean coupled model. J. Geophys. Res. 94 (C8), 10937–10954.

Midttun, L., 1985. Formation of dense bottom water in the Barents Sea. Deep Sea Res. A 32, 1233–1241.

O, Dwyer, J., Kasajima, Y., Nøst, O.A., 2001. North Atlantic Water in the Barents Sea opening. Polar Res 20 (2), 209–216.

Olsen, A., Johannessen, T., Rey, F., 2003. On the nature of the factors that control spring bloom development at the entrance to the Barents Sea and their interannual variability Sarsia 88 (6) , 379–393.

Padman, Erofeeva, S., 2004. A barotropic inverse tidal model for the Arctic Ocean. Geophys. Res. Lett. 31 (2), L02303.

Panteleev, G., Ikeda, M., Grotov, A., Nechaev, D., Yaremchuk, M., 2004. Mass, heat and salt balances in the eastern Barents Sea obtained by inversion of hydrographic section data. J. Oceanogr. 60, 613–623.

Parkinson, C.L., Washington, W.M., 1979. Large-scale numerical-model of sea ice. J. Geophys. Res. 84 (NC1), 311–337.

Pease, C.H., 1987. The size of wind-driven coastal polynyas. J. Geophys. Res. 92 (C7), 7049–7059.

Pfirman, S.L., Bauch, D., Gammelsrød, T., 1994. The Northern Barents Sea: water mass distribution and modification. In: Johannessen, O.M., Muench, R.D., Overland, J.E. (Eds.), The Polar Oceans and their Role in Shaping the Global Environment. Geophysical Monograph Series, vol. 85. AGU, Washington DC, pp. 77–94.

Quadfasel, D., Rudels, B., Kurz, K., 1988. Outflow of dense water from a Svalbard fjord into the Fram Strait. Deep Sea Res. A 35 (7), 1143–1150.

Rosenfeld, 1983. WHOI. Technical Report 85–35, 21.

Rudels, B., Jones, E.P., Anderson, L.G., Kattner, G., 1994. On the Intermediate depth waters of the Arctic Ocean. In: Johannessen, O.M., Muench, R.D., Overland, J.E. (Eds.), The Polar Oceans and their Role in Shaping the Global Environment. Geophysical Monograph Series, vol. 84. AGU, Washington DC, pp. 33–46.

Rudels, B., 1987. On the mass balance of the Polar Ocean, with special emphasis on the Fram Strait. Skrift 188, 1–53.

Sakshaug, E., Bjørge, A., Gulliksen, B., Loeng, H., Mehlum, F., 1994. Structure, biomass distribution and energetics of the pelagic ecosystem in the Barents Sea: a synopsis. Polar Biol. 14 (6), 405–411.

Schauer, U., Loeng, H., Rudels, B., Ozhigin, V.K., Dieck, W., 2002. Atlantic water inflow through the Barents and Kara Seas. Deep Sea Res. I 49 (12), 2281–2298.

Schauer, U., Muench, R., Rudels, B., Timokov, L., 1997. Impact of eastern Arctic shelf waters on the Nansen Basin intermediate layers. J. Geophys. Res. 102 (C2), 3371–3382.

Schiffer, R.A., Rossow, W.B., 1985. ISCCP global radiance data set — a new resource for climate research. Bull. Am. Met. Soc. 66 (12), 1498–1505.

Semtner, A.J., 1976. Model for thermodynamic growth of sea ice in numerical investigations of climate. J. Phys. Oceanogr. 6 (3), 379–389.
Shchepetkin, A.F., McWilliams, J.C., 2003. A method for computing horizontal pressure-gradient force in an oceanic model with a nonaligned vertical coordinate. J. Geophys. Res. 108 (C3). doi:10.1029/2001JC001047.
Simonsen, K., Haugan, P.M., 1996. Heat budgets of the Arctic Mediterranean and sea surface heat flux parameterizations for the Nordic Seas. J. Geophys. Res. 101 (C3), 6553–6576.
Skagseth, Ø., Furevik, T., Ingvaldsen, R., Loeng, H., Mork, K.A., Orvik, K.A., Ozhigin, V., 2008. Volume and heat transports to the Arctic via the Norwegian and Barents Seas. In: 'Arctic–Subarctic Ocean fluxes. In: Dickson, R., Meincke, J., Rhines, P. (Eds.), Defining the role of the Northern Seas in Climate. Springer, Netherlands. doi:10.1007/978-1-4020-6774-7.
Sorteberg, A., Kvingedal, B., 2006. Atmospheric forcing on the Barents Sea winter ice extent. J. Clim. 19 (19), 4772–4784.
Steele, M., Morley, R., Ermold, W., 2001. PHC: a global ocean hydrography with a high quality Arctic Ocean. J. Clim. 14 (9), 2079–2087.
Zhang, J.L., Hibler, W.D., 1997. On an efficient numerical method for modeling sea ice dynamics. J. Geophys. Res. 102 (C4), 8691–8702.
Zhang, J.L., Rothrock, D.A., Steele, M., 1998. Warming of the Arctic Ocean by a strengthened Atlantic inflow: model results. Geophys. Res. Lett. 25 (10), 1745–1748.

Paper II

V.S. Lien and A.G. Trofimov

Intermediate and deep water mass characteristics and transformations in the St. Anna Trough

Submitted to *Deep-Sea Research I*

II

Intermediate and deep water mass characteristics and transformations in the St. Anna Trough

Vidar S. Lien*[,a], Alexander G. Trofimov[b]

[a] *Institute of Marine Research, PO. Box 1870, N-5817 Bergen, Norway.*
[b] *Knipovich Polar Research Institute of Marine Fisheries and Oceanography, Murmansk, Russian Federation*

Abstract

We use CTD (Conductivity, Temperature and Depth) data from August/September 2008 to investigate the intermediate and deep water masses in the northeastern Barents Sea and the St. Anna Trough. Two distinct modes of Atlantic Water defined by potential temperature above 0 °C are observed between Novaya Zemlya and Franz Josef Land. One mode consists of Atlantic Water modified during its advection through the Barents Sea. The second mode consists of Atlantic Water from the Arctic Circumpolar Boundary Current following the topography into the St. Anna Trough. The Atlantic Water from the Barents Sea is slightly colder ($\Theta < 1$), more saline ($S > 34.9$) and has a higher potential density ($\sigma_\Theta > 28.0$) than the Atlantic Water advected south from the Nansen Basin ($\Theta \sim 1$; $S \sim 34.8$; $\sigma_\Theta \sim 27.9$). However, the Barents Sea Atlantic Water undergoes considerable modifications through mixing with colder and less saline water masses present in the northeastern Barents Sea and the St. Anna Trough, before entering the Arctic Ocean. Although the Barents Sea is currently in a climatologically

*Corresponding author
Email address: vidar.lien@imr.no (Vidar S. Lien)

warm phase with less than normal ice formation and subsequently reduced production of brine enriched water, the bottom water observed in the St. Anna Trough has a potential density high enough to sink to great depths and thereby ventilate the deep water masses in the Arctic Ocean.
Key words: Barents Sea, Kara Sea, Deep Water, Atlantic Water

1. Introduction

Production of cold and dense water at high latitudes plays an important role in the world ocean's thermohaline circulation. A most effective process in forming water masses with density high enough to sink to great depths in the world oceans, is ice-freezing connected with polynya activity and subsequent brine release in shelf areas (Morales Maqueda et al., 2004). Another process that produces such dense water masses, is direct atmospheric cooling of water masses with relatively high salinity. The Barents Sea is a shelf sea in which both of these processes occur, and it is one of the largest shelf seas adjacent to the deep Polar basin. Several formation sites of dense water have been observed (Nansen, 1906); (Midttun, 1985); (Quadfasel et al., 1988); (Ozhigin et al., 2000). This dense water contributes to the renewal of the deep water in the Arctic Ocean (Martin and Cavalieri, 1989); (Rudels et al., 1994)); (Jones et al., 1995); (Schauer et al., 1997); (Rudels et al., 2000) and thus the global thermohaline circulation (Meincke et al., 1997).

The northward advection of warm and saline Atlantic Water (AW; water mass definitions and abbreviations are summarized in Table 1) along the Norwegian coast splits into two branches west of the entrance to the Barents Sea, with one branch entering the Barents Sea while the other branch contin-

ues northward along the western coast of Svalbard as the West Spitsbergen Current (see e.g. Aagaard et al. (1987)). Several processes contribute to considerable modifications of the Barents Sea branch before it eventually enters the Arctic Ocean through the Barents Sea Exit and St. Anna Trough (Pfirman et al., 1994); (Rudels et al., 1994); (Ozhigin and Ivshin, 1999); (Rudels et al., 2004). These include freshwater input from runoff and ice melting (Coachman and Barnes, 1963); (Steele et al., 1995); wind and tidal mixing (e.g. Sundfjord et al. (2007)); and atmospheric cooling and ice-freezing (Aagaard et al., 1981); (Jones and Anderson, 1986); (Woodgate et al., 2001). Due to the advection of warm water masses, a substantial part of the Barents Sea is kept ice-free all year round (Kvingedal, 2005). This causes a large heat loss from the ocean to the atmosphere (Simonsen and Haugan, 1996); (Smedsrud et al., 2010). Availability of saline water masses in an area of substantial cooling favors production of water masses dense enough to sink to intermediate and deep parts of the Arctic Ocean.

The WSC enters the Arctic Ocean through the Fram Strait and is sometimes referred to as Fram Strait Branch Water (FSBW), as it submerges under the Arctic cold halocline water and forms a subsurface temperature and salinity maximum (see e.g. Rudels et al. (1999)). Some of the FSBW enters the Barents Sea from the north through submarine valleys and canyons (Matishov et al., 2009), mainly through Franz Victoria Trough on the western side of Franz Josef Land (Mosby, 1938); (Novitsky, 1961) and through the St. Anna Trough east of Franz Josef Land (Hanzlick and Aagaard, 1980); (Loeng et al., 1993); (Schauer et al., 2002a); (Gammelsrød et al., 2009).

The northeastern Barents Sea is connected to the Arctic Ocean through

the St. Anna Trough (see map, Fig. 1). A 350 m deep branch of the St. Anna Trough is oriented westward into the northeastern Barents Sea between Novaya Zemlya and Franz Josef Land. This branch is hereinafter called "Western St. Anna Trough" (WAT). Between the WAT and the Northeast Basin in the northeastern Barents Sea, a 200 m deep sill creates a saddle point. In the southern part, the depth of the St. Anna Trough varies between 500 and 300 m, while it reaches 1000 m at the entrance to the Arctic Ocean in the north. Between Novaya Zemlya and the WAT, there are several small banks and canyons, with depths ranging from 100 to 250 m. Between the WAT and Franz Josef Land is a bank with a depth of about 200 m, while the Northeast Basin is between 300 and 400 m deep.

The inflow of Atlantic Water to the Barents Sea in the west has been monitored since 1997 (Skagseth et al., 2008), and regular cruises measure both the physical and ecological state of the Barents Sea. As a consequence, southern and western parts of the Barents Sea are relatively densely sampled, and the physical conditions are described in several papers (see e.g. Loeng (1991); Pfirman et al. (1994); Ozhigin and Ivshin (1999)). The northern and northeastern parts, however, are less well sampled, partly due to the seasonal ice cover. Articles describing this area include Midttun (1985); Pfirman et al. (1994); Schauer et al. (2002a); Schauer et al. (2002b); Panteleev et al. (2004); Matishov et al. (2009). Also some model studies covering this area has been performed, see e.g. Kärcher et al. (2003); Maslowski et al. (2004). Some work has been done on the downstream conditions where the Atlantic Water advected through the Barents Sea becomes part of the Arctic Circumpolar Boundary Current in the Eurasian Basin, see e.g. Rudels

et al. (1999); Woodgate et al. (2001); Schauer et al. (2002b); Dmitrenko et al. (2008a); Dmitrenko et al. (2008b); Dmitrenko et al. (2009). Here, we present data from the poorly sampled area linking the Barents Sea to the Arctic Ocean. A dataset consisting of 142 CTD-stations (Conductivity, Temperature and Depth) covering the advection route from the Barents Sea to the Nansen Basin is used to analyze and discuss water mass properties and modifications and the exchanges between the northeastern Barents Sea and the Arctic Ocean through the St. Anna Trough.

In section 2, the data set used in this study is described. The results are presented and discussed in section 3, followed by a general discussion in section 4. Subsequently, a summary and conclusions are given.

2. Data

CTD-data from two cruises conducted from late August to mid-September 2008 are analyzed and presented. Fifty-six CTD-stations covering both the St. Anna Trough and the northeastern Barents Sea between Novaya Zemlya and Franz Josef Land were taken by the vessel "Obva" from August 26th to September 8th. Five CTD transects with a total of 86 stations between Novaya Zemlya and Franz Josef Land were taken by R/V "Professor Boyko" from September 9th to September 16th (see Fig. 2 for station positions). The R/V "Professor Boyko" was equipped with a FSI Micro CTD3, with an accuracy of 0.0002 (S/m) and 0.002 (°C) for conductivity and temperature, respectively. "Obva" was equipped with a SBE 19plus CTD system, with an accuracy of 0.0005 (S/m) and 0.005 (°C) for conductivity and temperature, respectively. The two surveys are partly overlapping spatially but not

temporally. Although the combined dataset spans a period of 3 weeks, we consider the datset to be more or less synoptic, especially since we focus our investigation on the water masses below the surface mixed layer.

The westernmost section was along 55°E sampled by "Obva", here called section A (see Fig. 2). This section crosses the northeastern part of the Northeast Basin. The 5 transects sampled by R/V "Professor Boyko" are hereinafter named sections 1 to 5, with section 1 being the westernmost section (see Fig. 2). Section 1 is crossing the saddle point separating the Northeast Basin in the Barents Sea from the WAT, while section 5 is located at the opening between the WAT and the main part of the St. Anna Trough. Sections 2, 3 and 4 cover the western and middle parts of the WAT. Section 3 corresponds to the transect covered by CTD-stations and moorings in 1991/92 (Loeng et al., 1993); (Schauer et al., 2002a); (Gammelsrød et al., 2009).

Cross trough sections show the east-west distribution of water masses in the St. Anna Trough. Two sections are investigated: one along 79°N (hereinafter section B) consisting of 6 stations, and one along 81°N (hereinafter section C) consisting of 3 stations (see Fig. 2). Section B crosses the St. Anna Trough just north of the entrance to the WAT, while section C crosses the St. Anna Trough east of Franz Josef Land. However, consisting of only 3 stations, section C has poor horizontal resolution.

In this study we adapt the water mass definitions from Gammelsrød et al. (2009), see Table 1, although other water mass definitions have been applied elsewhere, see e.g. Smolyar and Adrov (2003).

3. Water masses

A scatter-plot of the Θ-S properties at all the CTD-stations taken by R/V "Professor Boyko" shows the presence of three distinct intermediate and deep water masses and the mixing between them (Fig. 3). Contrary to earlier observations, indicating only one mode of AW (defined by $\Theta > 0$ °C) in the WAT (Schauer et al., 2002a); (Gammelsrød et al., 2009); two clearly distinct water masses with potential temperature above 0 °C were present in the WAT in 2008. Direct current measurements have revealed AW flowing southwestward along the northern slope of the WAT (Loeng et al., 1993); (Schauer et al., 2002a). This AW is therefore believed to originate from the Arctic Circumpolar Boundary Current and follow the topography into the St. Anna Trough and further southwestward into the WAT. These observations are in agreement with geostrophic calculations (Panteleev et al., 2004) and model studies (Kärcher et al., 2003); (Gammelsrød et al., 2009), indicating westward flow of water masses with temperatures above 0 °C in the WAT. Fig. 2 in Gammelsrød et al. (2009) shows that the westward flowing AW observed in 1991/92 exhibited similar Θ-S characteristics as the lower salinity AW observed in 2008.

In section A, only the more saline AW is present (Fig. 4). This confirms that the lower salinity AW must indeed be advected southwards from the Nansen Basin. It flows alongslope into the WAT and partly mixes with other water masses present and recirculates into the main part of the St. Anna Trough. This AW is hereinafter denoted recirculating Atlantic Water (rAW). The observations in section A show that the Barents Sea is the source of the high salinity Atlantic Water, hereinafter denoted Barents Atlantic derived

Water (bAW). The presence of Cold Bottom Water (CBW; see Table 1) in section A shows that the Barents Sea is also a source of CBW, which is advected eastwards into the St. Anna Trough, in agreement with earlier findings (e.g. Schauer et al. (2002a)).

In order to distinguish the two modes of Atlantic Water by their respective characteristics, we introduce new bounds on the water mass characteristics (Table 2). From inspection of the section plots, a temperature range between 0.5 and 1.5 °C is applied for the rAW (Fig.s 3 and 5; see also Table 1). rAW with temperature below 0.5 °C is considered "diluted rAW", due to mixing with Arctic Water (ARW; see Table 1), CBW or both. A salinity upper bound of 34.9 is applied to separate rAW from bAW (Figs. 3 and 5), while 34.75 is kept as the lower salinity bound for rAW (from Table 1). The upper temperature bound on rAW is to distinguish it from upper layer bAW that has become fresher due to either ice melt or mixing with coastal water. Using these bounds and averaging the water mass characteristics at all stations and depths where they are present in the R/V "Professor Boyko" dataset covering the WAT (Fig. 2), results in the following mean characteristics: Θ = 0.85 ± 0.21 °C; S = 34.82 ± 0.03 for rAW and Θ = 0.40 ± 0.26 °C; S = 34.97 ± 0.02 for bAW, where the ± denotes one standard deviation from the mean. The corresponding densities are σ_Θ = 27.91 ± 0.02 and σ_Θ = 28.06 ± 0.02 for rAW and bAW, respectively. Typical characteristics of the water masses present in the northeastern Barents Sea are summarized in Fig. 6 and Table 2. Characteristics of the FSBW are obtained from stations in the northwestern part of the St. Anna Trough in this dataset, and may therefore differ from those reported elsewhere, e.g. Dmitrenko et al. (2009); Schauer

et al. (2002b).

Vertical sections of potential temperature and salinity show that water mass characteristics vary geographically. In order to follow the advection and modification of rAW, bAW and CBW, vertical sections and Θ-S diagrams are investigated in the following sections, starting with the recirculating Atlantic Water.

3.1. Recirculating Atlantic Water

In the northwestern part of the St. Anna Trough (see Fig. 1), the Θ-S signature of the rAW is easily recognizable as an intermediate temperature maximum (see Θ-S properties in section B; Fig. 4). Based on observations from 1995, Schauer et al. (2002b) reported a maximum potential temperature of 3 °C and a maximum salinity of 34.95 in the inflowing AW in the northwestern St. Anna Trough. In our dataset, a maximum potential temperature of 2 °C and a salinity of just above 34.9 is observed (not shown). This apparent decrease in temperature from 1995 to 2008 is a bit surprising, due to reports of a warming of the Atlantic layer in the Arctic Ocean since the 1990s (Quadfasel et al., 1991); (Schauer et al., 2004); (Polyakov et al., 2005); (Dmitrenko et al., 2008a). However, with only two, closely placed stations at the western entrance to the St. Anna Trough, we likely missed the core of inflowing AW, and this may at least partly explain the difference.

Above the layer of rAW, upper layers consisting of ARW and less saline Surface Water (SW; see Table 1) are observed. These upper layer water masses are advected into the St. Anna Trough from the Nansen Basin together with the rAW. Advection of ARW from the Nansen Basin through the St. Anna Trough and into the northeastern Barents Sea was suggested

by Novitsky (1961) and Tantsiura (1973). However, our focus is the intermediate and deep water masses. Therfore, ARW and SW will not be discussed further in this work.

At the western slope of the St. Anna Trough, the rAW extends from the pycnocline at 50-80 meter depth to the bottom, with maximum temperature at about 200 meter depth (not shown). Horizontally, rAW occupies the western and central St. Anna Trough at intermediate depths (Fig. 7), in agreement with the observations by Schauer et al. (2002b). Southwards in the St. Anna Trough it encounters CBW towards the bottom, resulting in a cold bottom layer with temperatures below 0 °C. This is manifested by a thinning of the rAW layer resulting from an uplift of the 0 °C isotherm defining the boundary between rAW and CBW. In central and eastern parts of the St. Anna Trough, the thickness of the rAW layer is about 100 meter less than in western parts. The reduction is due to larger amounts of colder water masses in the deeper parts. This thinner layer is probably rAW that is recirculating and flowing northwards back into the Nansen Basin.

Geostrophic velocities through section B show a very weak flow ($\sim$0.01 ms^{-1}) in the west, indicating mostly barotropic flow (not shown). In the central region, however, a bottom intensified northward flow related to the CBW is seen. Thus, there is a horizontal gradient in the baroclinic velocity field in section B, with northward baroclinic flow in the central region and southward baroclinic flow in the western St. Anna Trough.

A core of the rAW enters the WAT along its northern slope, following approximately the 200 meter isobath (see Fig. 5). A sharp thermal front is seen at the top of the slope, extending from the bottom to about 60 m

depth. Between this depth and the thermocline at about 20 m, is a layer with water masses slightly warmer than ARW, thus isolating the warm rAW from the surface mixed layer. This water mass is probably a mixture of ARW and rAW, both advected southward from the Nansen Basin. The core of the rAW, with potential temperature above 1 °C, is located between 100 and 250 meter depth. As the rAW is advected westward into the WAT, the temperature in the core decreases slightly, and only a fraction of the core has potential temperature exceeding 1 °C in the westernmost sections. In section 3 (Fig. 5, middle), two cores of rAW are seen, with the larger core located above the northern slope of the WAT, and a less distinct core located in the center of the trough. The distance between the two cores is ∼40 km, while the distance between the stations is ∼20 km. In order to tell whether the two cores represent inflow and ourflow of rAW or represent a mesoscale feature, we use a two-layer model to calculate the internal Rossby radius, R_i, at the stations where the two cores are observed. The internal Rossby radius of deformation represents the typical length scale of mesoscale dynamics, and is given by:

$$R_i = \frac{\sqrt{g'H}}{f} \tag{1}$$

where $f = 2\Omega sin\phi$ is the Coriolis parameter and ϕ is the latitude. g' is the reduced gravity, given by

$$g' = \frac{g(\rho_2 - \rho_1)}{\rho_1}, \quad \rho_2 > \rho_1 \tag{2}$$

We divide the water column into two water masses separated by the pycnocline. Thus, ρ_1 and ρ_2 represent the density above and below the pycnocline,

respectively, with typical values being $\rho_1 = 1027.5$ kgm^{-3} and $\rho_2 = 1028$ kgm^{-3}. The depth H is set to the height between the midpoints of the two layers, with a typical value of ∼150 m. By the use of this simplified model, we get R_i ∼9km at the stations where the two cores are observed. Thus, the distance between the two cores is considerably larger than the typical length scale of mesoscale features in this area, and we conclude that the lesser core is rAW flowing eastward after recirculating in the WAT. It is also worth noting that the distance between the stations is larger than the internal Rossby radius as well, and therefore mesoscale features are not resolved by the observations.

Mixing between rAW and CBW can be inferred from Θ-S diagrams. See e.g. Fig. 3, showing water masses along the mixing line between rAW and CBW (see idealized mixing line in Fig. 6). Direct current measurements from 1991/92 in section 3 (Loeng et al., 1993); (Schauer et al., 2002a); (Gammelsrød et al., 2009), revealed a vertical velocity shear in the WAT, with southwestward flow in the upper layers and northeastward flow in the deep parts. A calculation of geostrophic velocities through section 3 (Fig. 8) indicate such a baroclinicity in the cross-section velocity field. Gammelsrød et al. (2009) suggested that the vertical velocity shear is due to downslope acceleration of dense bottom water flowing eastward, which favors turbulent mixing between rAW and CBW.

We examined the interaction between rAW and CBW using a Θ-S diagram for stations 9 to 13 in section 1 (Fig. 9). These stations cover the narrow region where rAW is observed as a subsurface temperature maximum (Fig. 5; left) and the neighbouring stations to the north (station 13) and

south (station 9) where there is no influence of rAW. According to the strict definition in Table 1, rAW is only observed at one station (station 10), but the two neighbouring stations to the north also reveal a strong influence of rAW. The rAW creates an intermediate temperature maximum between an upper temperature minimum associated with ARW, and a deeper temperature minimum associated with CBW. The presence of rAW creates horizontal density gradients, with a local density minimum at stations where rAW is present (not shown). At the stations where influence of rAW is observed, the core of the CBW is warmer, more saline and deeper in the water column compared to neighbouring stations (Fig. 9). The characteristics of the core of rAW in the WAT shows that the rAW looses heat to its surroundings as it flows from the Nansen Basin to the northeastern Barents Sea, resulting in a drop in core temperature from at least 2 °C in the northwestern parts of St. Anna Trough (keeping in mind that the core is poorly sampled in this area) to 1 °C in the WAT.

In the southern part of section 5 (Fig. 5; right), a layer of rAW with $\Theta <$ 0.5 °C and $S < 34.8$ is observed. This is colder and slightly less saline than the core of rAW observed in the WAT, and is probably eastward flowing rAW that has recirculated in the WAT. A bit further east, just off the northern tip of Novaya Zemlya, there is a layer of rAW with $\Theta \sim$0.5 °C, located below a fresher and warmer layer of surface waters. Below this diluted rAW there is a 150 m thick layer of CBW above a 200 m thick layer of bAW. Thus, FSBW flowing into the St. Anna Trough follows the topography all the way to the southernmost part of the St. Anna Trough. This rAW is modified by ARW and CBW, resulting in a colder and less saline water mass than the main

core of rAW. There is little evidence of this water mass in the sections at 79°N and 81°N, indicating that only a relatively small amount of rAW enters the WAT, while the bulk of the rAW circulates as a warm, subsurface water mass in the main part of the St. Anna Trough and returns to the Nansen Basin.

3.2. Barents Atlantic derived Water

In section A, the Barents Atlantic derived Water in the Northeast Basin consists of two layers. A vertical profile of temperature in the Northeast Basin is shown in Fig. 10. In the upper layer, the temperature decreases with depth, from close to 1.5 °C near the surface layer to just above 1 °C in the lower part. Below the eastern sill-depth of the Northeast Basin ($\sim$ 200 m depth), a colder (Θ $\sim$0.6 °C), homogeneous layer of bAW is separated from the upper layer bAW by a sharp thermocline. Both layers exhibit similar salinity, $\sim$35.0. The high salinity, which is close to the salinity of inflowing Atlantic Water in the western Barents Sea (35.07 reported by Skagseth et al. (2008) as the long-term mean), and the relatively high temperature imply that the bAW observed in the Northeast Basin is formed by atmospheric cooling of Atlantic Water with very little input of freshwater. The homogeneity of the deep, below sill-depth layer of bAW suggests that this deeper bAW is either formed locally in the basin and/or has a longer residence time than the above sill-depth bAW.

At the northern slope of the Northeast Basin, a front separating bAW and CBW is observed (Fig. 11). As seen from the Θ-S diagram in Fig. 4, the potential density of the CBW is lower than that of bAW and the CBW is advected into the Northeast Basin on top of the bAW. Thus, the CBW

observed in 2008 was actually represented by an intermediate temperature minimum rather than a bottom temperature minimum. At the interface between the bAW and the CBW, vertical profiles of temperature and salinity indicate the presence of double diffusive processes (not shown), which according to Sundfjord et al. (2007) were observed to contribute significantly to vertical heat fluxes in frontal areas further to the west in the Barents Sea.

In the frontal area, located above the deepest part of section A (Fig. 11), a layer influenced by CBW is manifested by an intermediate temperature minimum of about 0 °C. The Θ-S properties (Fig. 4) indicate mixing between bAW and CBW in the frontal area, which reduces the temperature and salinity of the bAW. Vertical profiles of potential temperature and salinity (not shown) indicate that CBW penetrates southwards both at intermediate depths and at the bottom, leaving the bAW as a relatively deep temperature maximum. However, the temperature minimum (Θ $\sim$-0.1 °C) close to the bottom is far from the freezing point. Thus, the convection associated with ice freezing on the nearby banks the preceding winter (2007/08) did not reach the bottom.

In section 1 (Fig. 5; left), across the saddle point just east of the Northeast Basin, the bAW displays similar characteristics to those in section A. The core of the bAW, detected at 2 stations, is located on the shelf north of Novaya Zemlya, with a maximum potential temperature of 1.3 °C and a salinity of 35.0. As observed in section A, the bAW consists of two layers. The upper layer occupies the depths between the pycnocline (located at about 50 m depth) and a deep thermocline at about 150 m, and is characterized by temperatures decreasing with depth. The deeper layer consists of a 30 meter

deep, well-mixed bottom layer, with a potential temperature of 0.8 °C.

East of section 1, the bAW loses more of its heat, and in section 2 the maximum temperature in the bAW core has dropped down to 0.7 °C. Vertical profiles of potential temperature and salinity through the core of the bAW reveal substantial differences between sections 1 and 2 (Fig. 12). Influence from CBW has lowered both the temperature and salinity throughout the water column, and the temperature and salinity maxima associated with the bAW core are located deeper (120 m) in section 2 (station 30) compared to section 1 (80 m; station 6). At both stations, the bottom layer is well mixed, but at station 30 the bottom layer is thicker than at station 6. This suggests more mixing near the bottom at the easternmost of the two sections, which could be explained by larger velocities/acceleration as the bottom water is moving downslope into the WAT. In section 2, the eastward moving bAW encounters CBW that resides over a shallow bank north of Novaya Zemlya. This bank causes the core of the bAW to split in two; one core flows eastward along the southern slope of the WAT, while the other core is deflected south towards Novaya Zemlya, beneath the Novaya Zemlya Coastal Current (NZCC).

The bAW entering the WAT partly submerges under the CBW occupying the deep layers in central parts of the WAT (Fig. 5; middle and right). This changes the front separating bAW and CBW from a vertical front in section 1 to a tilted front in section 2 and further eastward (see Fig. 5 for sections 1, 3 and 5), resulting in both a horizontal and a vertical velocity shear, as has been observed by direct current measurements in section 3 (Loeng et al., 1993); (Schauer et al., 2002a); (Gammelsrød et al., 2009). This favors

mixing between bAW and CBW in the WAT. There is evidence of isopycnal interleaving between bAW and CBW in the deep parts of the WAT. At station 50, located at the deepest part of section 3, there are several local temperature maxima and minima in the lower 100 meters (Fig. 13). Thus, east of the saddle point separating the Northeast Basin from the St. Anna Trough, bAW is mixing with CBW throughout the water column below the pycnocline. The temperature of the bAW is reduced substantially as it is advected through the WAT, but a relatively high salinity is maintained, due to the relatively high salinity of the CBW (Fig. 5; right).

As the bAW is advected through the southern parts of the St. Anna Trough, the temperature is further reduced. In section B, the deep temperature maximum associated with the bAW is below 0 °C (Fig. 4, see also Fig. 7) and this water mass is therefore no longer categorized as bAW, although the deep temperature maximum together with the high salinity (above 34.9) indicate that this is remnants of the bAW. This points to further cooling of the bAW by mixing between bAW and CBW in the St. Anna Trough (see Fig. 4). Thus, all the AW advected through the Barents Sea on its way towards the Arctic Ocean is transformed into water masses with potential temperature lower than 0 °C before entering the Nansen Basin. Therefore, it may be argued that the bAW does not contribute with any heat gain to the Arctic Ocean, if one uses -0.1 °C as an overall potential temperature of the water masses leaving the Arctic Ocean, as proposed by Aagaard and Greisman (1975).

3.3. Cold Bottom Water

Dense bottom water produced in the Barents Sea is reported to contribute to the ventilation of intermediate and deep layers in the Arctic Ocean (Rudels et al., 1994); (Jones et al., 1995); (Bauch et al., 1995); (Schauer et al., 1997); (Rudels et al., 2000). Several formation sites of CBW in the eastern Barents Sea are reported in the literature: Novaya Zemlya Bank (Nansen, 1906); (Midttun, 1985); (Martin and Cavalieri, 1989), Great Bank and Central Bank (Blindheim, 1989); (Loeng, 1991); and the Franz Josef Land area Martin and Cavalieri (1989). Midttun (1985) observed dense bottom water produced over Novaya Zemlya Bank at the bottom in the Northeast Basin.

In section A (Fig. 11), CBW is found north of the Northeast Basin, on the banks south of Franz Josef Land. However, no remnants from dense water production on the Novaya Zemlya Bank is found near the bottom in the Northeast Basin, as mentioned above. The core of CBW is found at intermediate depths, from just below the pycnocline at 50 m to about 150 m, with a minimum Θ of -1.6 °C at 75-80 m. The temperature increases with depth below the temperature minimum, indicating influence of Atlantic water masses (Fig. 11). The Θ-S diagram from section A (Fig. 4) suggests that this is bAW advected into the relatively deep basin just southwest of Franz Josef Land. The other possible source of Atlantic Water in this area, is the FSBW that enters the Barents Sea from the north through the Franz-Victoria Trough between Franz Josef Land and Victoria Islands (see e.g Pfirman et al. (1994)). The FSBW would need to cool substantially to match the observed mixing line. Such cooling of the subsurface FSBW would require mixing with ARW (or CBW), but this would also lower the salinity of the FSBW. Thus,

the relatively high salinity and low temperature needed to match the observed mixing line from mixing with CBW exclude the possibility that FSBW is the source of AW in this mixture. For a discussion on the characteristics of the FSBW on the northern Barents Sea slope, see e.g. Løyning (2001).

As the CBW flows eastward into the WAT, it submerges under the rAW and forms a tilted front (Fig. 5; middle and right). This creates a vertical velocity shear and enhances the mixing between CBW and rAW. In the southern part of the WAT, mixing between CBW and bAW is observed, as described earlier. Mixing with rAW and bAW raises the temperature of the CBW substantially. CBW and rAW exhibit similar salinity, while the bAW is more saline, resulting in a slight increase in salinity. From the northeastern Barents Sea to the St. Anna Trough, the minimum potential temperature of the CBW increases from -1.6 °C to -0.6 °C (Fig. 4).

In the WAT, the CBW occupies the intermediate and deeper layers of the trough, while the slightly more dense bAW sinks to the very bottom of the trough. Thus, the CBW separates the two different Atlantic water masses. In this regard, the term "Cold Bottom Water" is misleading, as the bAW penetrates below the CBW, leaving this cold water mass as an intermediate temperature minimum. There are, however, some indications of relatively large variations in the water mass characteristics on timescales of years to decades. Gammelsrød et al. (2009) reported that the deeper part of the WAT was mostly occupied by CBW, with very little or no bAW.

Although the CBW enters the St. Anna Trough as an intermediate water mass, it is transformed to bottom water as it is advected northward toward the Arctic Ocean. At all stations north of 78°30'N in the central and eastern

parts of the St. Anna Trough, the water mass in the deeper part of the water column is categorized as CBW (not shown). On the eastern slope it occupies the whole water column below the pycnocline, which is consistent with the findings of Schauer et al. (2002a). Thus, the water mass termed Barents Sea Branch Water (BSBW) in e.g. Schauer et al. (2002b), and which is observed downstream in the Nansen and Amundsen basins, is a mixture of CBW, bAW, and rAW.

Our observations indicate several sources of CBW. The presence of CBW in section A (Fig. 11), suggests the banks south of Franz Josef Land as a source of CBW. Another source is the shelf between the WAT and Novaya Zemlya. Here, CBW is produced locally by ice freezing and subsequent brine release the preceding winter, resulting in a relatively high salinity ($S =$ 34.95). However, the potential temperature at the bottom is -0.58 °C, which indicates a relatively large component of bAW. With a potential density as high as $\sigma_\Theta = 28.09$, this CBW is more dense than the bAW observed in this area. On the contrary, the CBW advected into the WAT from the Barents Sea is less dense than the bAW, as mentioned above. The local character of this dense CBW is evident from looking at the idealized water masses and corresponding idealized mixing lines, as seen in Fig. 6. If one uses the characteristics of the bAW found in the section at 55°E (Θ=1 °C and S=35.0), mixing between bAW and CBW from the northeastern Barents Sea would produce water masses with a salinity below 34.9 at temperatures around -0.6 °C.

A water mass with characteristics close to the CBW observed north of Novaya Zemlya (0.02 °C lower potential temperature and 0.01 lower salinity)

is observed at the bottom in section C (Fig. 14). The similar characteristics suggest a common source, although this CBW was neither observed in sections 4 and 5 (Fig. 5; right), nor section B (Fig. 7). The direct current measurements from 1991/92 show episodes of strong eastward flow (around 0.15 ms^{-1}) in the WAT, typically lasting from one to a few days. We speculate that the CBW north of Novaya Zemlya is flushed into the St. Anna Trough in pulses, and that this explains the apparent cooling of 0.2 °C at the bottom between 79°N (section B) and 81°N (section C) in the St. Anna Trough, although no water mass that can explain such cooling is observed. However, due to the coarse sampling in the northern St. Anna Trough, the presence of CBW produced locally by freezing of sea-ice around Franz Josef Land cannot be ruled out. Such brine enriched bottom water with temperature at the freezing point could enter the St. Anna Trough directly. However, it would have to descend through the southward flowing rAW, and thereby become substantially warmer before reaching the bottom of the St. Anna Trough.

4. Discussion

The rAW observed in the WAT in 2008 has similar characteristics as the water mass termed the northern Barents Atlantic-derived Water in Pfirman et al. (1994), originating from the Atlantic Water entering the Barents Sea from the north through the Franz-Victoria Trough. Pfirman et al. (1994) and Løyning (2001) discuss the difference between what is termed the northern and southern Barents Atlantic-derived Water (corresponding to rAW and bAW, respectively), and suggest that the difference in the water mass char-

acteristics may be due to the different advection time between the "long way" around the Svalbard archipelago and the "shortcut" through the Barents Sea. Thus, although both water masses originate from the Norwegian Atlantic Current (NwAC), they are different "vintages" and may therefore exhibit different characteristics. This is probably even more so when they meet in the WAT, after the rAW has traveled around Franz Josef Land as well. Fig. 15 shows that there is large annual and interannual variability in temperature and salinity in the NwAC, as observed at the western entrance to the Barents Sea. However, Pfirman et al. (1994) and Løyning (2001) focused on the area farther west in the Barents Sea, where the southern Barents Atlantic-derived Water has not been subject to as much modifications as further downstream in the northeastern Barents Sea. Therefore, the signal from the variability in the initial state at the entrance to the Barents Sea is expected to be weaker in the northeastern Barents Sea than in the western and northern parts.

Interannual variability is also seen in the water masses in the northeastern Barents Sea. In 1991, only rAW and CBW were observed in the transect corresponding to our section 3 (Gammelsrød et al., 2009). We propose two explanations for the lack of bAW in 1991. First, more mixing between bAW and CBW in the Northeast Basin and/or in the WAT may have resulted in BSBW with temperatures below 0 °C in the WAT, as observed further downstream in the St. Anna Trough in 2008. Secondly, and probably more importantly, lower temperature in both the bAW and the CBW in the Northeast Basin would have influenced the water mass resulting from mixing between the two. Fig. 15 shows that the bAW in the northeastern Barents Sea in

1991 and 2008 would have different characteristics when entering the Barents Sea in the west. According to Midttun and Loeng (1987), this influences the rate at which CBW is produced. However, annual variability in both atmospheric and sea-ice conditions will influence the air-sea heat fluxes and the availability of freshwater from ice melt, modifying both the temperature and salinity of the bAW en route to the WAT. A comparison of the net air-sea heat fluxes in the Barents Sea (obtained from the ERA Interim data set, see http://www.ecmwf.int/research/era/do/get/era-interim) the preceding year in 2007-2008 and 1990-1991, respectively (Fig. 16), shows substantial differences in the cooling pattern between the two years. In 2007-2008, by far the largest heat loss to the atmosphere took place in the southwestern quartile. This spatial pattern is in agreement with other studies of climatological heat loss in the Barents Sea (Smedsrud et al., 2010); (Årthun and Schrum, 2010). In 1990-1991, however, the largest heat loss took place in the northeastern quartile. A time series of the net heat fluxes averaged over the entire Barents Sea (not shown) reveals a difference between 1990/91 and 2007/08 in the months October through January only. This suggests that the bAW was subject to an anomalous cooling during the winter prior to the observations in 1991. According to the climatology for the period 1990-2008 (not shown), the 1991 spatial pattern was anomalous, while 2008 was similar to the climatology, although the cooling was somewhat skewed towards southwest in 2008. This may also explain the apparently weak winter convection in the northeastern Barents Sea in 2007/08.

To further investigate the difference between 1991 and 2008, the atmospheric conditions and sea-ice distribution the preceding winter are examined.

Here, we use the months where the time series of net heat fluxes showed a difference between the two years, October through January. The wind is important for the opening of lee-polynyas, and thus enhance the heat loss from the ocean to the atmosphere and also the production of sea-ice (see e.g. Morales Maqueda et al. (2004)). Fig. 17 shows a difference in the dominating wind direction in the Novaya Zemlya Bank area in the winter 1990/91 and the winter 2007/08. The offshore, southeasterly winds in 1990/91 favor polynya activity on the Novaya Zemlya Bank, while the alongshore, southwesterly winds in 2007/08 are less favorable for polynya activity. However, according to Fig. 16, the anomalous heat loss to the atmosphere in 1991 took place within the ice-free part of the eastern Barents Sea. Investigation of ice distribution (not shown), reveals less ice in the WAT, the Northeast Basin and over the Novaya Zemlya Bank in 2007/08 compared to 1990/91. This points to another mechanism than polynya activity explaining the anomalous cooling: the easterly winds in 1991 advected cold air masses from the east into the northeastern Barents Sea, while the southwesterly winds in winter 2007/08 brought warm and moist air from the Norwegian Sea into the northeastern Barents Sea, reducing the heat loss to the atmosphere in the winter 2007/08 compared to 1990/91. We are, however, aware that the conclusion of this investigation is weakened by both the spatial (1.5 times 1.5 degrees in longitude and latitude) and temporal (monthly averages) resolution of the data.

As the FSBW and BSBW meet again in the northern Kara Sea, both have undergone modifications which have resulted in different characteristics. According to Dmitrenko et al. (2009), the FSBW core typically has

a σ_Θ of 27.92. Although the rAW is modified in the St. Anna Trough and becomes colder and less saline due to mixing with surrounding water masses, the potential density is maintained, indicating isopycnal mixing. The BSBW is a product of both CBW, bAW, and rAW, and changes in the characteristics of these water masses may alter the characteristics of the BSBW further downstream. As discussed above, the characteristics of the bAW and the availability and characteristics of CBW in the northeastern Barents Sea varies from year to year. The BSBW is reported to be colder and less saline than the FSBW when it enters the Nansen Basin (e.g. Dmitrenko et al. (2009)). Although less saline, the lower potential temperature gives the BSBW a higher potential density than the FSBW, with a typical σ_Θ of 27.97 (Dmitrenko et al., 2009). However, Dmitrenko et al. (2009) also reported an increase in σ_Θ from 27.98 in 2005 to 28.02 in 2006, resulting from both a decrease in temperature (0.41 °C colder) and an increase in salinity (0.04 more saline). As seen in Fig. 15, the salinity of the inflowing Atlantic Water in the western Barents Sea peaked in 2006. In lack of any reliable estimates of advection time through the Barents Sea, we claculate an advection time of $\sim$1 year based on a distance of $\sim$1500 km between the western entrance to the Barents Sea and the Northeast Basin (assuming that the AW is advected via the Central Basin) and assuming an advection speed of 5 cms^{-1}. This implies that the salinity in the western Barents Sea influences the water mass properties of the bAW entering the WAT a year later. Advection from the WAT to the Nansen Basin require a further increase in advection time.

In the Nansen Basin, the BSBW is defined by an intermediate temperature and salinity minimum, and is easily identifiable in the Θ-S space

(Schauer et al., 2002b); (Dmitrenko et al., 2009). This characteristic Θ-S signature is also seen in the St. Anna Trough at 79°N and 81°N (not shown), and corresponds well to the BSBW core characteristics and potential density presented by Dmitrenko et al. (2009). However, the BSBW defined by a temperature and salinity minimum represents only the intermediate layer in the St. Anna Trough. In section B, the signature of the bAW, seen as a deep temperature maximum, is observed below the BSBW core (Fig. 4). Below the bAW, the bottom layer in the deep central parts of the St. Anna Trough is occupied by a water mass with constant salinity and temperature decreasing with depth, with similar characteristics as the CBW observed north of Novaya Zemlya (Fig. 14). Within the WAT, the mean σ_Θ of the bAW is 28.06 (Table 2), which is substantially higher than the typical potential density of the BSBW (27.97). Thus, the bAW is not only contributing to the maintenance of the water mass identified as the BSBW in the Nansen Basin, but it also contributes to water masses below the BSBW core.

The bottom layer observed in the St. Anna Trough in 2008 has a slightly higher potential density than reported in other recent work. The maximum σ_Θ of 28.09 observed in section C is higher than the maximum σ_Θ of 28.05 observed in the St. Anna Trough in 1996 (Schauer et al., 2002a) and as high as observed in 1965 (Hanzlick and Aagaard, 1980), although no evidence of high-salinity bottom water formed by sea-ice freezing in the northeastern Barents Sea is found. It is well documented that the NwAC follows the multidecadal oscillation of temperature in the North Atlantic (Sutton and Hodson, 2005). The temperature variability in the Barents Sea is also closely linked to this oscillation (Skagseth et al., 2008); (Levitus et al., 2009), as observed in the

Kola section (Tereshchenko, 1997), with the last decade being well inside a warm phase (Fig. 18). In a warmer climate with less ice freezing in the Barents Sea, one expects less production of CBW. However, our observations indicate that less high salinity CBW in the mixing process producing BSBW can be compensated by increased salinity of the inflowing AW in the western Barents Sea and reduced fresh water input from ice melt, resulting in an increase in the salinity of the bAW. As observed in this dataset, this can produce water masses that, according to Fig. 6 in Rudels et al. (2000), is dense enough to sink down to at least 2000 m depth in the Arctic Ocean and thereby ventilate the deep water masses.

5. Summary and conclusions

Data from a total of 142 CTD-casts covering the northeastern Barents Sea and the St. Anna Trough are analyzed and presented. Two modes of Atlantic Water with $\Theta > 0$ °C are observed in the area between Novaya Zemlya and Franz Josef Land. One mode consists of AW originating from the FSBW flowing eastward along the continental slope in the Arctic Ocean. This water mass, with a potential temperature well above 0 °C, enters the St. Anna Trough and circulates at intermediate depth within the trough. A fraction of this water mass is observed in the western St. Anna Trough between Novaya Zemlya and Franz Josef Land, where it mixes with CBW flowing eastwards from the Barents Sea. The other mode consists of AW that is modified during its advection through the Barents Sea. Contrary to earlier reports, the bAW has $\Theta > 0$ °C when it exits the Barents Sea. On its way toward the Arctic Ocean, the bAW mixes with CBW and forms what

is commonly termed BSBW, which has been observed downstream in the Nansen Basin.

There are three important factors determining the properties of the end product (BSBW): *i*) the initial water mass characteristics of the Atlantic Water entering the Barents Sea in the west; *ii*) the processes that modify the Atlantic Water on its way towards the Arctic Ocean; and *iii*) the water mass properties and availability of cold and saline water masses resulting from winter convection in the northeastern Barents Sea. Assessing the relative importance of these factors calls for further investigation. Thus, there is a need for more observations to study interannual variability of bAW and CBW, and to better understand the processes by which BSBW is formed in the St. Anna Trough. However, the data we have presented indicate that anomalies in two of the factors can compensate for an anomaly of opposite sign in the third factor. Therefore, the BSBW produced during a warm phase in the Barents Sea, may still be dense enough to ventilate the deep parts of the Arctic Ocean.

6. Acknowledgments

This work has been supported by the Norwegian Research Council through the IPY project Bipolar Atlantic Thermohaline Circulation (BIAC, grant no. 176082, IPY Cluster no. 23). Ilker Fer and Ken Drinkwater are acknowledged for constructive comments which helped improve the manuscript. The authors wish to thank the captains and crews onboard the R/V 'Fridtjof Nansen', R/V 'Professor Boyko' and 'Obva' for their good cooperation and hospitality.

References

Aagaard, K. and P. Greisman, "Toward new mass and heat budgets for the Arctic Ocean", *J. Geophys. Res.*, **80**(27), 3821-3827 (1975)

Aagaard, K., L.K. Coachman and E.C. Carmack, "On the halocline of the Arctic Ocean", *Deep-Sea Res. Part A*, **28**, 529-545 (1981)

Aagaard, K., A. Foldvik and S.R. Hillman, "The West Spitsbergen Current: Disposition and Water Mass Transformation", *J. Geophys. Res.*, **92**(C4), 3778-3784 (1987)

Bauch, D., P. Schlosser and R.G. Fairbanks, "Freshwater balance and the sources of deep and bottom waters in the Arctic Ocean inferred from the distribution of $H_2\,{}^{18}O$", *Prog. Oceanogr.*, **35**, 53-80 (1995)

Blindheim, J., "Cascading of Barents Sea bottom water into the Norwegian Sea", *ICES/CIEM*, **188**, 49-58 (1989)

Coachman, L.K. and C.A. Barnes, "Surface waters in the Eurasian Basin of the Arctic Ocean", *Arctic*, **15**, 251-277 (1963)

Dmitrenko, I. A., S. A. Kirillov, V. V. Ivanov and R. Woodgate, "Mesoscale Atlantic water eddy off the Laptev Sea continental slope carries the signature of upstream interaction", *J. Geophys. Res.*, **113**, C07005 (2008b) doi: 10.1029/2007JC004491

Dmitrenko, I. A., I. V. Polyakov, S. A. Kirillov, L. A. Timokhov, I. E. Frolov, V. T. Sokolov, H. L. Simmons, V. V. Ivanov and D. Walsh "Toward a warmer Arctic Ocean: Spreading of the early 21st century Atlantic Water

warm anomaly along the Eurasian Basin margins", *J. Geophys. Res.*, **113**, C05023 (2008a) doi: 10.1029/2007JC004158

Dmitrenko, I. A., D. Bauch, S. A. Kirillov, N. Koldunov, P. J. Minnett, V. V. Ivanov, J. A. Höleman and L. A. Timokhov, "Barents Sea upstream events impact the properties of Atlantic water inflow into the Arctic Ocean: Evidence from 2005 to 2006 downstream observations", *Deep-Sea Res. I*, **56**, 513-527 (2009) doi: 10.1016/j.dsr.2008.11.005

Gammelsrød, T., Ø. Leikvin, V. Lien, W. P. Budgell, H. Loeng and W. Maslowski, "Mass and heat transports in the NE Barents Sea: Observations and models", *J. Mar. Sys.*, **75**, 56-69 (2009) doi: 10.1016/j.jmarsys.2008.07.010

Hanzlick, D., K. Aagaard, "Freshwater and Atlantic Water in the Kara Sea", *J. Geophys. Res.*, **85(C9)**, 4937-4942 (1980)

Jones, E.P. and L.G. Anderson, "On the origin of the chemical properties of the Arctic Ocean halocline", *J. Geophys. Res.*, **91**, 10759-10767 (1986)

Jones, E. P., B. Rudels and L. G. Anderson, "Deep waters of the Arctic Ocean: origins and circulation", *Deep-Sea Res. I*, **42(5)**, 737-760 (1995)

Kärcher, M., M. Kulakov, S. Pivovarov, U. Schauer, F. Kauker and R. Schlitzer, "Atlantic Water flow to the Kara Sea: Comparing model results with observations", In: *Siberian River Run-off in the Kara Sea: Characterisation, Quantification, Variability and Environmental Significance [Stein, R., K. Fahl, D.K. Fütterer and E. Galimov (Eds.)]*, Proceedings in Marine Science, pp. 47-69 (2003)

Kvingedal, B., "Sea-Ice Extent and Variability in the Nordic Seas, 1967-2002", In: *The Nordic Seas: An integrated perspective [Drange, H., T. Dokken, T. Furevik, R. Gerdes and W. Berger (Eds.)], Geophysical Monograph Series*, **158**, AGU, Washington DC, 39-50 (2005)

Levitus, S., G. Matishov, D. Seidov and I. Smolyar, "Barents Sea multidecadal variability", *Geophys. Res. Lett.*, **36**, L19604 (2009) doi:10.1029/2009GL039847

Loeng, H., "Features of the physical oceanographic conditions of the Barents Sea", *Pol. Res.*, **10**, 5-18 (1991)

Loeng, H., V. Ozhigin, B. Ådlandsvik and H. Sagen, "Current measurements in the northeastern Barents Sea", *ICES CM*, **40**, 22pp (1993)

Løyning, T.B., "Hydrography in the north-western Barents Sea, July-August 1996", *Polar. Res.*, **20(1)**, 1-12 (2001)

Martin, S. and D.J. Cavalieri, "Contributions of the Siberian shelf polynyas to the Arctic Ocean Intermediate and Deep Water", *J. Geophys. Res.*, **94**, 12725-12738 (1989)

Matishov, G.G., D.G. Matishov and D.V. Moiseev, "Inflow of Atlantic-origin waters to the Barents Sea along glacial troughs", *Oceanologia*, **51**, 321-340 (2009)

Maslowski, W., D. Marble, W. Walczowski, U. Schauer, J.L. Clement and A.J. Semtner, "On climatological mass, heat, and salt transports through the Barents Sea and Fram Strait from a pan-Arctic coupled ice-ocean model simulation", *J. Geophys. Res.*, **109**, C03032 (2004)

Meincke, J., B. Rudels and H.J. Friedrich, "The Arctic Ocean - Nordic Seas thermohaline circulation", *ICES J. Mar. Sci.*, **54(3)**, 283-299 (1997)

Midttun, L., "Formation of dense bottom water in the Barents Sea", *Deep-Sea Res. A*, **32**, 1233-1241 (1985)

Midttun, L. and H. Loeng, "Climatic variations in the Barents Sea", In: *The effect of oceanographic conditions on the distribution and population dynamics of commercial fish stocks in the Barents Sea [Loeng, H. (Ed.)]*, Third Soviet-Norwegian symposium. Murmansk, May 1986, pp. 13-28 (1987)

Morales Maqueda, M.A., A.J. Willmott and N.R.T. Biggs, "Polynya dynamics: A review of observations and modeling", *Rev. Geophys.*, **42**, RG1004 (2004) doi:10.1029/2002RG000116

Mosby, H., "Svalbard Waters", *Geofysiske publikasjoner*, **12(4)**, 1-85 (1938)

Nansen, F., "Northern waters: Captain Roald Amundsens oceanographic observations in the Arctic seas in 1901", *Vitenskabs-Selskapets Skrifter,* **1**, Mathematisk-Naturv. Klasse., 3, 145pp (1906)

Novitsky, V. P., "Permanent currents of the Northern Barents Sea", *Trudy Gosudarstvennogo Okeanograficheskogo Instituda*, **64**, 1-32, Translated by U.S.N.O. 1967, Leningrad (1961)

Ozhigin, V.K. and V.A. Ivshin, "Water masses of the Barents Sea", *PINRO Press*, in Russian, Murmansk, 48 pp (1999)

Ozhigin, V.K., A.G. Trofimov and V.A. Ivshin, "The Eastern Basin Water and currents in the Barents Sea", *ICES CM*, **2000/L:14**, 19 pp (2000)

Panteleev, G., M. Ikeda, A. Grotov, D. Nechaev and M. Yaremchuk, "Mass, Heat and Salt Balances in the Eastern Barents Sea Obtained by Inversion of Hydrographic Section Data", *J. Oceanogr.*, **60**, 613-623 (2004)

Polyakov, I., A. Beszczynska, E. Carmack, E. Dmitrenko, E. Fahrbach, I. Frolov, R. Gerdes, E. Hansen, J. Holfort, V. Ivanov, M. Johnson, M. Kärcher, F. Kauker, J. Morison, K. Orvik, U. Schauer, H. Simmons, Ø. Skagseth, V. Sokolov, M. Steele, L. Timokhov, D. Walsh and J. Walsh, "One more step toward a warmer Arctic", *Geophys. Res. Lett.*, **32 (17)**, L17605 (2005) doi: 10.1029/2005GL023740

Pfirman, S. L., D. Bauch and T. Gammelsrød, "The Northern Barents Sea: Water Mass Distribution and Modification", In: *The Polar Oceans and their Role in Shaping the Global Environment [Johannessen, O. M., R. D. Muench and J. E. Overland (Eds.)], Geophysical Monograph Series*, **84**, AGU, Washington DC, 77-94 (1994)

Quadfasel, D., B. Rudels and S. Selchow, "Outflow of dense water from a Svalbard fjord into the Fram Strait", *Deep-Sea Res. Part A*, **35**, 1143-1150 (1988)

Quadfasel, D., A. Sy, D. Wells and A. Tunik, "Warming in the Arctic", *Nature*, **350**, 350 (1991)

Rudels, B., E. P. Jones, L. G. Anderson and G. Kattner, "On the Intermediate depth waters of the Arctic Ocean", In: *The Polar Oceans and*

their Role in Shaping the Global Environment [Johannessen, O. M., R. D. Muench and J. E. Overland (Eds.)], Geophysical Monograph Series, **84**, AGU, Washington DC, 33-46 (1994)

Rudels, B., H.J. Friedrich and D. Quadfasel, "The Arctic Circumpolar Boundary Current", *Deep-Sea Res. II*, **46**, 1023-1062 (1999)

Rudels, B., R.D. Muench, J. Gunn, U. Schauer and H.J. Friedrich, "Evolution of the Arctic boundary current north of the Siberian shelves", *J. Mar. Sys.*,**25**, 77-99 (2000)

Rudels, B., E.P. Jones, U. Schauer and P. Eriksson, "Atlantic sources of the Arctic Ocean surface and halocline waters", *Pol. Res.*, **23(2)**, 181-208 (2004)

Schauer, U., R.D. Muench, B. Rudels and L. Timokhov, "Impact of eastern Arctic shelf water on the Nansen Basin intermediate layers", *J. Geophys. Res.*, **102**, 3371-3382 (1997)

Schauer, U., H. Loeng, B. Rudels, V. K. Ozhigin and W. Dieck, "Atlantic water inflow through the Barents and Kara Seas", *Deep Sea Res. I*, **49**, 2281-2298 (2002a)

Schauer, U., B. Rudels, E. P. Jones, L. G. Anderson, R. D. Muench, G. Bjørk, J. H. Swift, V. Ivanov and A.-M. Larsson, "Confluence and redistribution of Atlantic water in the Nansen, Amundsen and Makarov basins", *Ann. Geophys.*, **20(2)**, 257-273 (2002b)

Schauer, U., E. Fahrbach, S. Østerhus and G. Rohardt, "Arctic warming

through the Fram Strait: Oceanic heat transport from 3 years of measurements", *J. Geophys. Res.*, **109**, C06026 (2004) doi: 10.1029/2003JC001823

Simonsen, K. and P.M. Haugan, "Heat budgets of the Arctic Mediterranean and sea surface heat flux parameterizations for the Nordic Seas", *J. Geophys. Res.*, **101**, 6553-6576 (1996)

Skagseth, Ø., T. Furevik, R. Ingvaldsen, H. Loeng, K. A. Mork, K. A. Orvik and V. Ozhigin, "Volume and heat transports to the Arctic via the Norwegian and Barents Seas", In: *Arctic-Subarctic Ocean fluxes. In: Defining the role of the Northern Seas in Climate [Dickson, R., J. Meincke and P. Rhines (Eds.)]*, Springer, Netherlands (2008) doi: 10.1007/978-1-4020-6774-7

Smedsrud, L.H., R. Ingvaldsen, J.E.Ø. Nilsen and Ø. Skagseth, "Barents Sea heat-transport, storage and surface fluxes", *Ocean Sci.*, **6**, 291-234 (2010)

Smolyar, I. and N. Adrov, "The quatitative definition of the Barents Sea Atlantic Water: mapping of the annual climatic cycle and interannual variability", *ICES J. Mar. Sci.*, **60**, 836-845 (2003)

Steele, M., J.H. Morison and T.B Curtin, "Halocline water formation in the Barents Sea", *J. Geophys. Res.*, **100**, 881-894 (1995)

Sundfjord, A,. I. Fer, Y. Kasajima and H. Svendsen, "Observations of turbulent mixing and hydrography in the marginal ice zone of the Barents Sea", *J. Geophys. Res.*, **112**, C05008 (2007) doi: 10.1029/2006JC003524

Sutton, R.T. and D.L.R. Hodson, "Atlantic forcing of the North American and European Summer Climate", *Science*, **309**, 115-118 (2005)

Tantsiura, A. I., "On Seasonal changes in currents in the Barents Sea", *Transactions of the Polar Scientific Research Institute of Marine Fisheries and Oceanography* - N. M. Knipovic (PINRO), in Russian, translated to English by the Norwegian Polar Research Institute, Tromsø (1973)

Tereshchenko, V.V., "Seasonal and year-to-year variation in temperature and salinity of the main currents along the Kola section in the Barents Sea", *Murmansk: PINRO Publ.*, in Russian, 71pp. (1997)

Woodgate, R.A., K. Aagaard, R.D. Muench, J. Gunn, G. Björk, B. Rudels, A.T. Roach and U. Schauer, "The Arctic Ocean Boundary Current along the Eurasian slope and the adjacent Lomonosov Ridge: Water mass properties, transports and transformations from moored instruments", *Deep-Sea Res. I*, **48**, 1757-1792 (2001)

Årthun, M. and C. Schrum, "Ocean surface heat flux variability in the Barents Sea", *J. Mar. Sys.*, accepted (2010)

Table 1: Water mass definitions and abbreviations used in the text.

Abbr.	Water mass	Θ (°C)	Salinity
SW	Surface Water	$T > -1$	$S < 34.3$
ARW	Arctic Water	$T < -1$	$34.3 < S < 34.7$
AW	Atlantic Water	$T > 0$	$S > 34.75$
bAW	Barents Atlantic derived Water	$T > 0$	$S > 34.9$
rAW	Recirculating Atlantic Water	$0.5 < T < 1.5$	$34.75 < S < 34.9$
CBW	Cold Bottom Water	$T < 0$	$S > 34.75$
Abbr.	Full name	Description	
BSBW	Barents Sea Branch Water	Barents Sea branch of the Atlantic layer in the Arctic Ocean	
FSBW	Fram Strait Branch Water	Fram Strait branch of the Atlantic layer in the Arctic Ocean	
NwAC	Norwegian Atlantic Current		
WAT	Western St. Anna Trough	Western branch of St. Anna Trough between Novaya Zemlya and Franz Josef Land	
NZCC	Novaya Zemlya Coastal Current		
WSC	West Spitsbergen Current		

Table 2: Core water mass characteristics in the northeastern Barents Sea. The ± denotes one standard deviation

Water mass	Θ (°C)	Salinity	σ_Θ
bAW	0.40 ± 0.26	34.97 ± 0.02	28.06 ± 0.02
rAW	0.85 ± 0.21	34.82 ± 0.03	27.91 ± 0.02
CBW			

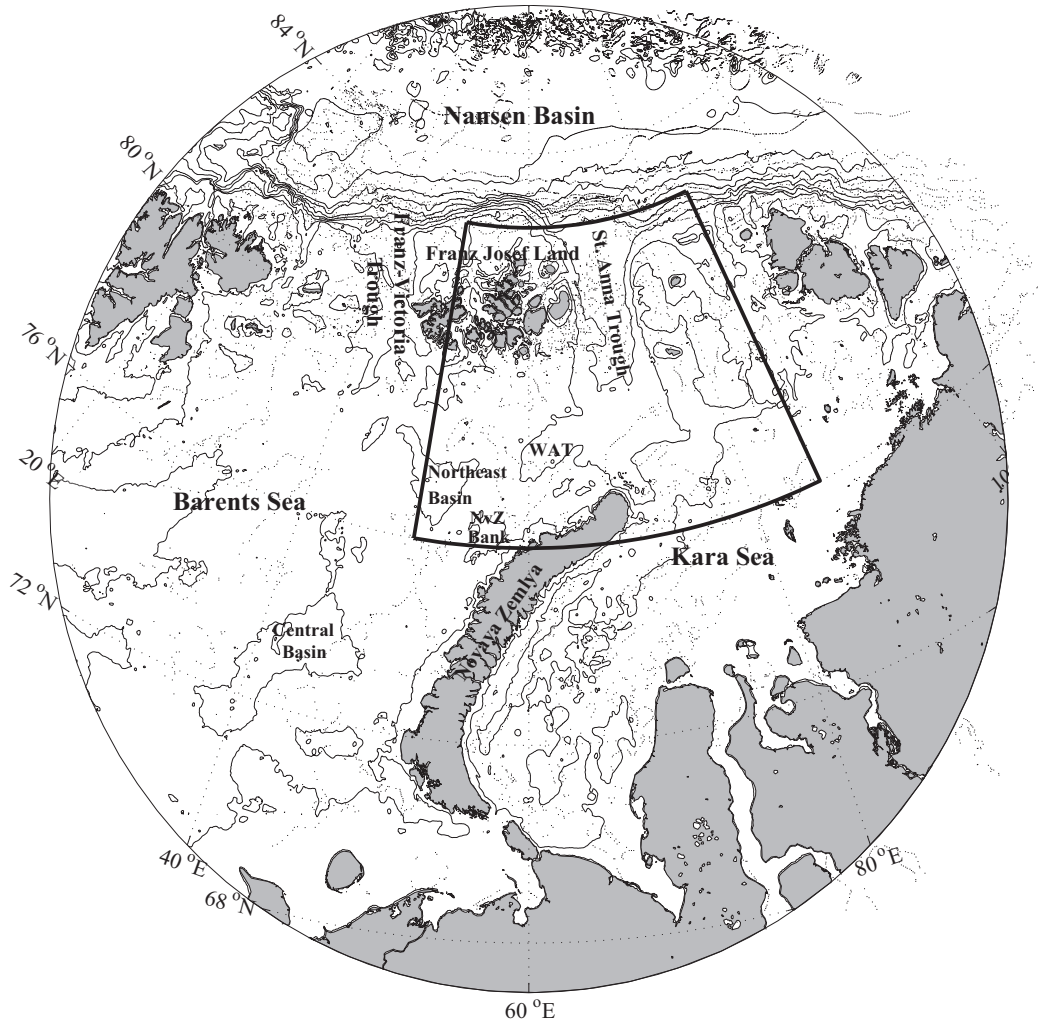

Figure 1: Bathymetric map of the Barents and Kara Seas. The marked box shows area of study (see Fig. 2).

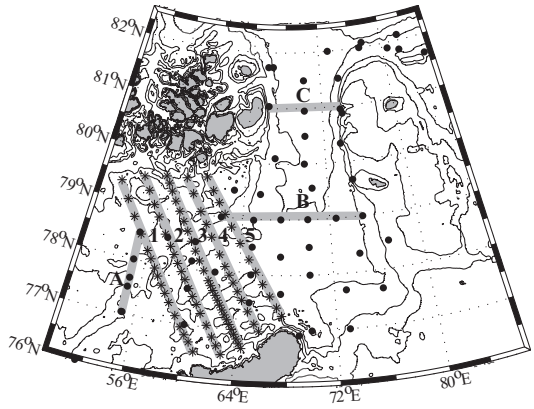

Figure 2: Bathymetric map showing the positions of the CTD-stations from the R/V "Professor Boyko" (stars) and "Obva" (dots). Sections discussed in the text are shown by thick, grey lines.

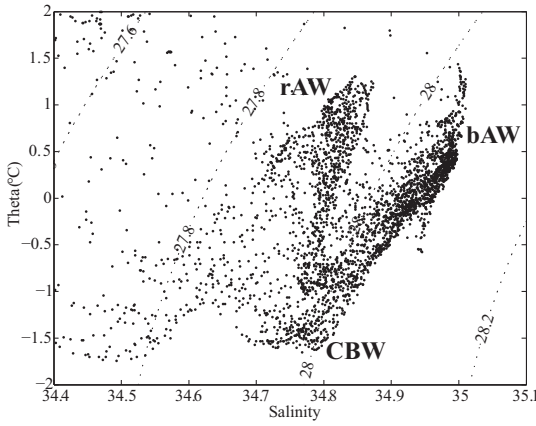

Figure 3: Θ-S diagram of all stations taken by R/V "Professor Boyko" 2008: rAW: Recirculating Atlantic Water; bAW: Barents Atlantic derived Water; CBW: Cold Bottom Water. See Table 1 for water mass definitions.

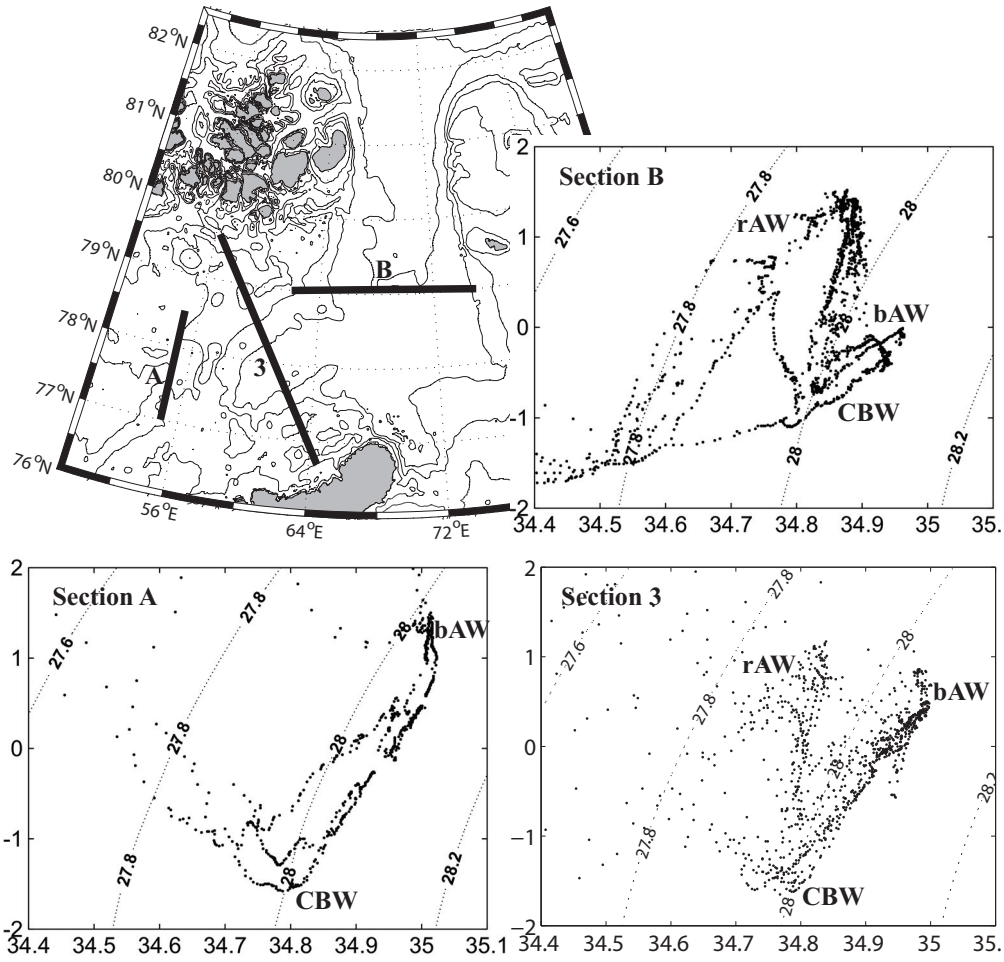

Figure 4: Θ-S diagrams for sections A, 3, and B, showing the origin and modification of recirculating Atlantic Water (rAW), Barents Atlantic derived Water (bAW) and Cold Bottom Water (CBW). See Table 1 for water mass definitions.

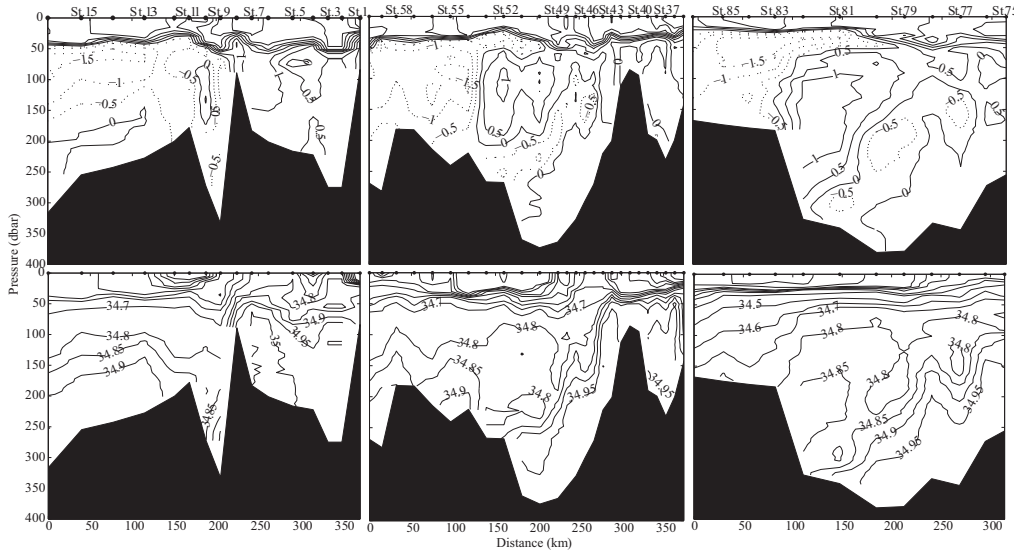

Figure 5: Vertical sections of potential temperature (top) and salinity (bottom) in section 1 (left), section 3 (middle), and section 5 (right). (South/Novaya Zemlya towards right.)

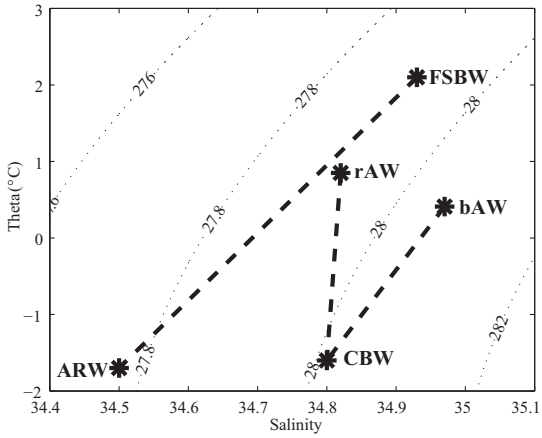

Figure 6: Idealized water masses in the northeastern Barents Sea: Fram Strait Branch Water (FSBW) as observed in northwestern St. Anna Trough; recirculated Atlantic Water (rAW); Barents Atlantic derived Water (bAW); Cold Bottom Water (CBW) as observed at 55E; Arctic Water (ARW). Note that rAW and bAW are represented by their mean characteristics, while CBW and ARW are represented by their characteristics at their respective temperature minima. Broken lines indicate mixing lines.

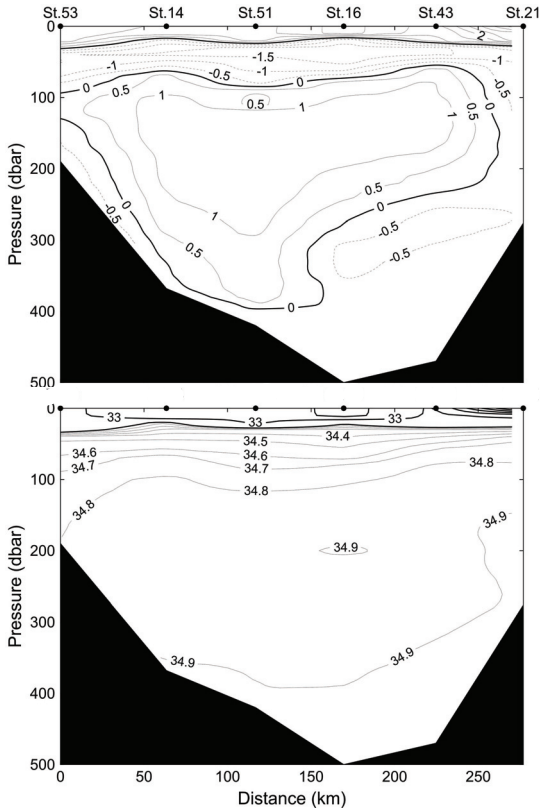

Figure 7: Vertical sections of potential temperature (top) and salinity (bottom) in section B. (East towards right)

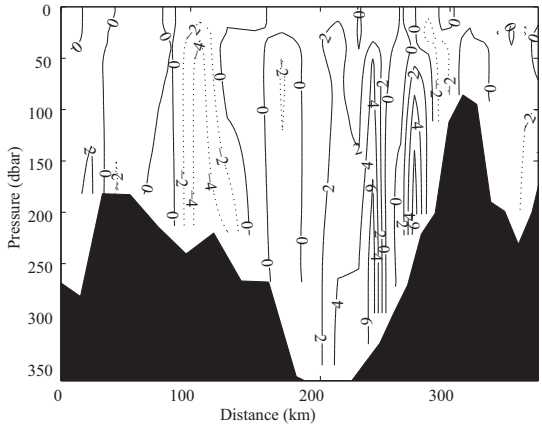

Figure 8: Geostrophic velocities (cms^{-1}) through section 3 in 2008. Zero velocity is assumed at the surface. (South/Novaya Zemlya towards right)

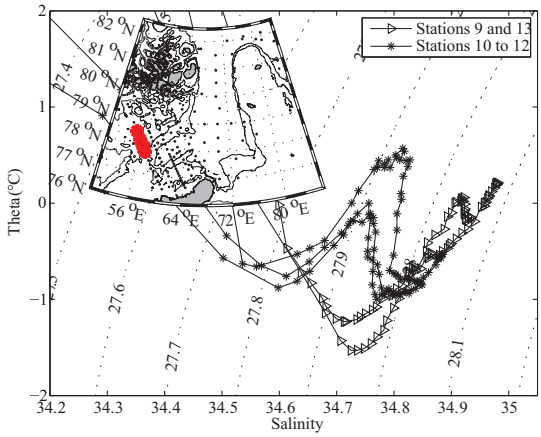

Figure 9: Θ-S diagram for stations 9 to 13 in section 1. Stars show stations with recirculated AW (stations 10-12) and triangles show stations with Barents derived AW (stations 9 and 13). Red stars show stations positions.

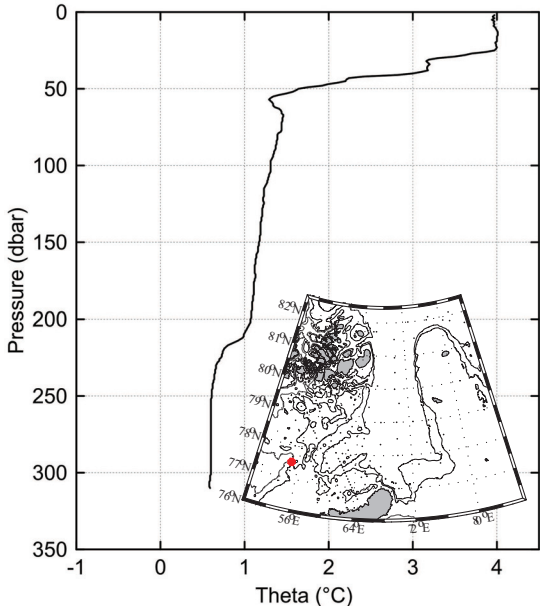

Figure 10: Potential temperature at station 3, in the section along 55E. Red star shows station position.

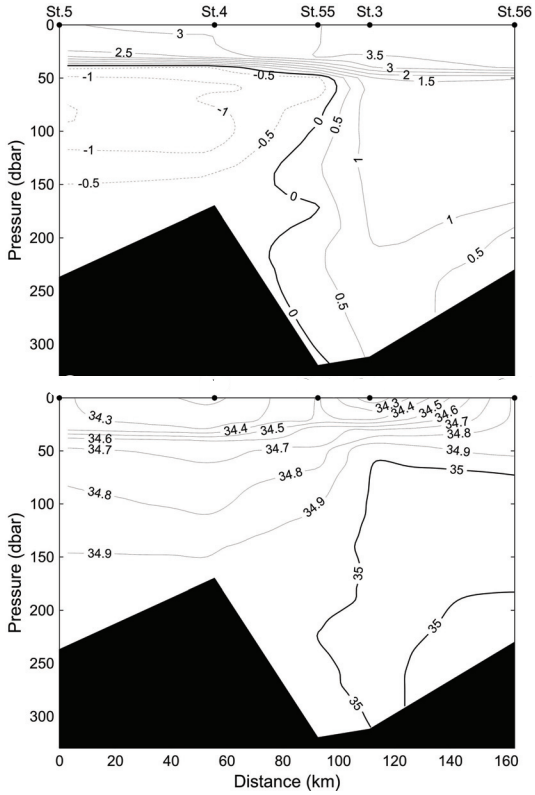

Figure 11: Vertical sections of potential temperature (top) and salinity (bottom) in section A. (South towards right.)

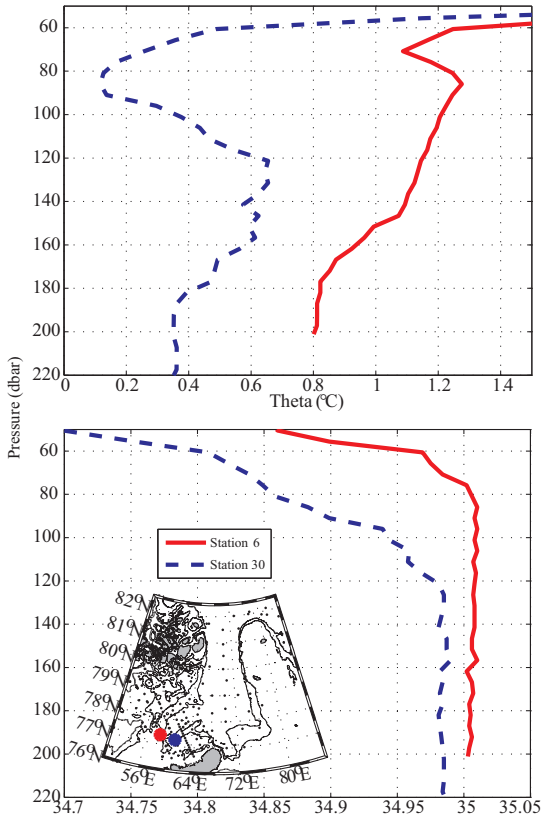

Figure 12: Vertical profiles of potential temperature (top) and salinity (bottom) at station 6 (section 1; solid, red line) and station 30 (section 2; broken, blue line). Stars show station positions.

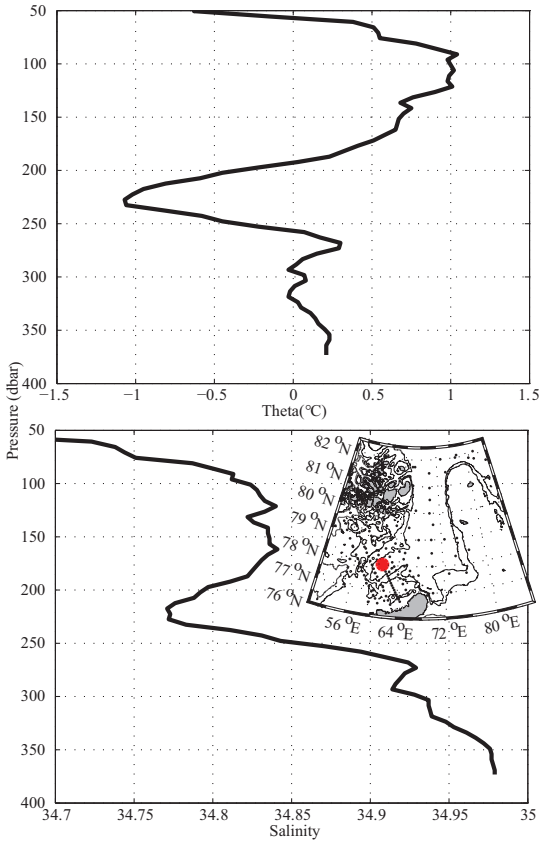

Figure 13: Vertical profile of potential temperature (top) and salinity (bottom) at station 50 (section 3). Red star shows station position.

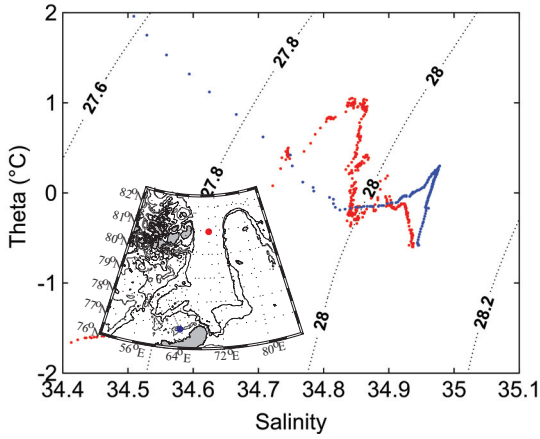

Figure 14: Θ-S diagram at stations 37 in the Boyko-dataset (blue; north of Novaya Zemlya) and 27 in the Obva-dataset (red; central St. Anna Trough). Stars show station positions.

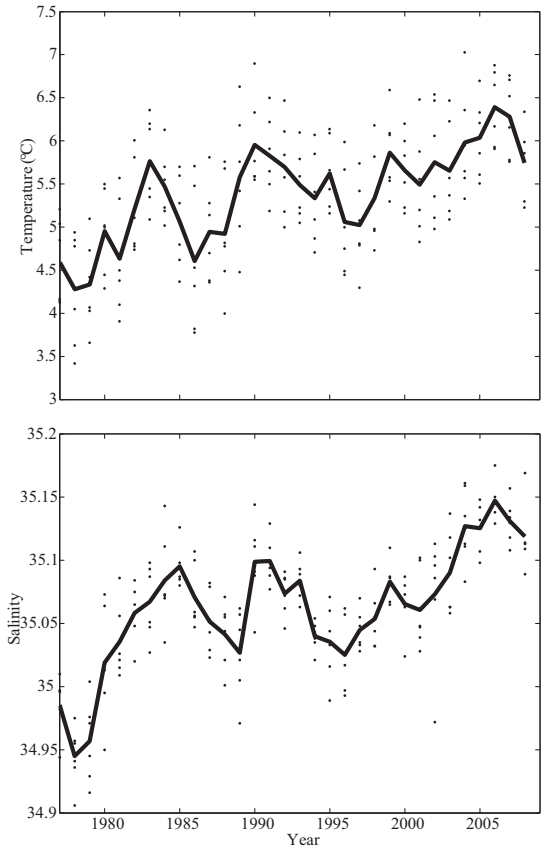

Figure 15: Average temperature (top) and salinity (bottom) between 50 and 200 meter from 71 30'N to 73 30'N in at the western entrance to the Barents Sea. Thick lines show yearly averages.

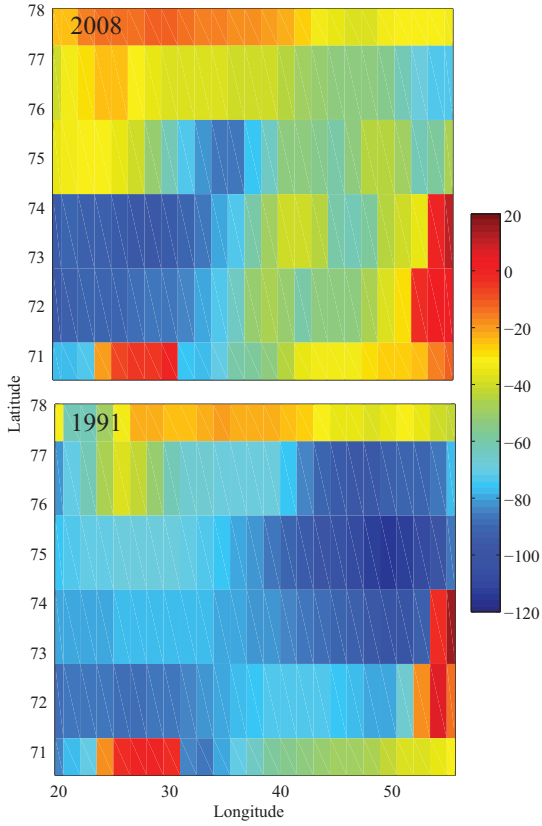

Figure 16: Average air-sea heatfluxes (Wm^{-2}) in the Barents Sea (20°E - 55°E; 71°N - 78°N) in the period October 2007 - September 2008 (top) and October 1990 - September 1991 (bottom). From ERA Interim.

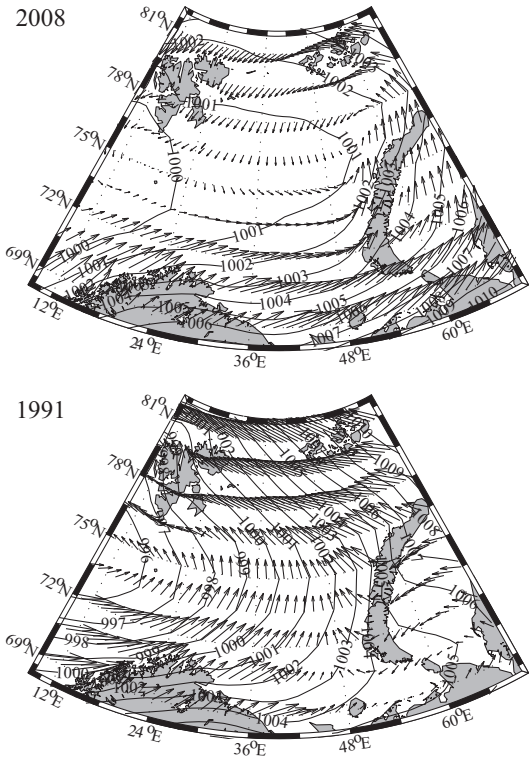

Figure 17: Mean sea level pressure and winds in the Barents Sea in the period October 2007 - January 2008 (top) and October 1990 - January 1991 (bottom). From ERA Interim.

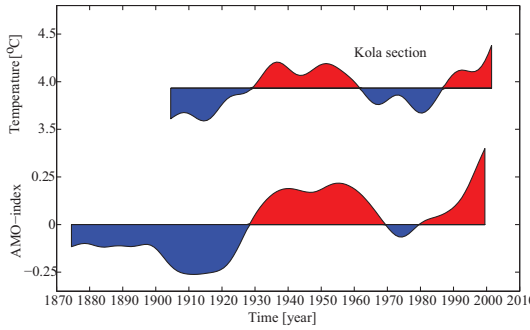

Figure 18: Time series of the Kola section mean temperature (upper graph) and the Atlantic Multidecadal Oscillation (AMO) index (lower graph). From Skagseth et al., 2008

Paper III

V.S. Lien and B. Ådlandsvik
The Barents Sea Polar Front - a model study
Manuscript

III

The Barents Sea Polar Front - A model study

Vidar S. Lien*,[a], Bjørn Ådlandsvik[a]

[a]*Institute of Marine Research, Nordnesgaten 33, 5817 Bergen, Norway.*

Abstract

The Barents Sea Polar Front is a dominating feature in the western Barents Sea. It forms the transition zone between the relatively warm and salty Atlantic Water in the south and the cold and fresh Arctic Water in the north. Here, we utilize an eddy-resolving numerical ocean model to investigate the structure and seasonal variability of the Barents Sea Polar Front. Observations of hydrography and sea-ice concentration are used to evaluate the model results. Two areas are investigated: Svalbardbanken (Svalbard Bank) and Storbanken (Great Bank). We find that the model does a good job in representing the front with respect to structure and position, but the model seems to lack some sub-mesoscale processes that may be important for the upslope advection of Atlantic Water in the frontal area. Two different factors dominate when the seasonal stratification develops on Svalbardbanken and Storbanken, respectively: On Svalbardbanken slope, we find that heating at the surface dominates, while at Storbanken freshwater from sea-ice melt contributes the most to stratify the water column. The model results suggest a mechanism where downslope advection of dense bottom water stratifies the water column and thereby makes the physical conditions favorable for pri-

*Corresponding author
Email address: vidar.lien@imr.no (Vidar S. Lien)

mary production. Due to this mechanism, the local spring-bloom can start up to one month earlier.
Key words: Polar Front, Barents Sea, Numerical model

1. Introduction

The Barents Sea Polar Front (BSPF) is a prominent feature in the Barents Sea, and separates the relatively warm and saline Atlantic Water (AW) in the south from the cold and fresher Polar Water (PW) in the north (Loeng, 1991). In the western region it is topographically steered (Johannessen and Foster, 1978), following Svalbardbanken (the Svalbard Bank) slope, east along the southern slope of Storbanken (the Great Bank), and southward along Sentralbanken (the Central Bank) (see Fig. 1). The BSPF is an area of complex interactions between different water masses, sea-ice, topography, and tidal mixing (Loeng, 1991); (Kowalik and Proshutinsky, 1995); (Sundfjord et al., 2007).

In a spring-bloom ecosystem like the Barents Sea, the seasonal stratification determines the timing of the onset of the algal bloom (Sakshaug et al., 2009). Two processes contribute to stratification in the marginal ice zone (MIZ) by reducing the density of the surface mixed layer: *i)* Freshwater input from sea-ice melt reduces the salinity, and *ii)* solar insolation increases the temperature in the surface mixed layer (Loeng, 1991). Sverdrup (1953) explained how the mixed layer depth (MLD) needed to be above a certain critical depth before a net primary production could start. The MLD is therefore an important indicator of whether the physical conditions are favorable for primary production.

The BSPF forms the transition zone between the ecosystems in the warm and cold parts of the Barents Sea (Loeng, 1991). During winter, cooling and salinization through ice freezing and brine rejection at the surface and strong wind induced mixing homogenize the water column. Thus, nutrients from the deeper layers are brought to the surface through mixing (Sakshaug et al., 2009). During spring, sea-ice melt adds freshwater at the surface, which stabilizes the water column and creates a thin mixed layer. This gives rise to an intense algal bloom that follows the retreating ice cover northwards (Sakshaug and Skjoldal, 1989).

Earlier studies of the physics and biology in the MIZ in general and the BSPF in particular include the extensive surveys during the 1980s (Sakshaug et al., 1991) and surveys focusing on the physics of the BSPF during the 1990s (Parsons et al., 1996); (Harris et al., 1998). Due to severe ice conditions, the BSPF region is sparsely sampled during winter. This has motivated several model studies of the area, including the early studies by Støle-Hansen and Slagstad (1991); Ådlandsvik and Hansen (1998), in addition to more recent studies, e.g. Sundfjord et al. (2008).

The dynamical processes associated with oceanic fronts were identified as an important gap in our knowledge within Arctic regions (ACIA, 2005; Arctic Climate Impact Assessment). The BSPF is an important feeding area for fish, in particular capelin (*Mallotus villosus*), and shifts in distribution appear linked to changes in frontal position.

In order to study the seasonal variation of the BSPF, a high-resolution numerical ocean model is set up for the Hopendjupet (Hopen Trench) area (see Fig. 1). The model domain includes Svalbardbanken, Hopendjupet

and Storbanken. The model has a horizontal resolution of 800 m, which is sufficient to resolve most of the mesoscale dynamics in the western Barents Sea. In order to resolve the strong seasonal pycnocline the vertical resolution is enhanced towards the surface.

A brief description of the observational data set, followed by a description of the model set-up, is given in section 2. An evaluation where the model results are compared with observations is performed in section 3. Results are presented in section 4, and a discussion is carried out in section 5. Finally, some concluding remarks are given in section 6

2. Data and Methods

2.1. Observational data

CTD-measurements (Conductivity-Temperature-Depth) from two cruises are used in the evaluation and the discussion of the model results. A total of 137 CTD-stations were taken from 31st of July to 17th of August, 2007, and a total of 138 CTD-stations were taken from 28th of April to 16th of May, 2008, as part of the IPY project NESSAR (Norwegian component of the Ecosystem Studies of SubArctic and Arctic Regions). During both cruises, the sampling were concentrated along two sections; one section across the Svalbardbanken slope and one section across the Storbanken slope (see Fig. 1 for position of sections). Satellite-derived (AMSR-E) daily snapshots used to evaluate the sea-ice distribution in the model are obtained from the University of Bremen (http://iup.physik.uni-bremen.de:8084/amsredata/asi_daygrid_swath/l1a/).

2.2. Mixed Layer Depth and Critical Depth

There are several ways of estimating the MLD (see e.g. Thomson and Fine (2003)). In this study, we apply the threshold method (Peters et al., 1989), where the MLD is defined as the depth z at which the potential density difference $\Delta\sigma_\Theta(z) = \sigma_\Theta(z) - \sigma_\Theta(z_0)$ between the surface z_0 and the depth z exceeds a specified threshold value. A critical point in this method is to choose an appropriate $\Delta\sigma_\Theta$, as the calculated MLD may be sensitive to the choice of threshold. Thomson and Fine (2003) argue that although $\Delta\sigma_\Theta$ = 0.01 kg m^{-3} has emerged as the standard, it is probably too narrow for biological applications. We therefore include the values $\Delta\sigma_\Theta$ = 0.03 kg m^{-3} and $\Delta\sigma_\Theta$ = 0.1 kg m^{-3} to investigate the sensitivity of the choices of $\Delta\sigma_\Theta$ on the estimated MLD.

The critical depth is estimated by an algorithm used in the primary production model NORWECOM, described in Skogen et al. (1995) and Skogen and Søiland (1998).

2.3. Model description

In this study, we use the Regional Ocean Modeling System (ROMS), coupled with a sea-ice model. ROMS is a three-dimensional baroclinic ocean general circulation model (OGCM) that uses normalized, topography-following sigma-coordinates in the vertical; see Shchepetkin and McWilliams (2005); Haidvogel et al. (2008) for a more detailed description of the model system. Vertical stretching that allows for enhanced resolution in the surface and bottom boundary layers is applied to the vertical coordinate. We have applied 40 sigma levels in the vertical, while the horizontal resolution is 800 by 800 m. Daily averages from a regional model with a horizontal resolution of

4 km, which covers the Nordic, Barents and Kara Seas, are used as forcing at the open boundaries. A nudging and radiation scheme is used for three dimensional momentum and advection of tracers through the open boundaries, as described in Marchesiello et al. (2001). A rather strong relaxation (3 days) towards the regional model is applied on incoming information, while a weaker relaxation (360 days) is applied to outgoing information. Tides are included, with free surface heights and velocities from eight tidal constituents from the Arctic Ocean Tidal Inverse Model (AOTIM; Padman and Erofeeva (2004)). Flather (1976) and Chapman (1985) open boundary conditions were used for barotropic normal velocity components and free surface, respectively, and the tides were added to the barotropic velocities and sea surface height at the open boundaries. The ERA Interim data set (see http://www.ecmwf.int/research/era/do/get/era-interim) from the European Center for Medium range Weather Forecasting (ECMWF) is applied as atmospheric forcing, providing 6-hourly atmospheric data at a resolution of 79 by 79 km.

Generic length scale (GLS) scheme (Umlauf and Burchard, 2003) is used for sub-gridscale mixing, with the two-equation *k-kl* model parameters, which is a modified form of the Mellor-Yamada 2.5 closure (Mellor and Yamada, 1982). The GLS *k-kl* scheme has been evaluated against 3 other mixing closures (Warner et al., 2005a) and was found to produce good results in coastal applications where tidal mixing is important (Warner and Geyer, 2005b). A dynamic-thermodynamic sea ice module is coupled to the ocean model, as described in Budgell (2005).

Thirteen locations coinciding with observation stations (Table 1 and Fig.

1) were selected where modeled station profiles were stored every 15 minutes. This enables a high time resolution for process studies in the frontal area.

Some challenges in this model experiment need to be adressed. The results from the small model domain with its four open boundaries will largely depend on the boundary forcing and the open boundary conditions applied. We therefore need some evaluation of the regional model used as boundary forcing and initialization. This evaluation is presented in section 3. Further, the northern Barents Sea has a seasonal ice cover, which generates a seasonal surface layer largely determined by ice-melt water. Together with seasonal heating of the surface water, this creates a strong pycnocline. A very high vertical resolution is needed in order to resolve the strong pycnocline in this area, which nearly forms a two-layer system in the summer season. Therefore, we have packed the vertical layers densely to increase the vertical resolution towards the surface.

High spatial resolution allows high resolution in topography, and hence local topographic effects. The resolution also determines whether eddies are resolved in the model grid. Based on the CTD-measurements, the internal Rossby-radius was estimated to be in the range 1-2 km. Thus, mesoscale dynamics are allowed to develop in the model, and it will be resolved to some degree (by a few gridcells). However, although both the mesoscale dynamics and effects from topography are fairly well represented in the model, the atmospheric forcing has a coarse resolution (79 by 79 km). This represents a limitation in high-resolution model studies. Regionally downscaled atmospheric forcing is needed in order to overcome this limitation, but that is beyond the scope of this study.

3. Model evaluation

A proper model evaluation is imperative in order to assess the validity of the model results. In our application, it is also important to evaluate the boundary forcing and the initial state, as mentioned above.

3.1. Evaluation of the regional 4 km model

The modeled hydrographic structure at the Barents Sea Opening (BSO; see Fig. 1 for position) corresponds well with the climatological mean based on hydrographic measurements (Kangas et al., 2006; not shown). Indices of temperature and salinity at the BSO are calculated by integrating over the 50 to 200 m depth range from 71°30'N to 73°30'N, in which the bulk of the Atlantic inflow to the Barents Sea is located. A comparison between the indices from the observations and from the model reveals that the model is biased low in both temperature (-0.36 °C) and salinity (-0.15) for the period 2006 to 2008. We are aware of a few weaknesses with this comparison. The section is sampled six times a year, which gives a good representation of the seasonal cycle. However, while the observations represent nearly synoptic snapshots within a given month, the model data are monthly averages. This potentially gives rise to some bias, as the temperature and salinity may vary within a single month. This problem is particularly large due to the short simulation period (three years). In addition, the spatial variability of the modeled Atlantic inflow may differ from reality. This potentially gives rise to biases between observations and model when using fixed locations.

The North Cape Current (NCaC) carrying AW into the Barents Sea, bifurcates in Bjørnøyrenna (Bear Island Trough), and one part flows into

Hopendjupet (Ingvaldsen, 2005). Thus, a bias in the properties of the Atlantic Water in the regional model is likely to occur also in the high-resolution model. Few hydrographic data exist from the northern parts of the Barents Sea, and therefore an evaluation of the regional model at the northern boundary of the high-resolution model is difficult.

Modeled ice concentration is in good agreement with observations with respect to both ice edge (defined by 15% ice concentration) and concentration (not shown), although the model tends to have more ice, especially on Svalbardbanken, and the ice edge is a bit further south compared to observations for most of the Hopendjupet area.

3.2. Evaluation of the high-resolution model

Sea-ice plays an important role in the hydrography on the cold side of the BSPF, as freezing of sea-ice adds salt to the water column, while melting sea-ice adds freshwater to the upper mixed layer. Thus, for the water masses to be correct, it is important that the model is able to reproduce both the seasonal ice zone (SIZ) and the amount of ice in the ice-covered regions. We evaluate the modeled sea-ice distribution by comparing 10-day averages of modeled concentration of sea-ice with 10-day averages of satellite-derived sea-ice concentrations. The position of the modeled ice edge in spring generally agrees very well with observations (Fig. 2). However, the modeled ice concentration is generally too low on Storbanken and also to some degree on Svalbardbanken (not shown). The modeled retreat of the ice edge through the melt season is in agreement with observations (not shown).

A comparison between modeled and observed hydrography at the model stations is carried out in Table 2. The results of the comparison need to

be interpreted with caution, as the stations are located in the frontal area, where spatial and temporal gradients are expected to be large. The observations consist of a various number of CTD-profiles (ranging from one to eight), usually spanning one to a few days in time. To account for temporal variability, 15 modeled daily averages (centered at the day(s) of the observation(s) ± 7 days) are averaged into one vertical profile. Average vertical profiles at stations 2, 8, and 13 are shown in Fig. 3. Spatial variability is not represented, except that the model stations represent 800 by 800 m squares. Also, the observations represent snapshots, while the model stations represent daily averages, hence tidal effects are removed in the modeled data. Root mean square error (RMSE) and bias of the modeled average vertical profile compared to the average observed vertical profile are computed, along with a correlation coefficient between the two vertical profiles. Both RMSE and bias are shown, in order to include the sign of the deviation as well as revealing a possible cancellation effect when the bias has opposite sign in the higher and lower parts of the water column (see e.g. Fig. 3; upper right). The correlation coefficient shows whether the modeled vertical structure agrees with observed vertical structure. R is chosen over R^2 in order to reveal the sign of the correlation, since a negative correlation may be considered as wrong as no correlation.

On the Atlantic side of the BSPF, the bias in salinity is close to the bias calculated at the BSO in the regional model, while the bias is lower at Svalbardbanken. There is also a generally good agreement in the vertical haline structure. The largest difference in temperature is found in the frontal area at the Svalbardbanken slope, where the model is colder than observed.

In this area we also find a large disagreement in vertical thermal structure, mainly owing to the lack of intrusion of AW in deeper layers in the model. The low biases in temperature at Storbanken (stations 11 to 13) is due to a cancelling effect from too high modeled temperatures near the surface and too low modeled temperatures near the bottom (Fig. 3; top right). The latter is due to lack of advection of AW onto the bank.

An observational based hydrographic atlas for the Barents Sea has been compiled at IMR (Sigrid Lind Johansen, pers.comm.). The data coverage is best in the arctic summer season (August-September-October). The temperature atlas is available in an equal-area grid with resolution 25 km.

The model results at 50 meters depth has been averaged to the same period and interpolated to the same equal-area grid for quantitative comparison. The comparison is done by computing the bias, the root mean square difference, the correlation coefficient, and a weighted bias defined as

$$\frac{1}{N}\sum^{N}\frac{F_{mod}-F_{obs}}{\sigma_{obs}} \tag{1}$$

where N is the number of atlas grid cells with values in the atlas that year, F_{mod} is the modeled value, F_{obs} the atlas value and σ_{obs} the standard deviation in the atlas cell based on the years 1970–2008.

The results are summarized in table 3. The temperature has a small negative bias. The larger RMS deviation indicate that there is some cancelling of errors. The salinity is also biased low. The weighted bias shows that this error is large, on the order of 1.5 to 2 standard deviations. The correlation coefficient is high both for salinity and temperature, indicating that the spatial structure of the modeled and observed fields are similar. As

the dominating spatial structure is the BSPF, this implies that the front is reproduced in correct position by the model. More details can be found from the T-S diagrams of the atlas data and model results in Fig. 4. As the diagrams are similar only 2008 is shown. The figure identifies the Atlantic water mass as the area with largest salt deficiency in the model. For temperature, the values are sligthly too low in the Atlantic water and too high in the Artic water, contributing to the cancellation in the bias.

4. Results

4.1. Structure of the Polar Front

The position of the modeled BSPF is determined by a topographically steered warm core jet (WCJ), carrying AW along Svalbardbanken with the shallow water on its left side (retrograde; Li and McClimans (1998)). This current has been observed by direct current measurements (Loeng and Sætre, 1997), as well as in both numerical studies (Li and McClimans, 1998); (Ådlandsvik and Hansen, 1998) and laboratory experiments (McClimans and Nilsen, 1993). In our model study, the WCJ is seen as a swift and narrow, approximately 25 km wide current, located between the 200 and 300 m isobaths (Fig. 5; top). A calculation of mean kinetic energy showed that the WCJ is a dominating and persistent dynamic feature in Hopendjupet (not shown).

East of Hopen, the WCJ turns east towards Storbanken, follows the 200 m isobath and flows between Storbanken and Sentralbanken towards the eastern parts of the Barents Sea. Using the net volume transport through the section shown in Fig. 5 to represent the strength of the WCJ, reveals a large variability on a monthly timescale (Fig. 6). The flow is strongest in

winter (February/March) and weakens during spring and summer, consistent with the seasonal pattern found at the BSO (Ingvaldsen et al., 2004). In 2007, a secondary maximum was found in the autumn (September/October), while in 2008, September and October represented a minimum with a net southeastward flow. This is also clearly seen in Fig. 5. Also evident is a current flowing southwestward, located downslope of the WCJ, and with the core located between the 300 and 400 m isobath. In October 2008, the WCJ was weak and pushed upslope, while the oppositely directed current downslope was intensified.

Although the WCJ exhibits a large temporal variability, the spatial variability (upslope extent) is small (Fig. 5). This is also reflected in the small changes in temperature between October 2007 and October 2008 (Fig. 7). Hence, the position of the BSPF changes little, in agreement with the findings of Johannessen and Foster (1978); Parsons et al. (1996). The modeled position of the BSPF at 50 m in May 2008 is shown in Fig. 8. The front is indicated as regions with strong gradient in temperature and salinity. The salt and temperature gradients give very similar position of the front, with more noise in the temperature along the south flank of Svalbardbanken. There is some indication of a front in temperature southwest of Sentralbanken, which is not visible in salinity. This may depend on the choice of contour levels. The front around Hopendjupet and towards Storbanken is particularly strong in both fields. In this area in May the front is well approximated by the 1 degree isoterm or the 34.8 isohaline (fig. 8). In the Hopendjupet/Storbanken area the front is strong all year round and the position quite fixed (not shown). Towards Svalbardbanken and in particular Sentralbanken the strength and

position of the front is more variable.

The BSPF is both thermal and haline (temperature shown in Fig. 9), but the two compensate, hence there is only a weak density gradient across the front (Fig. 10). During winter, wind mixing and thermal and haline convection homogenize the water column, and the BSPF extends from the bottom to the surface. When the melt season starts, usually in May, freshwater from sea-ice melt creates a sharp halocline. During this process, the upper pycnocline is de-coupled from the deeper part, which remains locked to the topography. Depending on the position of the ice edge, the fresh surface layer extends across the deeper BSPF and into Hopendjupet. This was observed on Storbanken in May, 2008, and the model results show a similar pattern in salinity (not shown). However, contrary to the observations, which show a thermal front coinciding with the haline front in Hopendjupet, the upper part of the modeled thermal front was still coupled to the deeper front in May, 2008.

During late spring and summer, the BSPF at Svalbardbanken develops into a two-front system (Fig. 9). The PW at the bank is heated through insolation and freshwater from sea-ice melt reduces the salinity. Tidal mixing homogenize the water column at the bank, and the tidal front located approximately at the 60 m isobath turns into both a thermal and a haline front, referred to as the summer front, e.g. Loeng (1991). Opposite to the front between AW and PW further downslope, the summer tidal front has a strong density gradient between the warm and fresh summer PW and the cold and more saline PW (Fig. 10). The PW trapped at the bottom between the summer front at the bank and the BSPF further downslope is present

throughout the year. This results in a minimum bottom temperature approximately along the 100 m isobath on the Svalbardbanken slope in summer, with a small temperature variability (∼2-3 °C through the year), compared to the temperature variability at the top of the bank (∼6 °C through the year).

On Storbanken, the observations show that a water mass of Atlantic origin, characterized by $T > 1$ °C and $S > 34.9$, occupies the bottom layer below an intermediate layer of water with -1 °C $< T <$ 0 °C. The cold intermediate layer consists of so-called "winter-water", which is a remnant of the thermal and haline convection the previous winter. The higher temperatures at the bottom indicate that the previous winter's convection did not reach the bottom. In the model, however, the "winter-water" extends all the way to the bottom. The surface layer above Storbanken is relatively fresh, and even the brine enriched bottom water has a salinity and also a potential density which is lower than the AW at the bottom of Hopendjupet. Therefore, severe ice freezing is needed for the winter convection to penetrate the stratification between the intermediate PW and the deep AW (Loeng, 1991).

4.2. Bio-physical dynamics

The Svalbardbanken section spans three different regimes. On the top of the bank (station 1), tidal mixing keep the water column well mixed and prevents stratification from developing. However, the bank is shallow enough for the critical depth to eventually reach the bottom, and hence sustain primary production. Station 10 is located close to the BSPF at the edge of the SIZ. At this station, the seasonal stratification is dominated by seasonal heating at the surface, although some advection of freshwater across the front

has been observed (Harris et al., 1998). Stations 2 to 9 are located within the SIZ and are deep enough for stratification to develop.

The model results indicate that heating at the surface is the dominating process when the stratification on the Svalbardbanken slope develops, while freshwater from sea-ice melt plays a less important role (Fig. 11; top). On the contrary, freshwater from sea-ice melt is dominating over heating at Storbanken early in the summer (Fig. 11; bottom). The stratification erodes gradually throughout the summer due to wind mixing (Loeng, 1991), as seen in Fig. 12; top. The sea-ice melt starts earlier than the heating of the surface layer (Loeng, 1991), hence the spring-bloom starts earlier on the Arctic side of the BSPF compared to the Atlantic side. This is seen in Fig. 12, where the MLD decreases earlier at station 11 (Storbanken slope) compared to station 10 (Svalbardbanken slope) in 2008. Although station 11 is located farther into Hopendjupet (260 m depth) than station 10 (215 m depth), melt water caused stratification at station 11 already in late April, because the ice edge extended out on the Storbanken slope in 2008. The gradual retreat of the sea-ice cover results in a later stratification on Storbanken than on the Storbanken slope. However, although the MLD was well above the critical depth at Storbanken by late May, the modeled ice cover was in excess of 50% until late June, which reduced the light available for algal growth.

Figure 12 (bottom) reveals large annual variability in MLD, which depends on ice conditions. Opposite changes are seen at stations 11 (Storbanken slope) and 13 (top of Storbanken), with a markedly later stratification at station 11 and an earlier start of the stratification at station 13 in 2007 compared to 2008. In 2007, there was less ice, hence station 11 was

outside the SIZ, leaving surface heating as the dominating mechanism to stratify the water column. At station 13, however, the earlier retreat of the ice edge in 2007 caused the MLD to reach the critical depth approximately a week earlier.

Large differences are also seen at Svalbardbanken, where there was a pronounced change in the timing of conditions favorable for primary production from 2007 to 2008. This was, however, only indirectly related to sea-ice, and the model results point to a third mechanism to stratify the water column, at least on a local scale. Most of the sea-ice on Svalbardbanken is formed during the period February-April. This produces brine-enriched water masses on the top of the bank. During April, this dense water flows down the slopes of the bank and creates a bottom layer with enhanced density, which stratifies the water column (Fig. 13; top). Such production of dense bottom water at the southeastern slope of Svalbardbanken was also pointed out by Sarynina (1969).

The advection of dense bottom water in 2008 is evident in Fig. 14, which shows the density at the surface and bottom at station 7 in both 2007 (top) and 2008 (bottom). A pulse of dense water cascading down the slope is seen as a sudden increase in density at the bottom in late April. The stratification due to the bottom water, here represented by the density difference between the surface and the bottom, persists until the seasonal heating reduces the density at the surface. To investigate whether this stratification is sufficient for the onset of an algal bloom, we compare the modeled and observed MLD and the estimated critical depth at station 7 (Fig. 15). From this comparison, we draw the following two conclusions: Firstly, there is

a good agreement between modeled and observed MLD in mid-May, while there is less agreement in late April (Fig. 15). Secondly, the comparison shows that the stratification due to the advection of dense bottom water is sufficient to raise the MLD above the critical depth, and thereby making the physical conditions favorable for primary production. This is supported by the observation of primary production at station 7 in the first half of May, 2008 (Kenneth F. Drinkwater, pers.comm). The comparison shows similar results at station 8, while the agreement between model and observations decreases upwards on the slope (not shown).

5. Discussion

5.1. Model evaluation

A nested setup has been used to model the Hopendjupet area in the Barents Sea with eddy-resolving resolution. The model setup is validated against available hydrographic and sea-ice data. The regional 4 km model is biased cold and fresh at the BSO. The high resolution model is also biased low in salinity and to a less degree temperature. As the problems are most pronounced in the inflowing AW the problem may be inherited from the regional model at the open boundaries. The horizontal frontal structures are well represented by the model. This may be a result of the strong topographic control on the front location, both in model and in nature. The position of the ice edge also agrees with observations. The model also reproduces the vertical salinity structure quite well, but there is problems with the temperature stratification on some stations at the flank of Svalbardbanken. This is further discussed below.

The model reproduced the WCJ at the flank of Svalbardbanken, as seen in other studies (Loeng and Sætre, 1997); (Li and McClimans, 1998); (Ådlandsvik and Hansen, 1998). Based on our two years there seems to be a seasonality in this current, with maximum flow in February-March and a weakening in spring and summer, with a net westward flow in some months. This supports the observations of a southwestward flow of AW along Svalbardbanken (Gawarkiewicz and Plueddemann, 1995); (Parsons et al., 1996), which was also supported by an idealized numerical model (Gawarkiewicz and Plueddemann, 1995). The conclusions of Gawarkiewicz and Plueddemann (1995), however, were based upon observations collected during summer, when the WCJ is relatively weak compared to the return current (Fig. 6).

5.2. Unresolved processes

According to Table 2, the vertical structure of the hydrography at the Svalbardbanken slope is poorly represented in the model. Several CTD-stations indicate advection of AW onto the slope, which was also observed by Parsons et al. (1996). They observed internal waves with amplitudes of $\sim$10 m, in addition to filaments of AW that were pinched off and dissipated underneath the front. During the cruise in summer 2007, interleaving was observed at the front. This was also reported by Parsons et al. (1996). These processes, however, seem to be lacking in the model. Although there are 40 vertical layers in the model, the vertical resolution is several meters near the bottom in the frontal area ($\sim$200 m bottom depth). Thus, internal waves with amplitudes of $\sim$10 m will be poorly represented in the model, hence the upslope advection of AW will be lacking in the model if such processes are important.

At Storbanken, Reigstad et al. (2002) found that locally produced cold and saline bottom water observed in March and May, 1998, was replaced by more Atlantic influenced water masses by July 1999. Such Atlantic influenced water masses were also observed in summer 2007, while due to heavy ice conditions, measurements were made only half way up the Storbanken slope in spring 2008. Therefore, we cannot conclude whether the AW was still present in 2008. This water mass is not found in the model and we anticipate that a lack of small scale processes may explain this discrepancy. Another factor could be the model diffusion, which tends to smooth gradients in temperature and salinity. Although the salinity is biased low in the modeled AW, the salinity and hence the density in the upper layers above Storbanken is in close agreements with observations (not shown). Thus, the density difference between a bottom layer of AW and an upper layer of PW would be less in the model and would therefore be more susceptible to vertical mixing and could easily be broken down.

5.3. Stratification and primary production

During the cruise in the first half of May, 2008, a stratified water column was observed (Fig. 13) along with primary production. The bloom appeared to be relatively recently started, as it was located in the surface layer and in the lowest salinity waters (Kenneth F. Drinkwater, pers.comm). Thus, Fig. 15 indicates that a MLD which is above the critical depth when defined by $\Delta\sigma_\Theta = 0.03$ kg m^{-3} is sufficient to sustain an algal bloom. According to the model, the onset of the bloom could then have occurred as early as the last days of April (station 7; Fig. 15) and the first days of May (station 8; not shown). At station 7, isolines of density show that the stratification is due

to the advection of dense bottom water (not shown). This is less clear at station 8 due to larger bottom depth (156 m compared to 104 m at station 7). We therefore conclude that, according to the model, advection of dense bottom water down the Svalbardbanken slope may create a stratification that is sufficient to start an algal bloom in areas where the bottom depth is close to 100 m or less.

The observational evidence for the production of high density water and its sinking along the Svalbardbanken slope is weak (Fig. 13). The absence of dense, brine-enriched bottom water in the observations could be due to differences in the sea-ice distribution. In the model, there is a substantial ice formation above the eastern part of Svalbardbanken during March and April (e.g. at station 3, there is a net production of 2.10 m of ice during this two-month period, compared to only 0.15 m at station 1). From the modeled and observed ice edges shown in Fig. 2 (bottom), it cannot be concluded that there is any difference in ice production between model and observations. However, in February and March (not shown), there was less ice on Svalbardbanken in the model, indicating a more severe ice production on the eastern side of the bank in the model compared to the observations in March and April. This conclusion is, however, not necessarily valid as long as observations of ice thickness and therefore also ice volume are unavailable. But regardless of the difference in ice distribution, the model results suggest a mechanism that stratifies the water column by advection of dense bottom water down the slope of Svalbardbanken, and that this may lift the MLD above the critical depth. Thus, it cannot be ruled out that following a winter with severe ice conditions on Svalbardbanken, such a mechanism may trigger

an earlier start of the primary production on the upper parts of the slope.

5.4. Sea-ice

Changes in sea-ice cover influence the stratification in the BSPF region through adding melt water at the surface and brine-enriched bottom water at the slope of Svalbardbanken. According to Fig. 14, this can lead to changes in the possible timing of the spring-bloom of up to one month at the Svalbardbanken slope, with a later start in years with less ice. At Storbanken, less ice leads to a later start of the spring-bloom at the slope, due to the retreat of the SIZ. On the bank, however, less ice leads to an earlier start of the melt season, and therefore conditions favorable for primary production occur earlier, due to both stratification caused by meltwater at the surface and less severe ice cover which allows for more light to penetrate down into the water column.

This is, however, a simplified picture purely based on some physical considerations. The ice cover in the Barents Sea is highly variable on timescales from days to decades, and the interannual to decadal variability may exceed the seasonal variability (Vinje and Kvambekk, 1991). Observations have shown that the simplified picture of a plankton bloom following the retreat of the ice edge is not always present (Falk-Petersen et al., 2000), due to a large variability in the physical conditions on a timescale of days and weeks.

According to the model, local ice production on Storbanken is negligible, and virtually all ice present on Storbanken is advected into the area, mainly from the northeast. However, this is based on data from the stations only, with the northeastermost station located in the southwestern part of Storbanken (Fig. 1). Thus, there may still be some local production fur-

ther to the north and east. Most of the sea-ice in the Barents Sea is locally produced, although there is also a considerable, yet variable import of ice mainly from the Kara Sea and also from the Arctic Ocean (Sakshaug et al., 2009). Based on 3 drifting buoys, Vinje (1988) found that simultaneous drift velocity could reach 0.2 ms^{-1}, while the average drift was 0.06 ms^{-1} towards southwest. A monthly average of modeled sea-ice drift (not shown), revealed a mean drifting velocity in the range 0.05-0.1 ms^{-1} in the Storbanken area in the high-resolution model, which is in good agreement with the findings of Vinje (1988). Still, a lack of local ice production on Storbanken may explain the discrepancy between the modeled and the observed ice concentration in this area.

6. Concluding remarks

In this study we have shown that the BSPF is trapped to the topography around Hopendjupet, and that it is determined by the WCJ flowing along the slope of Svalbardbanken and Storbanken. At the Svalbardbanken slope, bottom water formation may influence the timing of the spring-bloom, with an earlier start in years with large ice production on the bank. However, inclusion of more data, like direct measurements of light, turbulence, and primary production is needed in further investigations. More observations are needed in order to resolve the issue of dense bottom water induced stratification. This calls for high-frequency sampling of vertical profiles of hydrography and chlorophyll.

According to Ingvaldsen (2005), the position of the BSPF is dependent on the width of the NCaC. In this study, only two consecutive years (both are

considered "warm" years) are investigated, hence it is difficult to conclude how the WCJ is dependent on the width of the NCaC. A longer model hindcast, combined with observations is needed in order to investigate this relationship further.

Modeling sea-ice is still a challenge. Different bulk-flux algorithms are used in the regional 4 km model and the high-resolution model. Discussing the differences of these algorithms is beyond the scope of this work, but it is worth to mention that the routine used in the high-resolution model is designed for implementation in high-latitude simulations, compared to the more general bulk-flux algorithm applied in the regional model. We believe that a close study of the different parameterizations could be worthwhile.

7. Acknowledgements

This work was funded by the Norwegian Research Council through the IPY-project NESSAR (grant number 176057). We thank Morten D. Skogen for estimating the critical depth. Ken Drinkwater is acknowledged for his constructive comments which helped improve the manuscript.

References

Ådlandsvik, B. and R. Hansen, "Numerical simulation of the circulation in the Svalbardbanken area in the Barents Sea", *Cont. Shelf Res.*, **18**, 341-355 (1998)

Budgell, W.P., "Numerical simulation of ice-ocean variability in the Barents Sea region; Towards dynamical downscaling", *Ocean Dynamics*, **55**, 370-387 (2005)

Chapman, D.C., "Numerical treatment of cross-shelf open boundaries in a barotropic coastal ocean model", *J. Phys. Oceanogr.*, **15**, 1060-1075 (1985)

Falk-Petersen, S., H. Hop, W.P. Budgell, E.N. Hegseth, R. Korsnes, T.B. Løyning, J.B. Ørbæk, T. Kawamura and K. Shirasawa, "Physical and ecological processes in the marginal ice zone of the northern Barents Sea during the summer melt period", *J. Mar. Sys.*, **27**, 131-159 (2000)

Flather, R.A., "A tidal model of the northwest European continental shelf", *Mem. Soc. Roy. Sci. Liege*, **6(10)**, 141-164 (1976)

Gawarkiewicz, G. and A.J. Plueddemann, "Topographic control of thermohaline frontal structure in the Barents Sea Polar Front on the south flank of Spitsbergen Bank", *J. Geophys. Res.*, **100**, 4509-4524 (1995)

Haidvogel, D.B., H.G. Arango, W.P. Budgell, B.D. Cornuelle, E. Curchitser, E. Di Lorenzo, K. Fennel, W.R. Geyer, A.J. Hermann, L. Lanerolle, J. Levin, J.C. McWilliams, A.J. Miller, A.M. Moore, T.M. Powell, A.F. Shchepetkin, C.R. Sherwood, R.P. Signell, J.C. Warner and J. Wilkin, "Ocean forecasting in terrain-following coordinates: Formulation and skill assessment of the Regional Ocean Modeling System", *J. Comput. Phys.*, **227:7**, 3595-3624 (2008)

Harris, C.L., A.J. Plueddemann and G.G. Gawarkiewicz, "Water mass distribution and polar front structure in the western Barents Sea", *J. Geophys. Res.*, **103**, 2905-2917 (1998)

Ingvaldsen, R.B., L. Asplin and H. Loeng, "The seasonal cycle in the Atlantic

transport to the Barents Sea during the years 1997-2001", *Cont. Shelf Res.*, **24**, 1015-1032 (2004)

Ingvaldsen, R.B., "Width of the North Cape Current and the location of the Polar Front in the western Barents Sea", *Geophys. Res. Lett.*, **32**, L16603 (2005) doi: 10.1029/2005GL023440

Johannessen, O.M. and L.A. Foster, "A Note on the Topographically Controlled Oceanic Polar Front in the Barents Sea", *J. Geophys. Res.*, **83**, 4567-4571 (1978)

Kangas, T.-W., E. Svendsen and Ø. Strand, "Average value of salinity and temperature in the Institute of Marine Research's fixed sections", *Fisken og Havet*, **6**, in Norwegian, 51pp (2006)

Kowalik, Z. and A.Y. Proshutinsky, "Topographic enhancement of tidal motion in the western Barents Sea", *J. Geophys. Res.*, **100**, 2613-2637 (1995)

Li, S., "The dynamics of a slope current in the Barents Sea", Ph.D. Thesis, The Norwegian Institute of Technology, Trondheim, 151pp (1995)

Li, S. and T.A. McClimans, "The effects of winds over a barotropic retrograde slope current", *Cont. Shelf Res.*, **18**, 457-485 (1998)

Loeng, H., "Features of the physical oceanographic conditions of the Barents Sea", *Polar Res.*, **10(1)**, 1-18 (1991)

Loeng, H. and R. Sætre, "Current measurements in the Barents Sea in the period 1972-1994 - An overview", *Fisken og Havet*, Institute of Marine Research (1997)

Marchesiello, P., J.C. McWilliams and A.F. Shchepetkin, "Open boundary conditions for long-term integration of regional ocean models", *Ocean Modelling*, **3**, 1-20 (2001)

McClimans, T.A. and J.H. Nilsen, "Laboratory simulation of the ocean currents in the Barents Sea", *Dyn. Atmos. and Oceans*, **19**, 3-26 (1993)

Mellor, G.L. and T. Yamada, "Developement of a turbulence closure-model for geophysical fluid problems", *Rev. Geophys.*, **10(4)**, 851-875 (1982)

Padman, L. and S. Erofeeva, "A barotropic inverse tidal model for the Arctic Ocean", *Geophys. Res. Lett.*, **31**, (2004)

Parsons, A.R., R.H. Bourke, R.D. Muench, C.S. Chiu, J.F. Lynch, J.H. Miller, A.J. Plueddemann and R. Pawlowicz, "The Barents Sea Polar Front in summer", *J. Geophys. Res.*, **101**, 14201-14221 (1996)

Peters, H., M.C. Gregg and J.M. Toole, "Meridional variability of turbulence through the equatorial undercurrent", *J. Geophys. Res.*, **94**, 18003-18009 (1989)

Reigstad, M., P. Wassmann, C.W. Riser, S. Øygarden and F. Rey, "Variations in hydrography, nutrients and chlorophyll *a* in the marginal ice-zone and the central Barents Sea", *J. Mar. Sys.*, **38**, 9-29 (2002)

Sakshaug, E. and H.R. Skjoldal, "Life at the ice edge", *Ambio*, **18**, 60-67 (1989)

Sakshaug, E., C.C.E. Hopkins and N.A. Øritsland, "Proceedings of the Pro

Mare symposium on polar marine ecology", Trondheim, 12-16 May 1990, *Polar Res.*, **10(1-2)**, 662pp (1991)

Sakshaug, E., "Biomass and productivity distributions and their variability in the Barents Sea", *ICES J. Mar. Sci.*, **54**, 341-350 (1997)

Sakshaug, E., G. Johnsen and K. Kovacs, "Ecosystem Barents Sea", **ISBN 978-82-519-2461-0** 587pp, (2009)

Sarynina, R.N. "Conditions of origin of Cold Deep-Sea Waters in the Bear Island Channel", *Coun. Meet. Int. Coun. Explor. Sea*, **Symp:28**, 1-8 (1969)

Shchepetkin, A.F. and J.C. McWilliams, "The Regional Ocean Modeling System (ROMS): A split-explicit, free-surface, topography-following coordinates ocean model", *Ocean Modelling*, **9**, 347-404 (2005)

Skogen, M.D., E. Svendsen, J. Berntsen, D. Aksnes and K.B. Ulvestad, "Modeling the primary production in the North Sea using a coupled 3 dimensional Physical Chemical Biological Ocean model", *Est., Coast. Shelf Sci.*, **41**, 545-565 (1995)

Skogen, M.D. and H. Søiland, "A User's guide to NORWECOM v2.0. The NORWegian ECOlogical Model system", *Fisken og Havet*, **18** 42pp (1998)

Song, Y. and D.B. Haidvogel, "A semi-implicit ocean circulation model using a generalized topography-following coordinate system", *J. Comput. Phys.*, **115**, 228-244 (1994)

Støle-Hansen, K. and D. Slagstad, "Simulation of currents, ice melting, and

vertical mixing in the Barents Sea using a 3-D baroclinic model", *Polar Res.*, **10(1)**, 33-44 (1991)

Sundfjord, A,. I. Fer, Y. Kasajima and H. Svendsen, "Observations of turbulent mixing and hydrography in the marginal ice zone of the Barents Sea", *J. Geophys. Res.*, **112**, C05008 (2007) doi: 10.1029/2006JC003524

Sundfjord, A., I: Ellingsen, D. Slagstad and H. Svendsen, "Vertical mixing in the marginal ice zone of the northern Barents Sea - Results from numerical model experiments", *Deep-Sea Res. II*, **55**, 2154-2168 (2008)

Sverdrup, H.U., "On conditions for the vernal blooming of phytoplankton", *ICES J. Mar. Sci,*, **18**, 287-295 (1953)

Thomson, R.E. and I.V. Fine, "Estimating Mixed Layer Depth from Oceanic Profile Data", *J. Atmos. Oceanic Technol.*, **20**, 319-329 (2003)

Umlauf, L. and H. Burchard, "A generic length-scale equation for geophysical turbulence models", *J. Mar. Res.*, **61**, 235-265 (2003a)

Umlauf, L., H. Burchard and K. Hutter, "Extending the $k - \omega$ turbulence model towards oceanic applications" *Ocean Modelling*, **5**, 195-218 (2003b)

Vinje, T., "Dynamics and Morphology of the Barents Sea ice fields", *Proc. 9th Conf. Port and Ocean Engineering under Arctic Conditions 1*, 263-268. University of Alaska Fairbanks, Alaska, U.S.A. (1988)

Vinje, T. and Å.S. Kvambekk, "Barents Sea drift ice characteristics", *Polar Res.*, **10(1)**, 59-68 (1991)

Warner, J.C., C.R. Sherwood, H.G. Arango and R.P. Signell, "Performance of four turbulence closure methods implemented using generic length scale method", *Ocean Modelling*, **8**, 81-113 (2005a)

Warner, J.C. and W.R. Geyer, "Numerical modelling of an estuary: a comprehensive skill assessment", *J. Geophys. Res.*, **110**, (2005b)

Wilcox, D.C., "Reassessment of the scale-determining equation for advanced turbulence models", *AIAA Journal*, **26(11)**, 1299-1310 (1988)

Station	Latitude (N)	Longitude (E)
1	76° 08	23° 36
2	76° 06	24° 00
3	76° 03	24° 18
4	76° 00	24° 42
5	75° 57	25° 06
6	75° 54	25° 21
7	75° 50	25° 45
8	75° 46	26° 18
9	75° 42	26° 42
10	75° 36	27° 06
11	76° 26	32° 09
12	76° 35	32° 51
13	76° 57	34° 24

Table 1: Model station positions (see Fig. 1).

	Temperature			Salinity		
Sta	RMSE	Bias	R	RMSE	Bias	R
1	0.49	0.49	0.14	0.01	0.01	-0.09
2	0.16	0.15	0.81	0.02	0.02	0.95
3	0.22	0.21	0.73	0.05	0.05	0.94
4	0.14	0.06	0.29	0.09	0.08	0.98
5	0.60	-0.53	-0.80	0.09	-0.05	0.93
6	0.86	-0.81	-0.26	0.09	-0.08	0.91
7*	1.25	-1.22	-0.90	0.18	-0.18	0.91
8	1.06	-0.99	-0.14	0.21	-0.20	0.97
9	1.23	-1.17	-0.80	0.27	-0.27	0.84
10	0.22	0.00	0.86	0.17	-0.17	0.73
11	0.70	0.18	0.97	0.20	-0.18	0.97
12	0.88	-0.31	0.96	0.21	-0.17	0.95
13	1.20	0.07	0.83	0.19	-0.12	0.94

Table 2: Statistics on model and observation stations. Observations are based on mean profiles from ensambles of CTD-measurements. Model stations are based on 15-day means based around the midpoint of the observations (±7 days). Stations 1 to 10 represent spring conditions and stations 11 to 13 represent summer conditions. **16 day average used on station 7, due to CTD-stations spanning 16 days.*

Season	2007 ASO	2008 ASO
Number of cells	556	556
T bias	-0.05	-0.24
T weighted bias	0.09	-0.20
T RMSE	0.72	0.75
T correlation	0.95	0.95
S bias	-0.13	-0.12
S weighted bias	-1.89	-1.60
S RMSE	0.17	0.15
S correlation	0.94	0.92

Table 3: Statistics on model bias and RMSE from observations at 50 m depth.

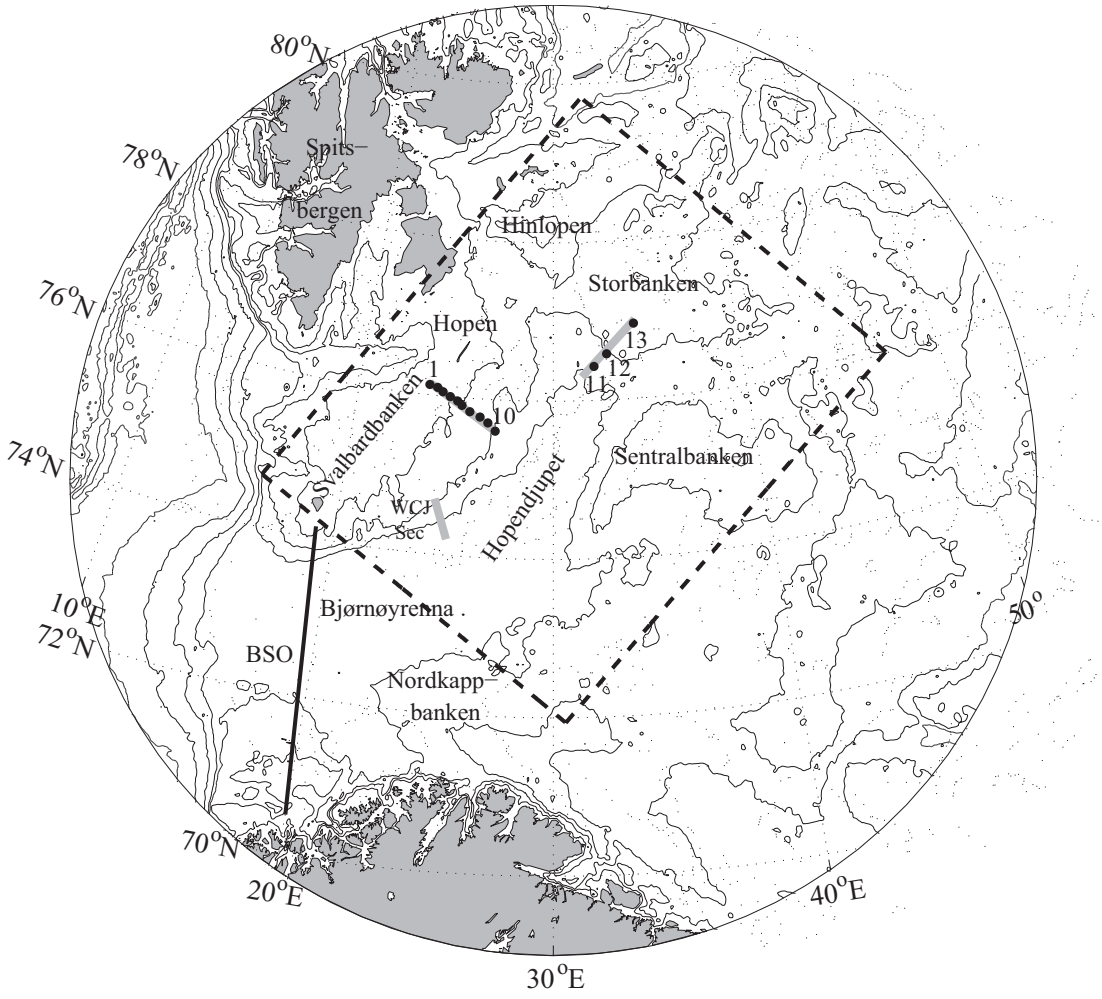

Figure 1: Bathymetric map of the western Barents Sea. Stipled rectangle shows model domain. Shaded gray lines indicate position of vertical sections and black dots show station positions. Black line labeled BSO show the Barents Sea Opening.

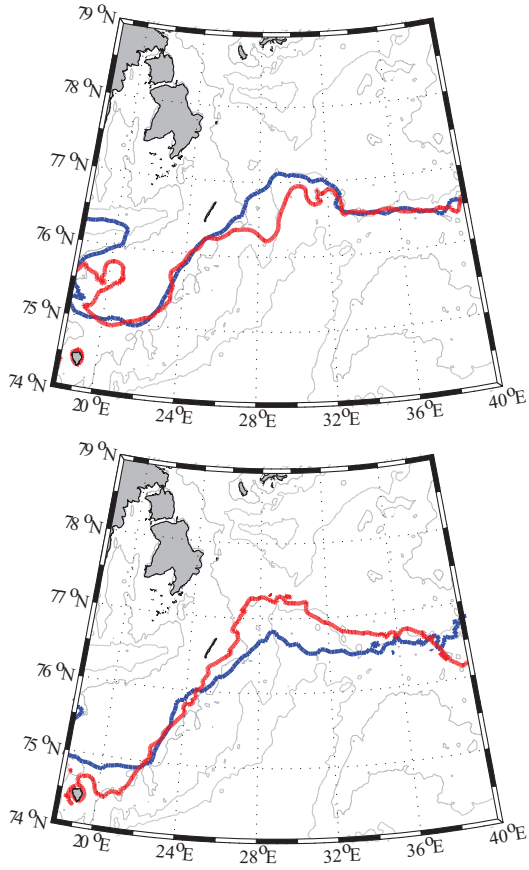

Figure 2: Position of the ice edge, defined by 15% ice concentration, at 15th of April in 2007 (top) and 2008 (bottom), based on observations (blue) and model (red).

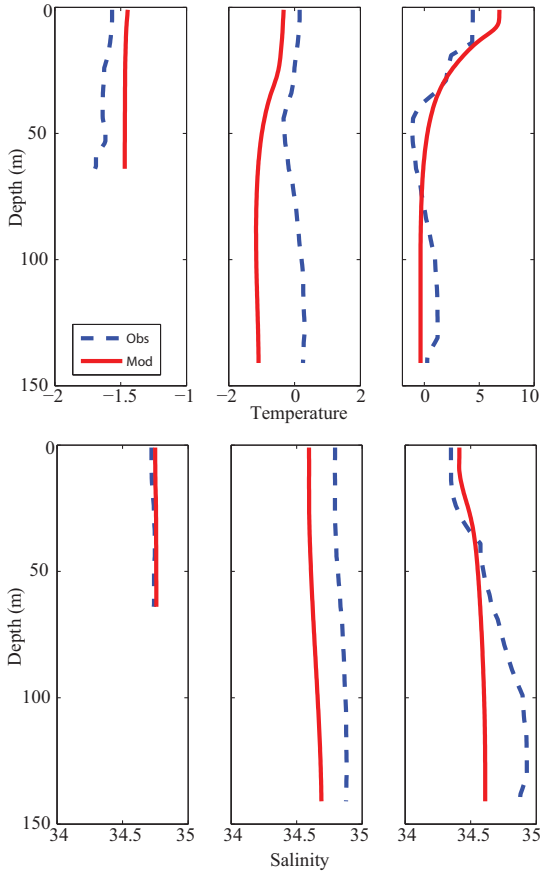

Figure 3: Vertical profiles of temperature (top) and salinity (bottom) at three selected stations: station 2 (left); station 8 (middle); station 13 (right). Blue, broken lines: Observations. Red lines: Model.

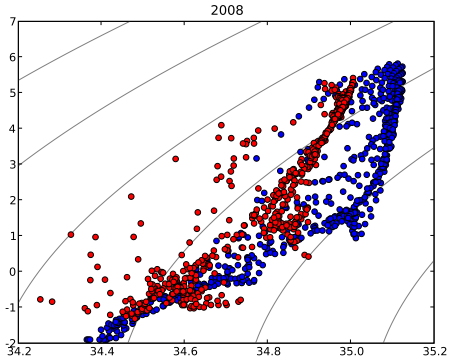

Figure 4: *T-S* diagram of the grid cell values from the hydrographic atlas in blue and the model values in the same cells in red. Both datasets are averages for August-September-October 2008 at 50 m.

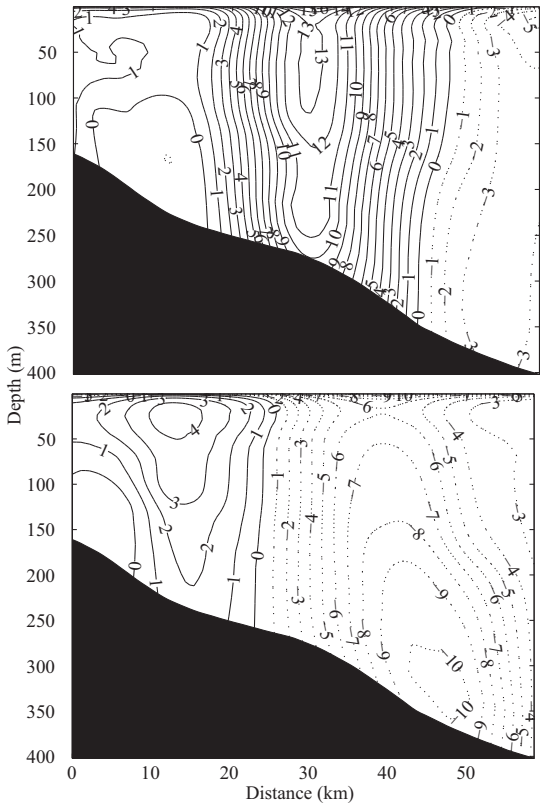

Figure 5: Vertical section through the Warm Core Jet, showing velocity perpendicular to the section (positive towards northeast) in March (top) and October (bottom). 2007 to the left and 2008 to the right. The position of the section is shown in Fig. 1

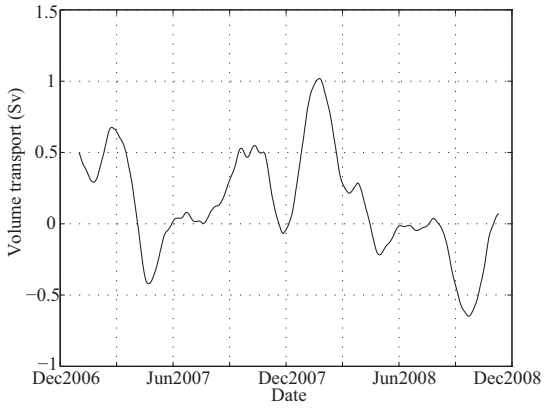

Figure 6: Net volume flux through the WCJ-section shown in Fig. 5. Positive values towards northeast. (See Fig. 1 for position of section)

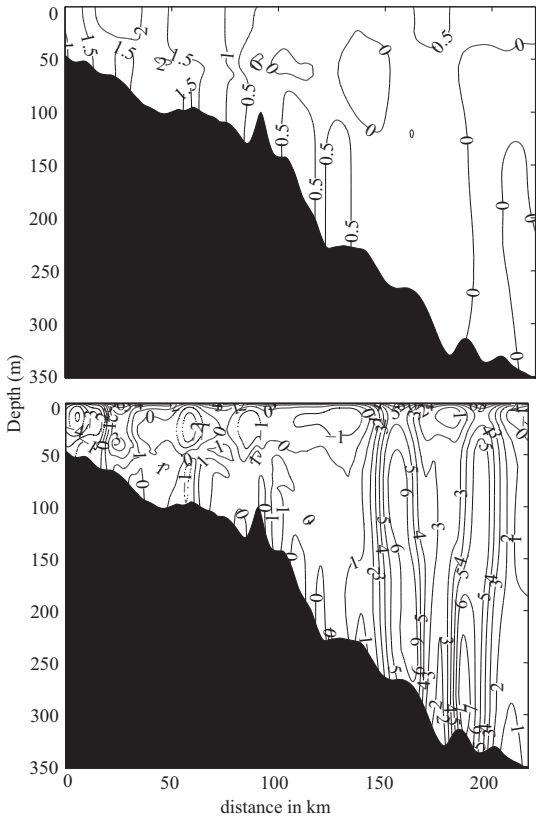

Figure 7: Temperature difference in °C (top) and cross-section velocity difference in cm s^{-1} (bottom) between October 2007 and October 2008.

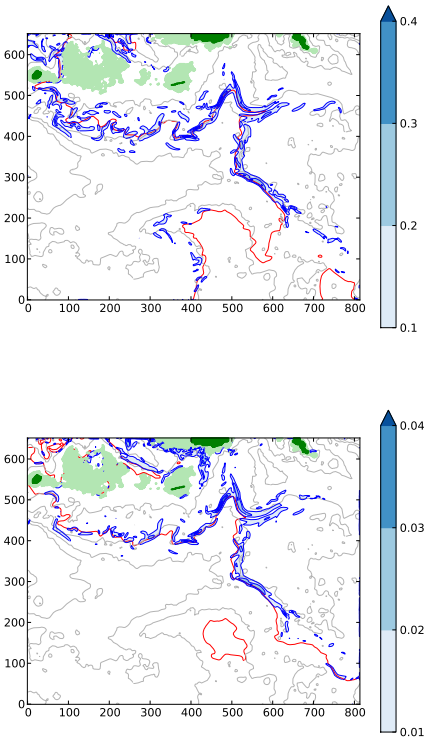

Figure 8: Modeled fronts in 50 meters depth in May 2008. Top: isolines of temperature gradient in deg C/km. The red line is the 1 degree isoterm. Bottom: isolines of salinity gradient in psu/km. The red line is the 34.8 isohaline. The grey lines in both panels are the 100,200,300, and 400 meter isobaths. Scales show model grid points (model domain shown in Fig. 1)

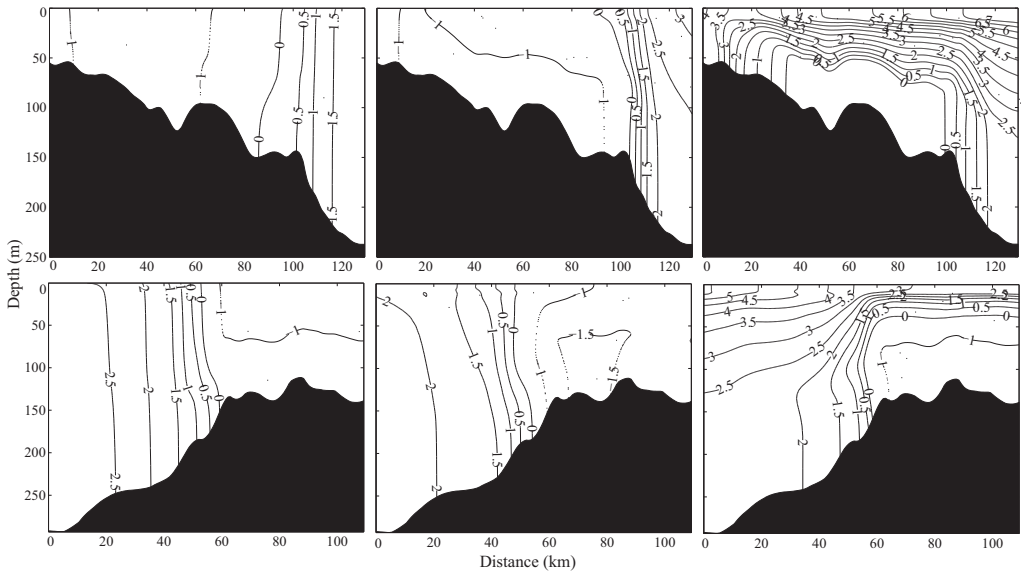

Figure 9: Temperature in the Svalbardbanken section (top) and the Storbanken section (bottom) in 2008. February (left), May (middle) and August (right). See Fig. 1 for position of the sections.

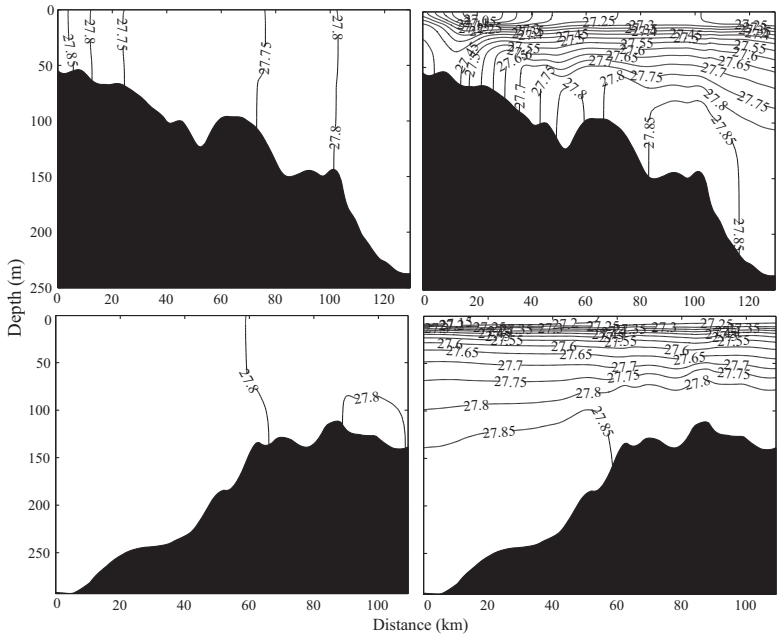

Figure 10: Density in the Svalbardbanken section (top) and the Storbanken section (bottom) in 2008. February (left) and August (right). See Fig. 1 for position of the sections.

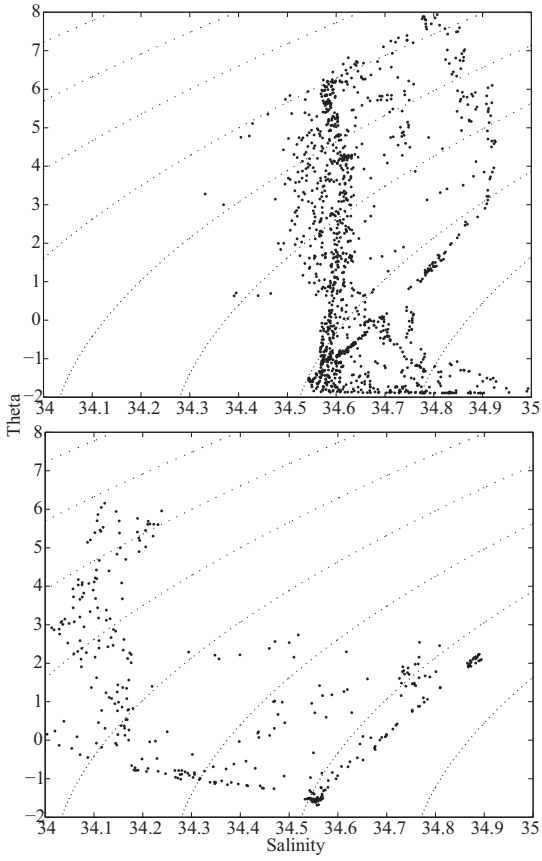

Figure 11: Θ-S at the surface at stations 1 to 10 (top) and stations 11 to 13 (bottom) in the period 1st of April to 31st of July, 2008. Dotted lines show isopycnals.

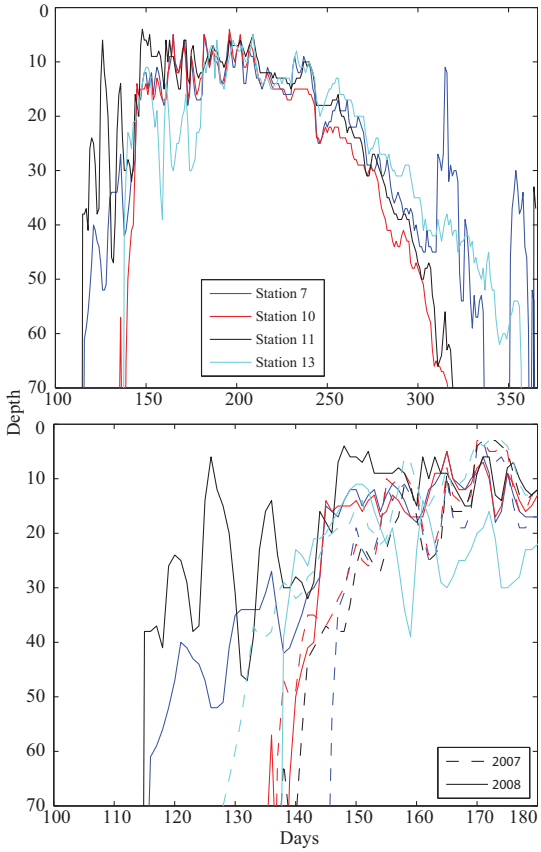

Figure 12: Mixed layer depth at 4 selected model stations. 2008 conditions (top) and a comparison between 2007 (broken lines) and 2008 (solid lines; bottom). (see Fig. 1 and Table 1 for position of stations)

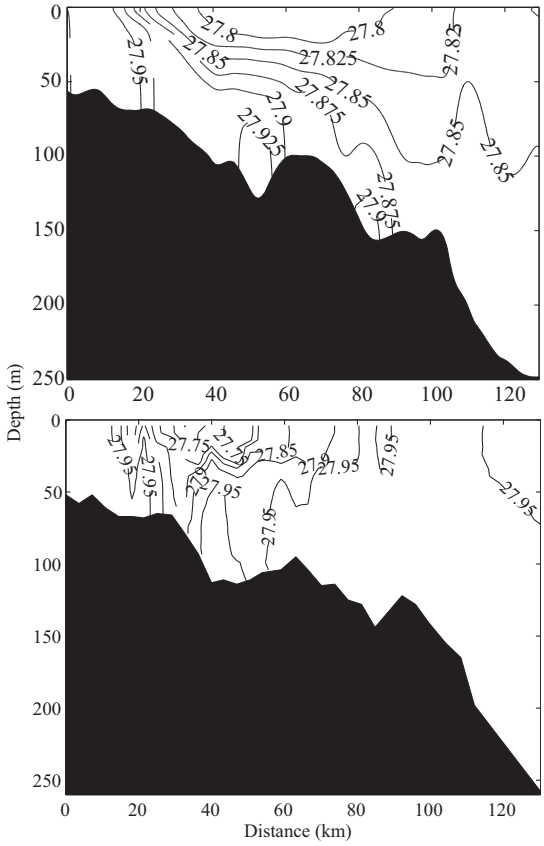

Figure 13: Potential density in the Hopen-section (13th to 15th of May 2008). Top: modeled average. Bottom: observations. (Note the different length scale).

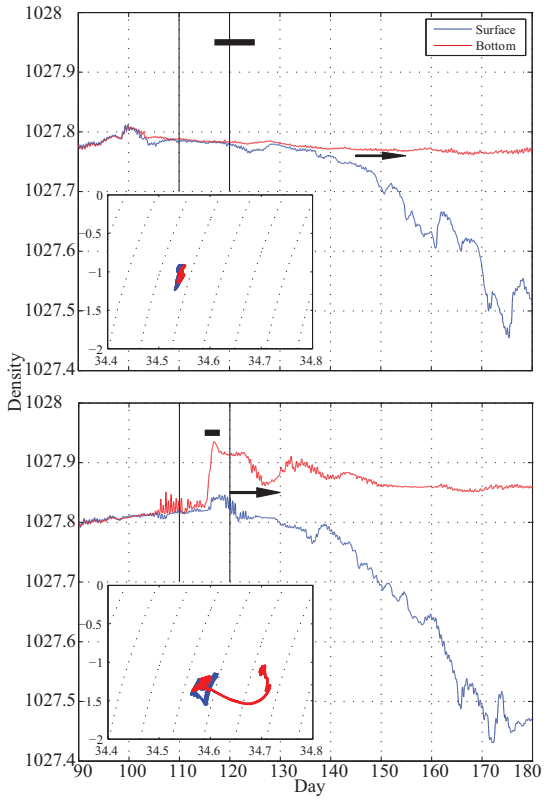

Figure 14: Modeled density at surface (blue) and bottom (red) at station 7; 2007 (top) and 2008 (bottom). Θ-S diagrams for the period indicated by black lines are shown in lower left corner. Arrows indicate 10-day periods in which the conditions become favorable for primary production and the start of the algal blooms can be expected (see also Fig. 15). Thick, black bars show periods in which the station has ice cover in excess of 15%.

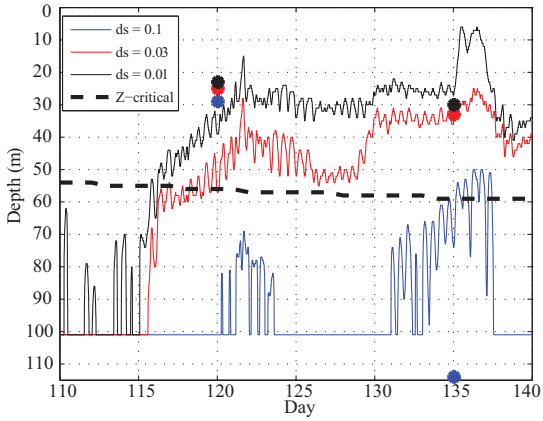

Figure 15: Modeled mixed layer depth for three different choices of $\Delta\sigma_\Theta(z)$ at model station 7 (see Fig. 1 and Table 1 for station location). Stars show corresponding mixed layer depths calculated from an average vertical profile based on 1 CTD-measurement (day 120) and 2 CTD-measurements (day 135) at the same location. Thick, broken line represents the estimated critical depth.

Paper IV

A. Melsom, V.S. Lien and W.P. Budgell

Using the Regional Ocean Modeling System (ROMS) to improve the oceanic circualtion from a GCM 20th century simulation

Ocean Dynamics, 59, 969-981, 2009

IV

Ocean Dynamics (2009) 59:969–981
DOI 10.1007/s10236-009-0222-5

Using the Regional Ocean Modeling System (ROMS) to improve the ocean circulation from a GCM 20th century simulation

Arne Melsom · Vidar Suren Lien · William Paul Budgell

Received: 4 March 2009 / Accepted: 30 July 2009 / Published online: 3 September 2009

Abstract Global coupled climate models are generally capable of reproducing the observed trends in the globally averaged atmospheric temperature. However, the global models do not perform as well on regional scales. Here, we present results from a 20-year, high-resolution ocean model experiment for the Atlantic and Arctic Oceans. The atmospheric forcing is taken from the final 20 years of a twentieth-century control run with a coupled atmosphere–ocean general circulation model. The ocean model results from the regional ocean model are validated using observations of hydrography from repeat cruises in the Barents Sea. Validation is performed for average quantities and for probability distributions in space and time. The validation results reveal that, though the regional model is forced by a coupled global model that has a noticeable sea ice bias in the Barents Sea, the hydrography and its variability are reproduced with an encouraging quality. We attribute this improvement to the realistic transport of warm, salty waters into the Barents Sea in the regional model. These lateral fluxes in the ocean are severely underestimated by the global model. The added value with the regional model that we have documented here lends hope to advance the quality of oceanic climate change impact studies.

Keywords Model validation · Barents Sea · Regional climate · Ocean modeling

Responsible Editor: Phil Dyke

A. Melsom (✉)
Norwegian Meteorological Institute,
P.O. Box 43 Blindern, 0313 Oslo, Norway
e-mail: arne.melsom@met.no

V. S. Lien · W. P. Budgell
Institute of Marine Research, Bergen, Norway

W. P. Budgell
Bjerknes Centre for Climate Research, Bergen, Norway

W. P. Budgell
Dept. of Physics and Physical Oceanography,
Memorial University of Newfoundland,
St. John's, Newfoundland and Labrador, Canada

1 Introduction

Climate and climate change affect the Barents Sea ecosystem by influencing species through changes in reproduction, recruitment (Sætersdal and Loeng 1987; Ellertsen et al. 1989), growth, and distribution (Nakken and Raknes 1987; Michalsen et al. 1998). Therefore, marine ecosystems are vulnerable to climate change, especially when key species are affected. In order to address the implications of future climate change on assessments of marine resources, results are needed with a resolution that resolves the relevant physical quantities, such as eddies and a realistic description of the bottom topography and the coastline. However, a horizontal resolution of the order of a few kilometers, which is needed for such purposes, is still not feasible when running global climate models.

The Barents Sea is a major heat sink for the Atlantic water on its way to the Arctic Ocean. Water mass transformation through freezing of sea ice and subsequent brine release and cooling of the ocean produces dense water that may sink to great depths in the Arctic Ocean (Midttun 1985). This contributes to the deep water formation in the Arctic (e.g., Rudels et al. 1994; Schauer et al. 2002; Quadfasel et al. 1988) and, thus, also to

the Atlantic thermohaline circulation. In order to get a realistic Barents Sea climate, it is therefore important to get a sufficient inflow of warm Atlantic water into the Barents Sea with a subsequent cooling of this water mass.

While model results for the northern hemisphere sea ice edge generally agree reasonably well with observations, Arzel et al. (2006) find that over half of the atmosphere–ocean general circulation models (AOGCMs) used in the fourth assessment report from the Intergovernmental Panel on Climate Change (IPCC-4AR) overestimate sea ice in the southern Barents Sea. Arzel et al. (2006) also note that models that perform well when validating the present climate sea ice extent are not necessarily also superior when it comes to results for the poleward heat transport. According to Parkinson et al. (2006), the oceanic heat transport by the North Atlantic Current in the Nordic Seas is underestimated in several of the IPCC-4AR climate models. This often leads to excessive sea ice cover in the Barents Sea region in the models. Moreover, the coarse resolution of these models makes it impossible to represent the topographic features with which the currents that transport heat into the Barents Sea are associated.

Here, we try to overcome some of these problems by applying atmospheric forcing from the atmospheric module of an AOGCM to a basin-scale, high-resolution, coupled ocean/sea ice model. Thus, some important processes that are not resolved or included in the coarser climate models are described in the high-resolution regional model. These differences include a more realistic bathymetry, shelf–ocean interactions, tides, and improved mixing. Our model will reproduce the Atlantic inflow to the Nordic Seas (Sandø and Furevik 2008), as well as to the Barents Sea, as long as the large-scale wind stress curl over the Atlantic and Nordic Seas is captured. The higher-resolution ocean model can then properly represent the roles of topography, tidal mixing, and fronts to produce a realistic ocean circulation. A similar effort has previously been performed for another shelf area, the North Sea (Ådlandsvik and Bentsen 2007).

Most evaluations of the performance of climate models in the Arctic have focused on atmosphere properties (e.g., Chapman and Walsh 2007; Walsh et al. 2008) and the seasonal variability and/or trends of sea ice extent (e.g., Parkinson et al. 2006; Arzel et al. 2006; Overland and Wang 2007). Regional sea ice/ocean circulation models for the Arctic forced with atmospheric reanalysis products have also been examined (e.g., Karcher et al. 2003; Maslowski et al. 2004). Walsh et al. (2008) compute the multi-model area-mean root-mean-square error (RMSE) of the surface temperature of the atmosphere. They find that the RMSE is in the range 3–6 K for the various seasons, when the region northward of 60°N is considered. Chapman and Walsh (2007) report negative biases during winter in the Barents Sea of 8–12 K in their examination of 14 IPCC-AR4 AOGCMs. In order to examine the relations between such relatively large errors in the atmospheric module of coupled climate models with the corresponding ocean circulation in the Arctic, we force a regional ocean/sea ice circulation model with atmosphere results from an AOGCM. The distribution of oceanic heat and salt in the problematic region of the Barents Sea are validated using various techniques, including a novel examination of how well the inter-annual variability is reproduced. Results for a 15-year present climate period are evaluated in this study, and we find that the results are substantially improved when compared to the corresponding results from the global model.

The aim of this paper is to validate the regional model for the Barents Sea and quantify the added value relative to a global simulation. Section 2 presents the AOGCM that is considered, and describes the high-resolution ocean/sea ice model from which results will be analyzed here. Then, the data sets used in the validation are described in Section 3. A brief introduction to the general hydrography and circulation at the entrance to the Barents Sea is given in Section 4. The validation follows in Section 5, and some conclusions are presented at the end of the paper in Section 6.

2 The model experiment

From the International Panel on Climate Change Fourth Assessment Report (IPCC WG-I/8 et al. 2007b), results from 20 AOGCMs are available. Ideally, all AOGCMs should be used in making an ensemble of regional simulations. However, due to both feasibility and the quality of the results of global AOGCMs on regional scales, results from only one AOGCM are used to force the regional ocean/sea ice model. In this study, a good representation of sea ice in the Arctic in general and the Barents Sea in particular is rated as the most important criterion when choosing an AOGCM. Overland and Wang (2007) use a limit of reproducing Arctic ice area within 20% and seasonal ice zone within 30% of observations as criteria for classifying a model as "good" in the present context. Then, out of the 20 AOGCMs, only three models perform well in both the Arctic as a whole and in the Barents Sea. In the present study, the Goddard Institute for Space Studies Atmosphere–Ocean Model (GISS AOM) is

chosen. The other two models passing the two "goodness" criteria in both the Arctic and the Barents Sea are Community Climate System Model version 3.0 of the National Center for Atmospheric Research and the Hadley Centre Global Environmental Model version 1 of the Hadley Centre for Climate Prediction and Research.

GISS AOM ran on a global grid with a resolution of four by three degrees in longitude and latitude, respectively, in both the atmosphere and the ocean. Geo-potential was used as the coordinate in the vertical direction in the ocean module, with a maximum of 16 z levels. The number of vertical layers in the ocean depends on the horizontal location but is constant in time. The layer thicknesses are adjusted at each horizontal location after computation by the dynamical subroutines at each time step such that the ratio of the mass of a grid box divided by the mass of the grid box below it is 8/11. A sea ice model calculating sea ice thickness and snow amount was coupled to the model system. Tides were not included. See the GISS AOM website http://aom.giss.nasa.gov/ for further details.

The coupled ice–ocean numerical model used for the regional simulation is the Regional Ocean Modeling System (ROMS), described in Shchepetkin and McWilliams (2005). The regional model is run on a stretched orthogonal curvilinear grid with an average resolution of 10 km, covering the Arctic and the Atlantic down to about 20°S. The domain and the variable resolution is displayed in Fig. 1. In the vertical, 40 generalized sigma (s-coordinate) levels are applied using the scheme of Song and Haidvogel (1994), with stretching that enhances the resolution towards the surface and the bottom. This provides a very good vertical resolution in shelf areas. For example, with a depth of 200 m and the parameter for surface stretching $\theta_s = 5.0$, the parameter for bottom stretching $\theta_b = 0.4$, and a critical depth of 10 m, at a pycnocline depth of about 20 m, the vertical grid resolution is better than 3.7 m. The method for computing the horizontal pressure gradient has been described by Shchepetkin and McWilliams (2003).

Daily mean sea level pressure, surface winds, surface air temperatures, surface specific humidity, downward long wave radiation at the surface, downward short wave radiation at the surface, and precipitation values were extracted from the GISS AOM results and used to provide atmospheric forcing for ROMS through the use of the bulk flux algorithm due to Fairall et al. (2003). At the lateral open boundaries of the ocean module, monthly mean climatological values from the Simple Ocean Data Assimilation (SODA) data set (Carton et al. 2000a, b) for the period 1981–2000 are used. Ice concentration, thickness, and velocity lateral boundary conditions for the sea ice module were taken from an annual monthly mean climatology constructed from GISS AOM fields for the period 1981–2000. Initial conditions were taken from January values from the SODA and GISS AOM climatologies for ocean and ice variables, respectively. Along the open boundary in the South Atlantic, SODA has a horizontal resolution of 50–55 km, while the corresponding resolution in GISS AOM is about 350 km.

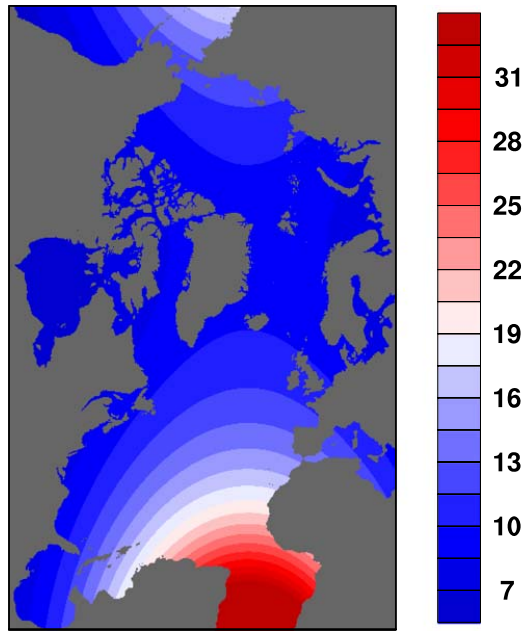

Fig. 1 Model domain and horizontal resolution. Land (dry grid cells) are displayed as *gray regions*, while the *color shading* corresponds to resolution in km as given by the *color bar* to the right. A contouring interval of 1.5 km was used

Tides are included in the ROMS simulation, with eight tidal constituents (M2, S2, N2, K2, K1, O1, P1, and Q1) from TPX 0.7 (Egbert and Erofeeva 2002) and tidal potential. Preliminary validation of model results with current meter data in the Barents Sea region suggests that modelled tidal current amplitudes are approximately 10% too large (G. Forristal, personal communication). The tides are important for mixing and ice freezing/melting in the Barents Sea and, thus, important for the heat transfer from ocean to atmosphere. In a numerical sensitivity study covering the Barents Sea, Harms et al. (2005) found an annual average of 15% increase in heat loss from ocean to atmosphere by

including M2 tide compared to a control run without tides.

The ice model dynamics are based on the elastic–viscous–plastic (EVP) rheology after Hunke and Dukowicz (1997) and Hunke (2001), and the ice thermodynamics are based on Mellor and Kantha (1989) and Häkkinen and Mellor (1992). The ice module used in ROMS has been ported from the Norwegian Meteorological Institute's Ice Model (MI-IM), documented by Røed and Debernard (2004).

The Barents Sea includes areas that are seasonally or permanently ice-covered. Atmosphere–ocean fluxes therefore have a large spatial and temporal variability. There is no coupling back from the regional model to the atmospheric boundary layer. However, feedback between the model surface temperature and the computed sensible, latent, and net long-wave radiation heat fluxes reduces the problem with drift in the surface temperature in ROMS. Still, wrong ice distribution in the climate model will affect the atmosphere–ocean fluxes in the high-resolution model. This is a major challenge.

To prevent long-term drift in the model salinity, the sea surface salinity is restored to climatology based on the Common Ocean-Ice Reference Experiment (CORE; see http://data1.gfdl.noaa.gov/nomads/forms/mom4/COREv2.html) (Large and Yeager 2008), with a restoration time of 360 days. Although restoring the sea surface salinity towards climatology, this allows for some inter-annual variability in the model salinity. Together with the flux correction, this reduces the regional model sensitivity to regional biases in the climate model atmosphere.

Surface freshwater runoff forcing was also obtained from CORE. The data are the annual mean river runoff distributed globally with a resolution of 1° in longitude and latitude. The data were interpolated to the model grid and took the same form as precipitation input, i.e., the freshwater supply altered the surface salt flux but no mass or momentum was added to the system. Hence, the diffuse nature of this runoff forcing does not allow for the evolution of coastal currents and salinity fronts at a distance of the order of 100 km off the coastline, even though the resolution in ROMS is sufficiently fine to describe such currents. Additional errors result from the lack of an annual cycle in the river runoff forcing.

The ROMS simulations have been performed for two periods, 1981–2000 representing the present climate and 2046–2065 representing the future scenario SRES A1B (IPCC WG-I/2 et al. 2007a). Five years is considered as spin-up, and only the remaining 15 years are used in the analysis. The first period will be used as a control run and is validated in this work, while analysis of results for the latter period will be reported in an upcoming publication.

3 Observations and model results

Hydrographic data along fixed cruise tracks and cast positions are available from the Institute of Marine Research (IMR; Kangas et al. 2006). The data have been subjected to a quality assurance process at IMR, using the The Integrated Global Ocean Services System standard. Observations were made as CTD casts with a vertical resolution ranging from 1 to 5 m. Here, the data were integrated over 10-m bins prior to the model validation. There are three cruise tracks that are frequently visited, from which the data are relevant for the present purpose. These tracks are "Bjørnøya west" (BW), "Fugløya–Bjørnøya" (FB), and "Vardø north" (VN). The number of CTD casts from these cruise tracks that are used in the present analysis is listed in Table 1. The cruise tracks and positions of the CTD casts are displayed in Fig. 2.

The results from GISS AOM are available as monthly means. Results were provided on a variable resolution grid in the vertical, consisting of 31 geopotential levels. As described in Section 2, the spatial resolution in GISS AOM is 4° in longitude, 3° in latitude. As can be seen from Fig. 2, each of the cruise tracks is spanned by very few grid cells in the GISS AOM (two to four cells). Hence, examination of horizontal gradients along the cruise tracks is of little value. Note also that a point-to-point comparison along the FB track will be tainted by the the poor local representation of the Norwegian coast in this region.

The present ROMS simulation uses variable resolution in the horizontal. As shown in Fig. 1, the resolution in the Barents Sea region is 8–9 km. Results from ROMS were available at the 40 s levels used in the simulation.

For the validation in Section 5, all model results are interpolated linearly in time. In the vertical direction, results are extracted from the model layer that corresponds to the observation depth. When a model's

Table 1 Hydrographic data used in the present study

Cruise track	Winter	Spring	Summer	Fall
Bjørnøya west	0	86	84	127
Fugløya–Bjørnøya	308	579	447	448
Vardø north	286	233	393	212

Values are no. CTD casts from the three cruise tracks from the period 1986–2000, sorted by season. Winter, spring, summer, and fall are defined as D-J-F, M-A-M, J-J-A, and S-O-N, respectively

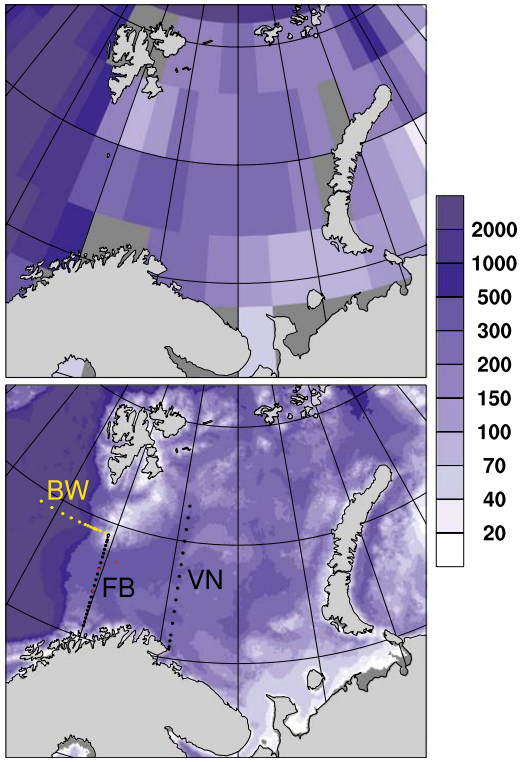

Fig. 2 The bottom topography in GISS AOM and ROMS for the Barents Sea region is displayed in the *top* and *bottom panels*, respectively. Grid cells that are dry are shown as *dark gray regions*. Actual land has been superimposed as *light gray regions*. The *shading* corresponds to model depth in m, as given by the *color bar* to the right. *Full circles* show the positions of the CTD stations where the observations were taken, along the labelled cruise tracks "Bjørnøya west" (*BW*), "Fugløya–Bjørnøya" (*FB*), and "Vardø north" (*VN*). *Red dots* indicate the positions of the moorings that are used in Section 5.3. Note that two of the mooring sites coincide with stations of the "Fugløya–Bjørnøya" cruise track

bottom depth is smaller than the observed bottom depth, the deepest model value is extrapolated downward. In the horizontal, bi-linear interpolation is applied.

The seasonal variability has a considerable magnitude in the present region, both in the atmosphere and in the upper ocean. Moreover, while sea ice has only rarely occurred in the tracks in recent years, more than half of the coupled ocean–atmosphere models have a seasonal ice cover in the entire Barents Sea in their baseline climate (1980–1999) (IPCC WG-I/8 et al. 2007b). Hence, we will conduct the present analysis on a seasonal basis. Here, we define the seasons as winter in December, January, and February, spring in March, April, and May, summer in June, July, and August, and fall in September, October, and November. Note that there were very few casts available from the BW track during winter, so hydrographic data and model results from BW for this season are discarded in the present analysis.

4 The regional ocean circulation and hydrography

The mean values for salinity and temperature from the upper 50 m reveal that all of the three tracks are dominated by water masses that are relatively saline and warm for such high latitudes. The main source is the poleward-flowing Norwegian Atlantic Current, which splits into two branches as it leaves the coast of northern Norway.

The western branch continues northward along the continental shelf break and becomes the West Spitsbergen Current. The BW cruise track intersects this current. The eastern branch flows eastward into the Barents Sea as the North Cape Current. This current is first intersected by the FB track, and further to the east by the VN track.

Coastal water in the Norwegian Coastal Current (NCC), occupying the southernmost part of the FB track, accounts for an additional volume and heat transport into the Barents Sea. This water mass is distinguishable from Atlantic water by its lower salinity range ($S < 34.7$). A common definition of Atlantic water in the Barents Sea is by temperature ($T > 3\ ^\circ C$) and salinity $S > 35.0$ (Loeng 1991). Based on an array of moorings along the FB track and using these criteria, Skagseth et al. (2008) found that this branch carries 1.8 Sv of Atlantic water on average, with a corresponding heat flux of 48 TW. The inflow was reported to show an upward trend of 0.1 Sv/year from 1997 to 2006 and a relatively large temporal variability on several time scales.

The data show that the saltiest water is found in the BW track, reaching an average value of 34.99 in the upper 50 m of the cross-section during spring. The corresponding maxima for the FB and VN tracks are 34.88 and 34.83, respectively. There is a general freshening in the upper 50 m as the water flows eastward from FB to VN, ranging from 0.01 during fall to 0.09 during spring.

The coldest cross-sectional average of the upper ocean water is found in BW, which is the northernmost track. Here, the average temperature reaches a high of 5.3 °C during summer. In FB and VN, the seasonal highs are attained during fall, with values of 7.1 °C and

6.3 °C, respectively. There is a cooling in all seasons of the upper ocean as the water flows eastward in the southern part of the Barents Sea. The largest cooling from FB to VN is 1.3 K, which occurs during winter when the overlying atmosphere is at its coldest.

5 Model validation

The model validation is performed by comparing model results that are interpolated in space and time to the observed data, as outlined in Section 3. It is important to realize that the atmospheric forcing in this region has considerable variability, which, to a large extent, is associated with the North Atlantic Oscillation (NAO; Hurrell 1995; Hurrell et al. 2003). NAO is due to processes that are internal to the atmosphere (Thompson et al. 2003) and has a random and unpredictable character on time scales ranging from months to decades (Hurrell et al. 2003). The GISS AOM simulation does not include assimilation of observations; hence, the local atmospheric circulation in GISS AOM from a particular month and year will generally correspond to a NAO signal that is different from the observed index value at that time. The validation that follows in Subsections 5.1–5.3 is restricted to the upper 50 m of the water column, which is significantly impacted by the ocean–atmosphere fluxes. In order to account for the discrepancy regarding NAO, we compare observations with model results at the corresponding time of the year, but the actual year is chosen randomly from the 15 years with available model results from ROMS.

Most of the NAO variability occurs at time scales less than 3 years (see, e.g., Fig. 12 in Hurrell et al. 2003). Hence, statistical measures such as biases and probability distributions that are derived from a 15-year analysis are representative, since errors that are associated with mismatching conditions and different NAO indices will tend to cancel each other. Even the temporal variability itself can be validated by examining the scatter in time in the observations and model results.

There is an underlying trend in the global atmospheric surface temperature for the period in question due to trends in the composition of Earth's atmosphere (IPCC WG-I/2 et al. 2007a). Changes in the radiative forcing are included in the coupled GISS AOM simulation, which this study is based upon. However, the amplitude of the regional internal atmospheric variability in the Arctic is of a much larger magnitude than the global trends (Räisänen 2002).

Due to the poor match between the horizontal resolution in GISS AOM and the distance between the positions of the CTD stations, we will limit the validation of results from GISS AOM to integrated statistics (mean bias) for the BW track (which represents the water masses in the Nordic Seas adjacent to the Barents Sea) and VN track (the longest of the cruise tracks). Validation of integrated quantities (fluxes of mass and heat) from GISS AOM is also provided.

5.1 Overall validation

The biases of the model results with respect to the observations are listed in Table 2. We note that, in the upper 50 m, ROMS is somewhat warmer than the observations in the west (BW and FB), and generally slightly too salty in the east (FB and VN). Overall, the ROMS results are remarkably close to the observations. GISS AOM is too cold (by about 1 K) and too fresh (by 0.2–0.3) when compared to data from the BW track. Moreover, the validation of GISS AOM exhibits a significant deterioration inside the Barents Sea, with biases of 5 K and 1 in temperature and salinity, respectively.

In order to gain more insight into the performance of ROMS, we compute the probability density function (pdf) for temperature and salinity in the upper 50 m,

Table 2 Biases in hydrography results relative to the observations

Results for the upper 50 m for temperature (in K) and salinity are shown in the upper and lower half of the table, respectively

Cruise track	Model	Winter	Spring	Summer	Fall
Temperature					
Bjørnøya west	GISS AOM		−1.0	−1.1	−0.5
Vardø north	GISS AOM	−4.2	−4.2	−5.3	−4.3
Bjørnøya west	ROMS		0.3	0.1	0.2
Fugløya–Bjørnøya	ROMS	0.6	0.6	0.2	−0.2
Vardø north	ROMS	−0.0	−0.5	−0.8	−1.0
Salinity					
Bjørnøya west	GISS AOM		−0.26	−0.27	−0.19
Vardø north	GISS AOM	−0.79	−0.76	−1.33	−1.43
Bjørnøya west	ROMS		−0.04	−0.02	0.10
Fugløya–Bjørnøya	ROMS	−0.04	0.04	0.12	0.18
Vardø north	ROMS	0.06	0.05	0.15	0.20

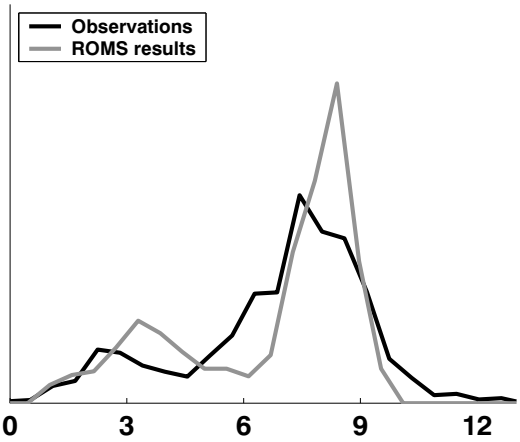

Fig. 3 Probability density function for temperature for the fall (S-O-N) season from the "Fugløya–Bjørnøya" track. The analysis was restricted to observations and model results from the upper 50 m. Values along the *horizontal axis* are temperatures in °C. The amplitude has been scaled so that the area under each curve is the same

based on observations and model results from the fall season. The results for temperature and salinity from the FB track are shown in Figs. 3 and 4, respectively.

With the exception of the higher peak, the pdfs for temperature are similar in most aspects. The skewness parameter is −0.72 and −0.90 for observations and ROMS, respectively. The pdfs for temperature from the VN track are similar to those from the FB track.

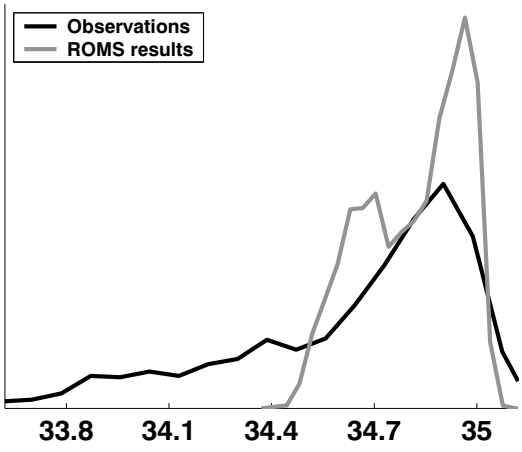

Fig. 4 Same as Fig. 3, but for salinity

The pdf from the ROMS results for salinity is also similar to the observed distribution in most aspects.

The most striking misrepresentation is that salinity values that are smaller than 34.4 are absent in the model. These results are representative for all seasons from the FB track. The lack of water masses in the model that have the signature of a coastal current is a primary cause for the narrower distributions and higher peaks in the pdfs of ROMS results. This discrepancy is due to the use of a 1° product for the runoff forcing.

The pdfs provide valuable information about the overall variability in the sampled region. However, they give no information about how the variability is distributed in space and time.

5.2 Variability in space

The cross-sectional averages of temperature and salinity in the FB track for the fall season are displayed in Figs. 5 and 6, respectively. Model results were interpolated to the observations' positions prior to averaging.

Again, we find that the results from ROMS are strikingly similar to the observations, particularly for temperature. There are horizontal fronts in the ROMS results that are in the correct positions when compared to the observed fronts; the ROMS salinity fronts are too weak, though. Observations and ROMS results for other seasons exhibit similar features to those from the fall season.

The results for the BW track (not shown) are similar to those from FB, with a temperature front near Bjørnøya in the observations and in the results from ROMS. For the VN track (also not shown), there are no well-defined temperature fronts in the cross-sectionally averaged fields, although the observations and the ROMS results are somewhat colder in the north. The salinities from ROMS are close to the observed values in the interior, but ROMS underestimates the gradient near the coast, as it does not reproduce the magnitude of the salinity minimum in this region. This is due to the coarse resolution of the freshwater runoff forcing from the CORE data set, as discussed in Section 2.

In order to assess the magnitude of the differences between model results and observations, it is useful to scale these differences by a spatially dependent quantity that represents variability. Here, we compute the standard deviation of temperature and salinity for each season, from each CTD station and each 10 m bin in the vertical, based on all of the observations available from 1980 to 2007.

The absolute values of the normalized model vs observation differences are then computed, and results are weighted spatially by the distance between the

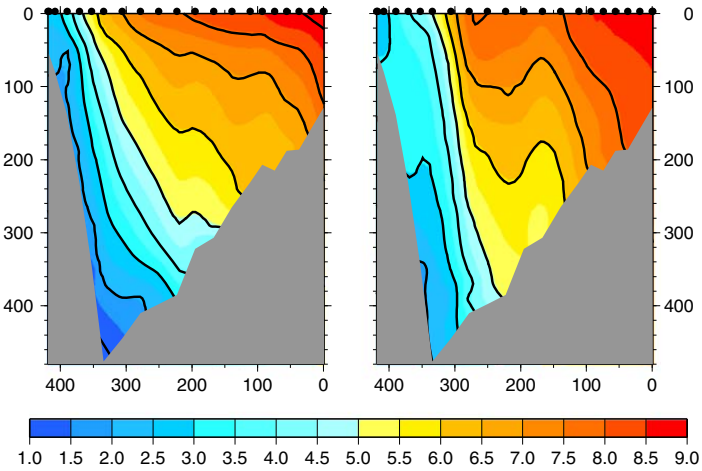

Fig. 5 Temperature cross-section of the "Fugløya–Bjørnøya" cruise track, based on all dates in the fall season (S-O-N) with cruise data for the period 1986–2000. Results based on observations and the ROMS model are displayed to the *left* and *right*, respectively. The *shading* corresponds to temperature values as given in °C by the *color bar* at the bottom, and *contour lines* have been added for each 1° value. The *vertical axes annotation values* are depths in m, while *values along the horizontal axes* are distances from the southernmost CTD station, in km. The positions of the stations are shown as *full black circles* at the top of each panel, and the figures are drawn to view the cross-section from west towards east

various CTD stations. The resulting mean normalized differences are listed in Table 3. Note that results from GISS AOM are not given, due to its insufficient horizontal resolution for the present purpose.

As explained above, there is no inter-annual phase lock between model results and observations. Hence, any mean normalized difference significantly smaller than 1 should be treated with suspicion. However, since the validation is performed with monthly means from the models, and instantaneous measurements, even a "perfect" model will have a normalized difference that is not 1. Presently, the normalization is carried out based on the observed variability, which has a higher variability than that from monthly mean values. Thus, we expect normalized differences to be somewhat lower than 1 for a "perfect" model. From Table 3, we

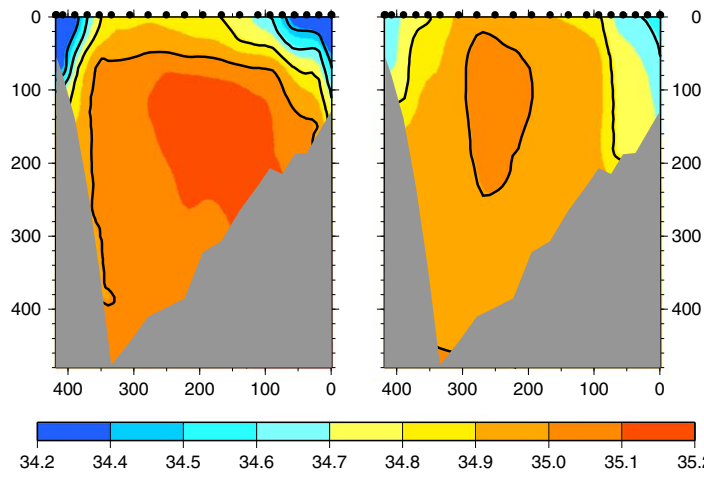

Fig. 6 Same as Fig. 5, but for salinity

Table 3 Normalized model vs observation differences for hydrography

Cruise track	Model	Winter	Spring	Summer	Fall
Temperature					
Bjørnøya west	ROMS		1.0	0.8	0.9
Fugløya–Bjørnøya	ROMS	1.0	1.3	0.8	0.9
Vardø north	ROMS	0.8	1.3	0.7	1.1
Salinity					
Bjørnøya west	ROMS		1.4	1.3	1.8
Fugløya–Bjørnøya	ROMS	1.4	1.4	1.0	1.0
Vardø north	ROMS	1.3	1.0	1.1	0.9

Results for the upper 50 m for temperature (in K) and salinity are shown in the upper and lower halves of the table, respectively

see that, with one exception, the normalized ROMS model vs observation differences are in the range 0.7–1.4.

5.3 Variability in time

As discussed above, it is difficult to assess the normalized model vs observation differences due to the lack of an optimal result. In order to shed more light on this topic, we propose to take advantage of the fact that the inter-annual variability in the observations and model results are de-coupled. Then, we can examine how well the observed temporal variability is described by the model by applying the method of ranking that is used for validation of an ensemble (Hammill 2001). Based on the mean temperature from ROMS in the upper 50 m of the FB track, we find that the auto-correlation at lags of 1 and 2 years are 0.4 and −0.3, respectively. Hence, we set the de-correlation time scale to 2 years and can construct an eight-member ensemble of the results for 1986–2000.

Another topic that needs to be addressed in this context is the mismatch in the sampling from the model and instruments. Model results are available as monthly means, whereas observations from the CTD casts are instantaneous. An analogous issue in the analysis of ensembles in weather forecasting is that, in order to correctly analyze the ensemble, one needs to take errors in the instrumental records into account. This can be done by adding noise to the observations to mimic instrument errors (Saetra et al. 2004).

In the present case, the mismatch introduced by monthly averaging of model results is much greater than the instrument errors. We have four time series of continuous temperature observations in the vicinity of the FB track at our disposal, their locations are displayed as red dots in Fig. 2. From two of the moorings, no data were available at depths smaller than 50 m. As an estimate of the variance that is lost by application of a monthly average, we compute the root mean square (RMS) offset from a least squares fit to each month of data from all moorings, at the 50-m level. We find that, during spring, the RMS offsets range from 0.1 to 0.4 K, while the corresponding range from the fall season is 0.1 to 0.55 K. For both seasons, the RMS differences increase from south to north. In the analysis that follows, we have thus added Gaussian noise with standard deviation given by the RMS values after the model results for each year were found by interpolating linearly in time between the monthly averages.

If the statistical properties of the inter-annual variability in the observations and the model results are the same, the probability that the observed value is smaller than the ensemble minimum, between the ensemble minimum and the second smallest ensemble value, etc., is the same for each interval (Hammill 2001). In an eight-member ensemble, there are nine different possible outcomes of such a ranking. Here, we simplify by restricting the analysis to count the frequency of observations that are inside the range of the ensemble. This corresponds to seven of the nine intervals, so ideally, the frequency should be $7/9 = 0.78$.

The aim here is to validate variability in time. However, the representation of spatial scales will also have an effect on ranking. If fronts such as those displayed in, e.g., the left panel of Fig. 5 are not resolved in the model, ranking will show that the model underestimates variability even if the temporal variability is described correctly. Hence, due to the coarse horizontal resolution in GISS AOM, we will limit the ranking analysis to the results from ROMS.

The results from the analysis for the FB track are provided as Table 4, for the low and high estimates of the RMS offsets in the data from the moored instruments. The probability of observed values falling inside either ensemble range is lower than the optimal value of 0.78, for both seasons and the whole RMS range.

Table 4 Fraction of temperature observations from the Fugløya–Bjørnøya track that falls within the ensemble range based on results from ROMS, based on observations at levels in the range 40–50 m

Season	RMS	Raw	De-biased
Spring	0.10	0.43	0.51
	0.40	0.56	0.58
Fall	0.10	0.52	0.55
	0.55	0.70	0.72

The optimal value for a eight-member ensemble is 0.78. RMS temperature offsets are in K. De-biasing was performed by subtracting the average of differences between model results and observations for levels between 40 and 50 m from the entire FB track. See the text for additional details

Nevertheless, given the slight underestimation of spatial variability that is evident from Fig. 5, we find that the temperatures from ROMS give a reasonable representation of the observed variability. A crude measure of the model performance in this context is "variability percentage," as given by the fraction between the tabulated values and the optimal value (0.78). Using the debiased model results, the percentage from the average of the low and high RMS estimates becomes 70% and 81% for spring and fall, respectively.

5.4 Volume and heat fluxes

It is difficult to make a consistent comparison between observed and modeled volume and heat fluxes. Observations are based on point measurements, while model data provide area averages over a grid box, but with higher spatial resolution than the observations. The distance between observation points is larger than the eddy scale, which would influence the comparison between model and observations even for a "perfect" model. Bias and possible drift in modeled salinity often complicate the comparison further, by obscuring the water mass definitions that are appropriate for the analysis of model results.

Figures 4 and 6 show that the salinity in the ROMS results is biased. They also show that water masses such as coastal water are underestimated in the model, seen by the lack of a tail at the lower end in the salinity pdf (Fig. 4). Two different approaches to separate Atlantic water from coastal water in the model include using temperature only and restrict the analysis to the geographical extent of the moorings, or using both temperature and salinity adjusted for model bias. In this validation, the first method is applied. This is consistent with the observations by Ingvaldsen et al. (2004), and will effectively distinguish between water masses of Atlantic origin and water masses in the NCC, as the NCC is situated south of the mooring section. The latter method, however, gave only slightly different results. In GISS AOM, the criterion is applied on the whole opening between Norway and Svalbard.

For the period 1986–2000, the modeled net inflow to the Barents Sea is 2.4 Sv in GISS AOM and 2.1 Sv in ROMS for all water masses. Using the definition above gives a corresponding Atlantic inflow of 1.1 Sv in GISS AOM and 1.8 Sv in ROMS. The observations reported by Skagseth et al. (2008) give an average Atlantic inflow of 1.8 Sv. The different results from the two models are mainly due to too-low temperatures in GISS AOM, as shown in Fig. 5.

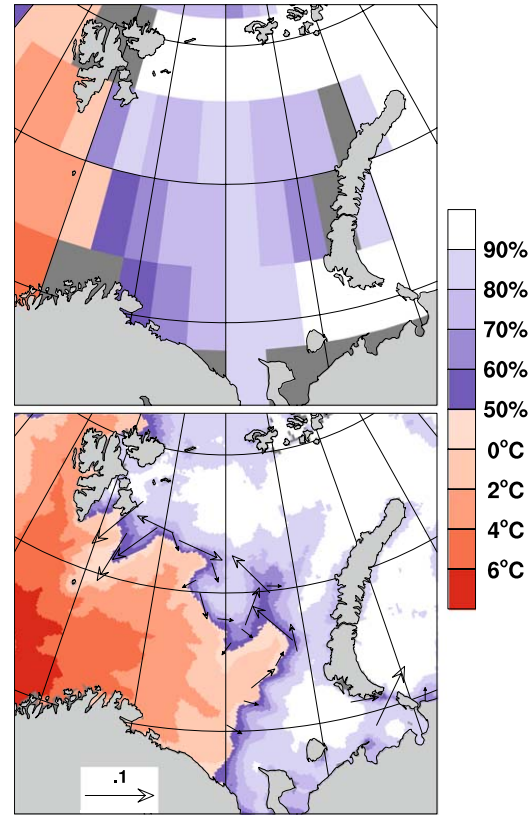

Fig. 7 Mean ice concentration and sea surface temperature (SST) in the Barents Sea during May, based on results from GISS AOM (*top*) and ROMS (*bottom*). The *shading* corresponds to ice cover area fractions wherever this exceeds 50% and SST values elsewhere, as given by the *color bar* to the right. Vectors display the velocity of sea ice in regions where the concentration is in the range 50–70%. The lengths of the vectors have been scaled by the *caption arrow inside the white box* in the bottom panel, which corresponds to a speed of 0.1 m/s. Vectors are only displayed when the speed is larger than 0.02 m/s. This threshold was not exceeded anywhere in the GISS AOM results for this region

In winter/spring, no water masses are classified as Atlantic water in GISS AOM, resulting in zero inflow of Atlantic water in the months February through May. The net inflow of all water masses, however, only shows a slight decline throughout winter and spring, and varies between 2.1 Sv in June and 2.9 Sv in October. The heat flux reflects the low temperatures and varies between 13 TW in March (0 TW for Atlantic water) and 45 TW in October (42 TW for Atlantic water), with an average of 27 TW (16 TW for Atlantic water) for

the whole period 1986–2000. This agrees poorly with observations (Skagseth et al. 2008), which suggest that the average heat flux carried by the Atlantic water into the Barents Sea is 48 TW. The heat flux is greatly increased in ROMS, despite a reduction in the total volume flux. For the whole period, the average net heat flux from all water masses amounts to 65 TW in the ROMS simulation, while the Atlantic water contributes with 46 TW.

Further, Skagseth et al. (2008) find that variability in heat flux through FB track is dominated by fluctuations in volume transport rather than temperature fluctuations: They found a higher heat flux in winter, when temperatures are lower, and attributed this to the stronger volume transports in winter.

GISS AOM shows the opposite behavior, with temperature changes being the dominant factor for the variability of heat flux in the inflow to the Barents Sea. The extensive Barents Sea ice cover in winter in GISS AOM (see Fig. 7 for the results from May) is attributed to the low heat flux into the Barents Sea in winter.

Although the ROMS results agree very well with observations regarding average fluxes on decadal timescales, the temporal variability is too low in the model. Skagseth et al. (2008) found the 12-month running mean volume transport into the Barents Sea to vary between a minimum of 0.8 Sv and maximum of 2.9 Sv within the 10-year period 1997–2006 (see Table 5 here). For the heat flux, the minimum and maximum values were 29 and 70 TW, respectively. The corresponding values from the 15-year period with results from ROMS are 1.5 and 2.1 Sv for volume transport minimum and maximum, respectively, and 41 and 51 TW for heat transport minimum and maximum, respectively.

Table 5 Volume fluxes (in Sv) and heat fluxes (in TW) through Barents Sea opening for Atlantic water only (defined geographically, see text)

Source	Mean	Min	Max
Volume flux			
GISS AOM	1.1	0.6	1.5
ROMS	1.8	1.5	2.1
Observations	1.8	0.8	2.9
Heat flux			
GISS AOM	16	8	25
ROMS	46	41	51
Observations	48	29	70

Min and max values are minimum and maximum values in 12-month filtered time series

GISS AOM shows a larger relative variability than the ROMS results, but the average fluxes are substantially underestimated, as described above. As also revealed by Table 5, ROMS produces realistic inflow of both volume and heat into the Barents Sea.

6 Conclusion

In the ROMS simulation that is examined here, ROMS was coupled to a dynamic–thermodynamic sea ice model as described in Budgell (2005). The results for sea ice from the GISS AOM and ROMS experiments are connected to the ocean temperature results as expected, since the Barents Sea has a much larger ice cover in the colder GISS AOM. We particularly observe that the sea ice retreat in GISS AOM is delayed in the spring season, as can be seen from Fig. 7. The GISS AOM results for sea ice, where the Barents Sea is, e.g., almost completely ice-covered during winter, does not at all correspond to the observations. The sea ice results can be compared to the observations from 1990 that are displayed in Rayner et al. (2003), see, e.g., their Fig. 1c,d. While the ROMS results also display a too-extensive sea ice cover, it is much closer to the observations than the GISS AOM ice cover.

The excess heat carried into the Barents Sea by Atlantic water in ROMS, as compared to GISS AOM, has an average value of 30 TW (see Table 5), or $8 \cdot 10^{19}$ J per month. If all of this energy is consumed by ice melting, this corresponds to a 1-m-thick ice cover over the entire Barents Sea being melted during a period of 4 months. We also note from Fig. 7 that ice retreat in ROMS due to advection only has an impact locally. Advection of sea ice in GISS AOM is slow-paced everywhere in the Barents Sea. Hence, most of the improvement in the description of sea ice in ROMS can be attributed to its realistic heat transport.

The same atmospheric forcing is applied to both of the ocean and sea ice models, albeit in different ways, since GISS AOM is a fully coupled system. Obviously, one must expect that the ROMS results are at least somewhat tainted by the GISS AOM atmosphere that has a lower boundary that is much too cold. Hence, it is encouraging to find that, even under these conditions, ROMS can provide results that constitute a realistic description of the hydrographic conditions in the upper water masses of the Barents Sea.

We have demonstrated that a regional ocean circulation model, run with a much higher horizontal resolution than what is feasible with a coupled general circulation model, is capable of a realistic representation of the

ocean circulation in a shelf sea. However, it is important to realize that the impact of the large-scale circulation may differ from one shelf sea to another. The Barents Sea is characterized by a strong impact from relatively warm waters that enter in the west, making it a much warmer shelf sea with less sea ice than other shelf seas at similar latitudes.

This study gives us reason to believe that much value can be added to projections of the future ocean climate from coupled AOGCMs by down-scaling using regional modeling. While AOGCMs that are eddy resolving in the ocean are not likely to transpire in the foreseeable future, regional models can provide information with a resolution that is more relevant for, e.g., oceanic biota.

The present results are generated on a variable mesh grid that is sufficient for resolving important large-scale circulation features such as the Gulf Stream separation (Smith et al. 2000), but too coarse to reproduce the circulation on the scales at which most meso-scale activity is found at high latitudes. Hence, extending the methodology by nesting an even smaller domain into a regionally downscaled model may be useful from the viewpoint of climate change impact studies.

Acknowledgements This work has been supported by the Climate of Norway and the Arctic in the 21st Century (NorClim) and Norwegian Ecosystem Studies of Sub-Arctic Seas (NESSAS) projects and the NOTUR supercomputing project, which are financed by the Research Council of Norway. GISS AOM results were downloaded from IPCC AR4 data archive at Lawrence Livermore National Laboratory. Computations were performed on the Atlantic Computational Excellence Network (ACEnet) of Canada facilities. Figures 1, 2, and 7 were made using NCAR Command Language (NCL; http://ncl.ucar.edu).

References

Arzel O, Fichefet T, Goosse H (2006) Sea ice evolution over the 20th and 21st centuries as simulated by current AOGCMs. Ocean Model 12:401–415. doi:10.1016/j.ocemod.2005.08.002

Ådlandsvik B, Bentsen M (2007) Downscaling a 20th century global climate simulation to the North Sea. Ocean Dyn 57:453–466

Budgell WP (2005) Numerical simulation of ice-ocean variability in the Barents Sea region: towards dynamical downscaling. Ocean Dyn 55:370–387. doi:10.1007/s10236-005-0008-3

Carton JA, Chepurin G, Cao X, Giese BS (2000a) A Simple Ocean Data Assimilation analysis of the global upper ocean 1950–1995, part 1: methodology. J Phys Oceanogr 30: 294–309

Carton JA, Chepurin G, Cao X (2000b) A Simple Ocean Data Assimilation analysis of the global upper ocean 1950–1995, part 2: results. J Phys Oceanogr 30:311–326

Chapman WL, Walsh JE (2007) Simulations of Arctic temperature and pressure by global coupled models. J Climate 20:609–632. doi:10.1175/JCLI4026.1

Egbert GD, Erofeeva SY (2002) Efficient inverse modeling of barotropic ocean tides. J Atmos Ocean Technol 19:183–204

Ellertsen B, Fossum P, Solemdal P, Sundby S (1989) Relations between temperature and survival of eggs and first feeding larvae of the North-East Arctic cod (*Gadus morhua L.*). Rapports et Procs-verbaux des Runions du Conseil international pour lExploration de la Mer 191:209–219

Fairall CW, Bradley EF, Hare JE, Grachev AA, Edson JB (2003) Bulk parameterization of air–sea fluxes: updates and verification for the COARE algorithm. J Climate 16:571–591

Häkkinen S, Mellor GL (1992) Modelling the seasonal variability of a coupled arctic ice–ocean system. J Geophys Res 97:20285–20304

Hammill TM (2001) Interpretation of rank histograms for verifying ensemble forecasts. Mon Weather Rev 129:550–560

Harms IH, Schrum C, Hatten K (2005) Numerical sensitivity studies on the variability of climate-relevant processes in the Barents Sea. J Geophys Res 110:C06002. doi:10.1029/2004JC002559

Hunke E, Dukowicz J (1997) An elastic–viscous–plastic model for sea ice dynamics. J Phys Oceanogr 27:1849–1867

Hunke E (2001) Viscous-plastic sea ice dynamics with the EVP model: linearization issues. J Comput Phys 170:18–38

Hurrell JW (1995) Decadal trends in the North Atlantic Oscillation and relationships to regional temperature and precipitation. Science 269:676–679

Hurrel JW, Kushnir Y, Ottersen G, Visbek M (2003) An overview of the North Atlantic oscillation. In: Hurrell JW, Kushnir Y, Ottersen G, Visbeck M (eds) The North Atlantic Oscillation: climate significance and environmental impact. Geophysical Monograph Series, vol 134. Amer. Geophys. Union, pp 1–35

Ingvaldsen RB, Asplin L, Loeng H (2004) The seasonal cycle in the Atlantic transport to the Barents Sea during the years 1997–2001. Cont Shelf Res 24:1015–1032

IPCC WG-I/2, Trenberth KE, Jones PD, Ambenje P, Bojariu R, Easterling D, Tank AK, Parker D, Rahimzadeh F, Renwick JA, Rusticucci M, Soden B, Zhai P (2007a) Observations: surface and atmospheric climate change. In: Solomon S, Qin D, Manning M, Chen Z, Marquis M, Averyt KB, Tignor M, Miller HL (eds) Climate change 2007: the physical science basis. Contribution of working group I to the fourth assessment report of the intergovernmental panel on climate change. Cambridge University Press, Cambridge

IPCC WG-I/8, Randall DA, Wood RA, Bony S, Colman R, Fichefet T, Fyfe J, Kattsov V, Pitman A, Shukla J, Srinivasan J, Stouffer RJ, Sumi A, Taylor KE (2007b) Climate models and their evaluation. In: Solomon S, Qin D, Manning M, Chen Z, Marquis M, Averyt KB, Tignor M, Miller HL (eds) Climate change 2007: the physical science basis. Contribution of working group I to the fourth assessment report of the intergovernmental panel on climate change. Cambridge University Press, Cambridge

Kangas T-V, Svendsen E, Strand Ø (2006) Average value of salinity and temperature in the Institute of Marine Research's fixed sections (in Norwegian). Report series "Fisken og Havet" 6/2006. Institute of Marine Research, Bergen, 53 pp

Karcher MJ, Gerdes R, Kauker F, Köberle (2003) Arctic warming: evolution and spreading of the 1990s warm event in the

Nordic seas and the Arctic Ocean. J Geophys Res 108:3034. doi:10.1029/2001JC001265

Large WG, Yeager SG (2008) The global climatology of an interannually varying airsea flux data set. Clim Dyn 33:341–364. doi:10.1007/s00382-008-0441-3

Loeng H (1991) Features of the physical oceanographic conditions of the Barents Sea. Pol Res 10:5–18

Maslowski W, Marble D, Walczowski W, Schauer U, Clement JL, Semtner AJ (2004) On climatological mass, heat, and salt transports through the Barents Sea and Fram Strait from a pan-Arctic coupled ice-ocean model simulation. J Geophys Res 109:C03032. doi: 10.1029/2001JC001039

Mellor GL, Kantha L (1989) An ice-ocean coupled model. J Geophys Res 94:10937–10954

Michalsen K, Ottersen G, Nakken O (1998) Growth of Northeast Arctic cod (*Gadus morhua L.*) in relation to ambient temperature. ICES J Mar Sci 55:863–877

Midttun L (1985) Formation of dense bottom water in the Barents Sea. Deep Sea Res A 32:1233–1241

Nakken O, Raknes A (1987) The distribution and growth of Northeast Arctic cod in relation to bottom temperatures in the Barents Sea, 1978–1984. Fish Res 5:243–252

Overland JE, Wang M (2007) Future regional Arctic sea ice declines. Geophys Res Lett 34:L17705 doi:10.1029/2007GL030808

Parkinson CL, Vinnikov KY, Cavalieri DJ (2006) Evaluation of the simulation of annual cycle of Arctic and Antarctic sea ice coverages by 11 major global climate models. J Geophys Res 111:C07012. doi:10.1029/2005JC003408

Quadfasel D, Rudels B, Kurz K (1988) Outflow of dense water from a Svalbard fjord into the Fram Strait. Deep Sea Res A 35:1143–1150

Räisänen J (2002) CO_2-induced changes in interannual temperature and precipitation variability in 19 CMIP2 experiments. J Climate 15:2395–2411

Rayner NA, Parker DE, Horton EB, Folland CK, Alexander LV, Rowell DP, Kent EC, Kaplan A (2003) Global analyses of sea surface temperature, sea ice, and night marine air temperature since the late nineteenth century. J Geophys Res 108(D14):4407. doi:10.1029/2002JD002670

Røed LP, Debernard J (2004) Description of an integrated flux and sea-ice model suitable for coupling to an ocean and atmosphere model. met.no Report 4/2004. Norwegian Meteorological Institute, Oslo, 56 pp. http://met.no/filestore/MI-IM-Documentation.pdf

Rudels B, Jones EP, Anderson LG, Kattner G (1994) On the intermediate depth waters of the Arctic Ocean. In: Johannessen OM, Muench RD, Overland JE (eds) The polar oceans and their role in shaping the global environment. Geophysical Monograph Series, vol 84. AGU, Washington, DC, pp 33–46

Sandø AB, Furevik T (2008) Relation between the wind stress curl in the North Atlantic and the Atlantic inflow to the Nordic Seas. J Geophys Res-Oceans 113. doi:10.1029/2007JC004236

Schauer U, Loeng H, Rudels B, Ozhigin VK, Dieck W (2002) Atlantic water inflow through the Barents and Kara Seas. Deep Sea Res I 49:2281–2298

Sætersdal G, Loeng H (1987) Ecological adaption of reproduction in Northeast Arctic cod. Fish Res 5:253–270

Saetra Ø, Hersbach H, Bidlot J-R, Richardson DS (2004) Effects of observation errors on the statistics for ensemble spread and reliability. Mon Weather Rev 132:1487–1501

Shchepetkin AF, McWilliams JC (2003) A method for computing horizontal pressure-gradient force in an oceanic model with a non-aligned vertical coordinate. J Geophys Res 108:1–34

Shchepetkin AF, McWilliams JC (2005) The Regional Ocean Modeling System (ROMS): a split-explicit, free-surface, topography-following coordinates ocean model. Ocean Model 9:347–404

Skagseth Ø, Furevik T, Ingvaldsen R, Loeng H, Mork KA, Orvik KA, Ozhigin V (2008) Volume and heat transports to the Arctic via the Norwegian and Barents Seas. In: Dickson R, Meincke J, Rhines P (eds) Arctic-subarctic ocean fluxes. Defining the role of the northern seas in climate. Springer, Netherlands. doi:10.1007/978-1-4020-6774-7

Smith RD, Maltrud ME, Bryan, FO, Hecht MW (2000) Numerical simulation of the North Atlantic Ocean at $\frac{1}{10}^{\circ}$. J Phys Oceanogr 30:1532–1561

Song Y, Haidvogel, DB (1994) A semi-implicit ocean circulation model using a generalized topography-following coordinate system. J Comp Phys 115(1):228–244

Thompson DWJ, Lee S, Baldwin MP (2003) Atmospheric processes governing the Northern Hemisphere Annular Mode/North Atlantic Oscillation. In: Hurrell JW, Kushnir Y, Ottersen G, Visbeck M (eds) The North Atlantic Oscillation: climate significance and environmental impact. Geophysical Monograph Series, vol 134. American Geophysical Union, Washington, DC, pp 81–112

Walsh JE, Chapman WL, Romanovsky V, Christensen JH, Stendel M (2008) Global climate model performance over Alaska and Greenland. J Climate 21:6156–6174. doi:10.1175/2008JCLI163.1